Selective Surface Chemistry of Bifunctional Carboxylic acid, Aldehyde and Alcohol on Si(100)2×1: Exploring Competition between Alkyl, Alkenyl, Carboxyl, Hydroxyl, and Carbonyl Groups in Surface Functionalization

by

Maryam Ebrahimi

A thesis
presented to the University of Waterloo
in fulfillment of the
thesis requirement for the degree of
Doctor of Philosophy
in
Chemistry

Waterloo, Ontario, Canada, 2008

AUTHOR'S DECLARATION

I hereby declare that I am the sole author of this thesis. This is a true copy of the thesis, including any required final revisions, as accepted by my examiners.

I understand that my thesis may be made electronically available to the public.

Abstract

The dissociative adsorption of three carboxylic acids (acetic acid, propanoic acid, and acrylic acid), allyl alcohol, and allyl aldehyde on Si(100)2×1 at room temperature has been investigated by X-ray photoelectron spectroscopy (XPS) and temperature programmed desorption (TPD), as well as density-functional theory (DFT) calculations. The C 1s features obtained by XPS measurement for acetic acid, propanoic acid, and acrylic acid show that formation of bidentate carboxylate at a low exposure is followed by that of unidentate carboxylate at a higher exposure, with approximately equal population for both adstructures. The signatures of C 1s features attributed to methyl (285.7 eV), ethyl (285.3 eV), ethenyl (285.0 eV), and bidentate carboxyl (286.8 eV) and unidentate carboxyl (289.8-289.3 eV) carbons were observed for the studied carboxylic acids. The results showed that the carboxyl group is more reactive than the alkyl or alkenyl group towards the Si(100)2×1 surface, with O−H dissociation preferred over [2+2] C=C cycloaddition and the other plausible reaction products. This was also supported by our DFT calculation which showed that the bidentate carboxylate adstructure is the most stable configuration among the calculated adstructures for the aforementioned carboxylic acids. The combined temperature-dependent XPS and TPD studies provided strong evidence for the formation of ketene, acetaldehyde and CO from acetic acid, CO and ethylene from propanoic acid, and CO, ethylene, acetylene, and propene from acrylic acid. Furthermore, the TPD results provided further evidence for the preferred structure of the adsorbate from each of the carboxylic acid on the surface.

In addition to carboxyl group, reactivity of the hydroxyl and carbonyl functional groups relative to that of ethenyl group was studied by investigating the reaction of allyl alcohol and allyl aldehyde on Si(100)2×1 at room temperature. The C 1s XPS results supported O−H dissociation for allyl alcohol and [2+2] C=O cycloaddition for allyl aldehyde over the [2+2] C=C cycloaddition. The similarity between the observed C 1s features for allyl alcohol and allyl aldehyde helped to identify the structure of the adsorption products of these two molecules on the surface. The presence of the related C 1s feature of C=C for allyl alcohol and allyl aldehyde, and the absence of C 1s feature of C=O for allyl aldehyde provided strong evidence to support that [2+2] C=C cycloaddition does not occur in the

presence of hydroxyl or carbonyl groups. Furthermore, by comparing the experimental results and the adsorption energies of the adstructures calculated by DFT, it was concluded that these molecules do not react with the Si dimers through both of their functional groups, while the reaction of only one of the two functional groups is preferred on the surface. Formation of ethylene, acetylene, and propene from allyl alcohol and allyl aldehyde, simultaneously to CO from allyl alcohol, was concluded from the corresponding TPD results, which also confirm the structure of the adsorbates on the surface.

The present research shows that reactions involving oxygen-containing functional groups are favoured over the other plausible reactions including [2+2] C=C cycloaddition on the Si(100)2×1. The preference of the surface to react with one of the two functional groups calls for future studies for the selective functionalization of Si(100)2×1 with potential applications in molecular electronics.

Acknowledgements

I would like to thank my supervisor Professor Leung who gave me the opportunity to do my Ph.D in his research group, and widely supported me during the last four years in many aspects. I would like to appreciate his patience in teaching me how to better express and present my research work besides spending a lot of his time to improve my thesis. I would like to thank all the other Professors with whom I was delighted to get acquainted, including my committee members Dr. Goddard, Dr. Aziz, Dr. Karanassios, Dr. Thomas, and Dr. Lu during the last four years, Dr. Lau as the external examiner, and Dr. Nooijen and Dr. Chong with whom I was grateful to discuss science.

I would like to express my thanks to Dr. Thiam, as a friend and a teacher, who made me familiar with different aspects of surface science, and taught me how to precisely run the experiments and analyze the data. He gave me all the confidence that I needed to overcome the challenges related to the ultra-high vacuum project, and he encouraged me not to stop in any stage of life. I would also like to thank Dr. Zhou, Abdullah Radi, Fernando Rios, and all the other members of WatLab. My special thank to Dr. Fisher who unsparingly answered my questions. His friendship is so valuable to me, and I will never forget all the nice time that I was grateful to serve as his TA for several courses. I would like to thank Mrs. Cathy van Esch, the administrative coordinator of the Department of Chemistry. Her responsibility together with her nice character has made her a very special person in my mind. I am grateful to all the members of the Machine Shop and the Electronics Shop, who always did their best to facilitate my research project. I am thankful to Dr. Hu and Mr. Sean McLeod for their assistance to use SHARCNET and WEPIL. My thanks to all of my friends for their company that gave me the great pleasure to enjoy the time we spent together in Waterloo. Finally, I would like to thank my family specially my parents, my sister and brothers who have been the main reason for me to do my best and achieve my success.

Dedication

To my father and my mother

Table of Contents

List of Figures ix
List of Tables xii
Chapter 1 Introduction 1
1.1 Background and motivation 1
1.1.1 Structure of Si(100)2×1 surface 2
1.1.2 Reactions of diverse organic molecules on Si(100)2×1 3
1.2 Overview of surface analysis techniques 5
1.2.1 X-ray photoelectron spectroscopy (XPS) 5
1.2.2 Temperature Programmed Desorption (TPD) 7
1.3 Experimental setup 7
1.4 Computational Details 11
1.5 Objectives and scope 13
References 16
Chapter 2 18
2.1 Introduction 18
2.2 Results and Discussion 21
2.2.1 DFT computational study of adsorbate-substrate configurations 21
2.2.2 XPS study of the adspecies at room temperature 24
2.2.3 XPS and TPD studies of the thermal evolution of adspecies 27
2.3 Summary 35
References 36
Chapter 3 40
3.1 Introduction 40
3.2 Results and Discussion 43
3.2.1 DFT computational study of adsorbate-substrate configurations 43
3.2.2 XPS study of room-temperature adsorption of acrylic acid and propanoic acid 48
3.2.3 XPS and TPD studies of the thermal evolution of acrylate adspecies 53
3.3 Summary 62
References 63
Chapter 4 66

4.1 Introduction 66
4.2 Results and Discussion 68
4.2.1 DFT computational study of adsorbate-substrate configurations 68
4.2.2 Room-temperature adsorption of allyl alcohol and allyl aldehyde on Si(100)2×1 72
4.2.3 Thermal evolution of allyl alcohol and allyl aldehyde adspecies on Si(100)2×1 74
4.3 Summary 85
References 86
Chapter 5 Conclusion 89

List of Figures

Figure 1.1 Schematic diagram of the constructed Si(100)2×1 surface. 3

Figure 1.2 Schematic diagram for the cycloaddition reaction. 4

Figure 1.3 Schematic diagram of the XPS process. 6

Figure 1.4 Photograph of the Experimental Set up. 10

Figure 1.5 Geometry and the total energy calculated by using DFT/B3LYP with 6-31++G(d,p) for (a) acetic acid, (b) propanoic acid, (c) acrylic acid, (d) allyl alcohol, and (d) allyl aldehyde. The energy is reported in units of hartree or atomic unit (a.u.). All the bond lengths are in unit of pm. 12

Figure 2.1 Optimized geometries of the adsorption structures of acetic acid on Si(100)2×1: (a) inter-dimer bidentate, (b) intra-dimer bidentate, (c) unidentate I, (d) unidentate II, (e) C–OH dissociation, (f) ene I, (g) ene II , and (h) [2+2] C=O cycloaddition reaction products. The corresponding adsorption energies (ΔE) calculated by 6-31++G(d,p) basis set are given in parentheses. All the bond lengths are in unit of pm. 23

Figure 2.2 Schematic diagrams of (a) unidentate and (b) bidentate adstructures, and (d) the plausible resonance forms of the hybrid resonance structure (b). (c) XPS spectra of the C 1s region for a saturated exposure (100 L) and a 5-L exposure of acetic acid on Si(100)2×1 at 300 K. 26

Figure 2.3 XPS spectra of the C 1s region for a saturated exposure of acetic acid on Si(100)2×1 at (a) 300 K, and upon sequential flash-annealing to (b) 489 K, (c) 711 K, (d) 933 K, (e) 1154 K, and (f) 1376 K. (g) shows the corresponding temperature profiles of the C 1s intensities ($I_{C\ 1s}$) for SiC at 283.3 eV, C_a at 284.0-285.7 eV, C_b at 286.9 eV, and C_c at 289.8 eV, along with the total C 1s intensity (C_{tot}), all with respect to the intensity of Si 2p ($I_{Si\ 2p}$). 28

Figure 2.4 XPS spectra of the O 1s region for a saturated exposure of acetic acid on Si(100)2×1 at (a) 300 K, and upon sequential flash-annealing to (b) 489 K, (c) 711 K, (d) 933 K, (e) 1154 K, and (f) 1376 K. (g) shows the corresponding temperature profile of the O 1s intensity ($I_{O\ 1s}$) with respect to the intensity of Si 2p ($I_{Si\ 2p}$). 29

Figure 2.5 TPD profiles of the selected fragments of m/z (a) 2, (b) 15, (c) 28, (d) 29, (e) 42, (f) 43, and (g) 44 for a saturation coverage of acetic acid on Si(100)2×1 at 300 K. 33

Figure 2.6 Schematic models for thermal evolution of unidentate acetate (structure I) and bidentate acetate (structure II), depicting the formation of (a) ketene, (b) acetaldehyde, (c) CO, and (d,e) CO_2 desorbates, and (f) their interconnection 34

Figure 3.1 Optimized geometries of the adsorbate-substrate configurations of acrylic acid on Si(100)2×1: (a) inter-dimer bidentate, (b) intra-dimer bidentate, (c) unidentate, (d) [O,C] bidentate, (e) C–OH dissociation, (f) [2+2] C=C cycloaddition reaction, (g) [2+2] C=O cycloaddition reaction, and (h) ene products. The corresponding adsorption energies (ΔE) calculated with a 6-31++G(d,p) basis set are given in parentheses. All the bond lengths are given in unit of pm. 46

Figure 3.2 Optimized geometries of the adsorbate-substrate configurations of propanoic acid on Si(100)2×1: (a) inter-dimer bidentate, (b) intra-dimer bidentate, (c) unidentate, (d) C–OH dissociation, (e) ene, and (f) [2+2] C=O cycloaddition reaction products. The corresponding adsorption energies (ΔE) calculated with a 6-31++G(d,p) basis set are given in parentheses. All the bond lengths are given in unit of pm. 47

Figure 3.3 Schematic diagrams of (a) unidentate and (b) bidentate acrylate adstructures, and the plausible resonance structures of (d) bidentate and (e) unidentate acrylate, and of (f) unidentate and (g) bidentate propanoate. XPS spectra of the C 1s and O 1s regions for (c) a saturation exposure (130 L) and a 2-L exposure of acrylic acid and (h) a saturation exposure (30 L) and a 2-L exposure of propanoic acid, all on Si(100)2×1 at 300 K. 52

Figure 3.4 XPS spectra of the C 1s region for (a) a saturated exposure (130 L) of acrylic acid on Si(100)2×1 at 300 K, and upon sequential flash-annealing to (b) 525 K, (c) 770 K, (d) 1050 K, (e) 1185 K, and (f) 1350 K. (h) shows the corresponding temperature profiles of the C 1s intensities ($I_{C\ 1s}$) for SiC at 283.3 eV, C_a at 284.0-285.0 eV, C_b at 286.8 eV, and C_c at 289.3 eV, along with the total C 1s intensity (C_{tot}), all with respect to the intensity of Si 2p ($I_{Si\ 2p}$). 55

Figure 3.5 XPS spectra of the O 1s region for (a) a saturated exposure (130 L) of acrylic acid on Si(100)2×1 at 300 K, and upon sequential flash-annealing to (b) 525 K, (c) 770 K, (d) 1050 K, (e) 1185 K, and (f) 1350 K. (g) shows the corresponding temperature profile of the O 1s intensity ($I_{O\ 1s}$) with respect to the intensity of Si 2p ($I_{Si\ 2p}$). 56

Figure 3.6 TPD profiles of selected fragments of (A) m/z (a) 2, (b) 26, (c) 27, (d) 28, (e) 39, (f) 41, and (g) 42 for a saturation coverage (130 L) of acrylic acid, and (B) m/z (a) 2, (b)

25, (c) 26, (d) 27, and (e) 28 for a saturation coverage (30 L) of propanoic acid, on Si(100)2×1 at 300 K. 60

Figure 3.7 Schematic models for thermal evolution of unidentate and bidentate (A) acrylate and (B) propanoate on Si(100)2×1, depicting the formation of CO, ethylene, and acetylene, and of CO and ethylene, respectively. 61

Figure 4.1 Optimized geometries of the adsorbate-substrate configurations (ASCs): (a) O−H dissociation ASC I, (b) [2+2] C=C cycloaddition ASC II, and (c) [O, C, C] tridentate ASC III products of allyl alcohol, and (d) [2+2] C=O cycloaddition ASC IV, (e) [2+2] C=C cycloaddition ASC V and (f) [O, C] bidentate ASC VI products of allyl aldehyde, all on Si(100)2×1. The corresponding adsorption energies calculated with the 6-31++G(d,p) basis set are given in parentheses. 71

Figure 4.2 XPS spectra of the C 1s (left column) and O 1s regions (right column) for (a) a 0.45 L and (b) a saturated exposures (106 L) of allyl alcohol deposited on Si(100)2×1 at 300 K, and for sample (b) upon sequential flash-annealing to (c) 425 K, (d) 545 K, (e) 800 K, (f) 1090 K, and (g) 1390 K. (h) Corresponding temperature profiles of the C 1s intensities ($I_{C\ 1s}$) for SiC at 283.1 eV, C_a at 284.3-284.8 eV, and C_b at 286.4 eV, along with the total intensity for C 1s (C_{tot}), and of the total O 1s intensity ($I_{O\ 1s}$), all with respect to the intensity of Si 2p ($I_{Si\ 2p}$). 77

Figure 4.3 XPS spectra of the C 1s (left column) and O 1s regions (right column) for (a) a 0.2 L and (b) a saturated exposures (60 L) of allyl aldehyde deposited on Si(100)2×1 at 300 K, and for sample (b) upon sequential flash-annealing to (c) 425 K, (d) 545 K, (e) 800 K, (f) 1090 K, and (g) 1390 K. (h) Corresponding temperature profiles of the C 1s intensities ($I_{C\ 1s}$) for SiC at 283.0 eV, C_a at 284.3-284.7 eV, and C_b at 286.3 eV, along with the total intensity for C 1s (C_{tot}), and of the total O 1s intensity ($I_{O\ 1s}$), all with respect to the intensity of Si 2p ($I_{Si\ 2p}$). 78

Figure 4.4 TPD profiles of selected fragments of m/z (a) 2, (b) 26, (c) 27, (d) 28, (e) 39, (f) 40, (g) 41, and (h) 42 for a saturation exposure of (A) allyl alcohol and (B) allyl aldehyde on Si(100)2×1 deposited at 300 K. 83

Figure 4.5 Schematic models for thermal evolution of the O−H dissociation and [2+2] C=O cycloaddition products to ethylene, acetylene, and propene for (A) allyl alcohol and (B) allyl aldehyde, respectively, on Si(100)2×1, and to additional CO desorption for allyl alcohol. 84

List of Tables

Table 2.1 Comparison of the adsorption energies ΔE and total energies (in square parentheses) for the three most stable adsorbate-substrate configurations (ASCs) of acetic acid on Si(100)2×1 obtained by DFT/B3LYP calculations with 6-31G(d), 6-31+G(d), 6-31++G(d), and 6-31++G(d,p) basis sets. 22

Table 3.1 Comparison of the adsorption energies ΔE and total energies (in square parentheses) for the three most stable adsorbate-substrate configurations (ASCs) of acrylic acid and of propanoic acid on Si(100)2×1 obtained by DFT/B3LYP calculations with 6-31G(d), 6-31+G(d), and 6-31++G(d,p) basis sets. 45

Table 4.1 Comparison of the adsorption energies, ΔE, and total energies (in square parentheses) for plausible adsorbate-substrate configurations (ASCs) of allyl alcohol and allyl aldehyde on Si(100)2×1 obtained by DFT/B3LYP calculations with 6-31G(d), 6-31+G(d), 6-31++G(d), and 6-31++G(d,p) basis sets. 70

Chapter 1
Introduction

1.1 Background and motivation

Fabrication of smaller transistors has been one of the most important goals in the semiconductor manufacturing industry since 1960's. It is expected that the quest for continued miniaturization will not stop until the size of a single molecule is reached. Miniaturized transistors, therefore, will have a direct impact on device scaling and on fabricating even faster processors. As the fundamental aspects of this subject, molecular-level phenomena that control the chemical reactions occurring at the semiconductor interfaces have attracted a lot of attention. In addition to the extensive development of inorganic materials being used in the semiconductor industry, significant progress has also been made to incorporate organic materials by taking advantages of their diverse functionality and properties. It is expected that hybrid organic-inorganic devices will exhibit the best properties of both inorganic and organic materials. This has created a new field of research generally known as "Organic Functionalization of Semiconductor Surfaces" that makes use of novel surface chemistry not found in "Classical Chemistry".[1−14]

Investigating the properties of the hybrid organic-inorganic materials is one of the fundamental steps that link organic functionalization of silicon surface to molecular electronics. The future advancement of electronics at the molecular level depends on the synthesis of materials with specific properties, in addition to developing the methods needed for assembling the molecules. However, besides the problem relating to the contact of the single molecule in a molecular device, assembling individual molecules is another challenge associated with molecular electronics. Despite a wide range of materials with potential electronic applications have been studied, the stability, conductivity, and control of the direct and reverse charge transfer have been among the main challenges associated with these materials. It is known that the conjugated π-electrons of a material with a well-defined electronic structure readily transfer the electron. In order to provide electron conduction through a molecule, as prerequisite in a molecular electronic device, the molecule should be

strongly attached to the surface. If the bonded species contain unpaired electrons or π electrons, electronic conduction will occur through the delocalized electrons. To make a fundamental contribution toward this area of research, the reaction products for the adsorption of the molecules containing O and π-electrons were studied in the present research.

1.1.1 Structure of Si(100)2×1 surface

Silicon crystals have the diamond structure, in which Si atoms with the sp^3 hybridization are bonded to four nearest atoms in tetrahedral coordination.[5] Each covalent bond is 2.35 Å with the bond energy of 226 kJ mol^{-1}. A perfect crystal of Si can be cut along any arbitrary direction. As the simplest planes, the low-index Miller planes represent the basic building blocks of surface structure. The three low-index planes for an element with the diamond structure such as silicon include (100), (110), and (111). The so-called dangling bonds are created on the surface where the crystal is cut. It should be noted that cutting the surface requires the cleavage of bonds. Bond breakage results in having surface atoms with a lower coordination number, creating the so-called dangling bonds.[15] The silicon atoms on the surface of Si(100) will pair their two dangling bonds to minimize the surface energy and to reduce the number of dangling bonds. This process is called "surface reconstruction" that results in the Si dimer rows with a (2×1) pattern on the surface. Figure 1.1 shows different views of the reconstructed Si(100)2×1 surface.

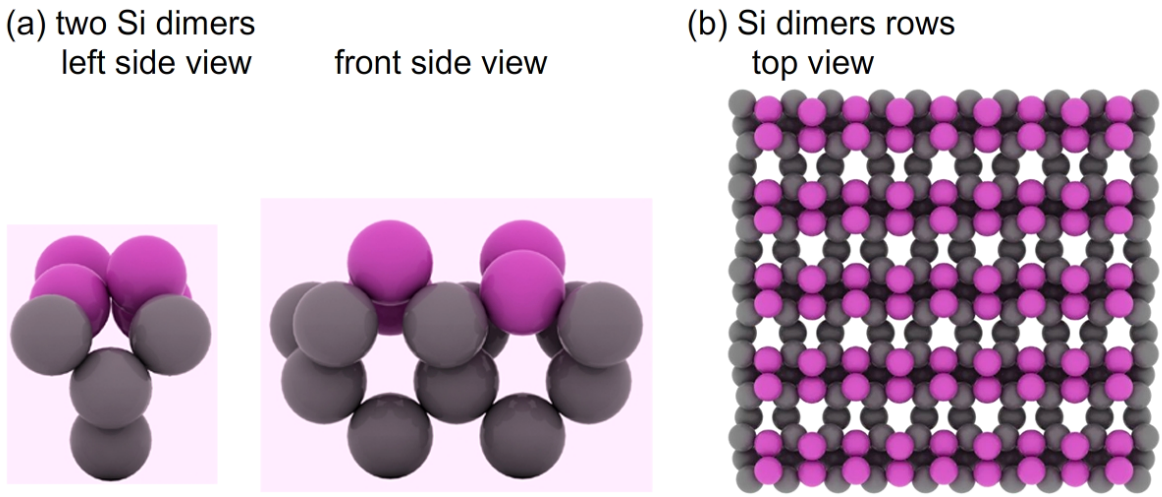

Figure 1.1 Schematic diagram of the constructed Si(100)2×1 surface.

Si(100)2×1 is the most widely used semiconductor surface in the electronics industry. The reactivity of Si(100)2×1 is related to the dimer bond, which may be considered as comprising of a full σ bond and a partial π bond.[1,2,5,6] The asymmetric charge distribution in the Si dimer results in nucleophile and electrophile sites as $Si^{\delta+}=Si^{\delta-}$ (known as buckled dimer), which ultimately control the reactivity and selectivity of the Si(100)2×1 surface. The asymmetrically tilted dimer has been earlier confirmed by low temperature (LT) scanning tunneling microscopy (STM).[16] The dimer rows provide unique reactive sites on Si(100)2×1 for organosilicon chemistry.

1.1.2 Reactions of diverse organic molecules on Si(100)2×1

Si dimer is known to react with different types of organic functional groups through a diverse range of reaction mechanisms. The similarity of the Si dimer to the carbon double bond has enabled a large number of reactions to occur on the Si(100)2×1 surface. Pericyclic reactions including [2+2] and [4+2] cycloaddition, also known as Diels-Alder reactions, are some of the typical reactions on Si(100)2×1 involving molecules containing C=C and/or C=O. The reactivity of the Si=Si dimer to form the [2+2] and [4+2] cycloaddition products at room temperature (RT) has been demonstrated by many studies.[1,2,9,10] It should be noted

that the [2+2] cycloaddition reactions are symmetry-forbidden in the classical organic chemistry, while [4+2] cycloaddition reactions are symmetry-allowed according to the Woodward-Hoffman selection rules.[17] Figure 1.2a illustrates the interaction between a pair of π electrons between two alkenes in the [2+2] cycloaddition reaction, which does not lead to the formation of a four-membered ring. However, this reaction can take place only by ultraviolet light excitation or at high temperatures. In contrast, the reaction between a diene (with two alternating C=C) and an alkene can readily lead to [4+2] cycloaddition reaction in which two new σ bonds are formed (Figure 1.2b). In comparison to classical chemistry, it has been proposed that the buckled Si(100)2×1 dimers , shown in Figure 1.2c, allow the alkene to form the σ bond with the Si(100)2×1 surface resulting in the formation of [2+2] cycloaddition products. The mechanisms of these reactions on Si(100)2×1 are largely unclear. The reactions of unsaturated hydrocarbons, including alkene, alkyne, and aromatic hydrocarbons, aldehyde, and ketones, belongs to this general class of reactions.[1,2,4,9,10]

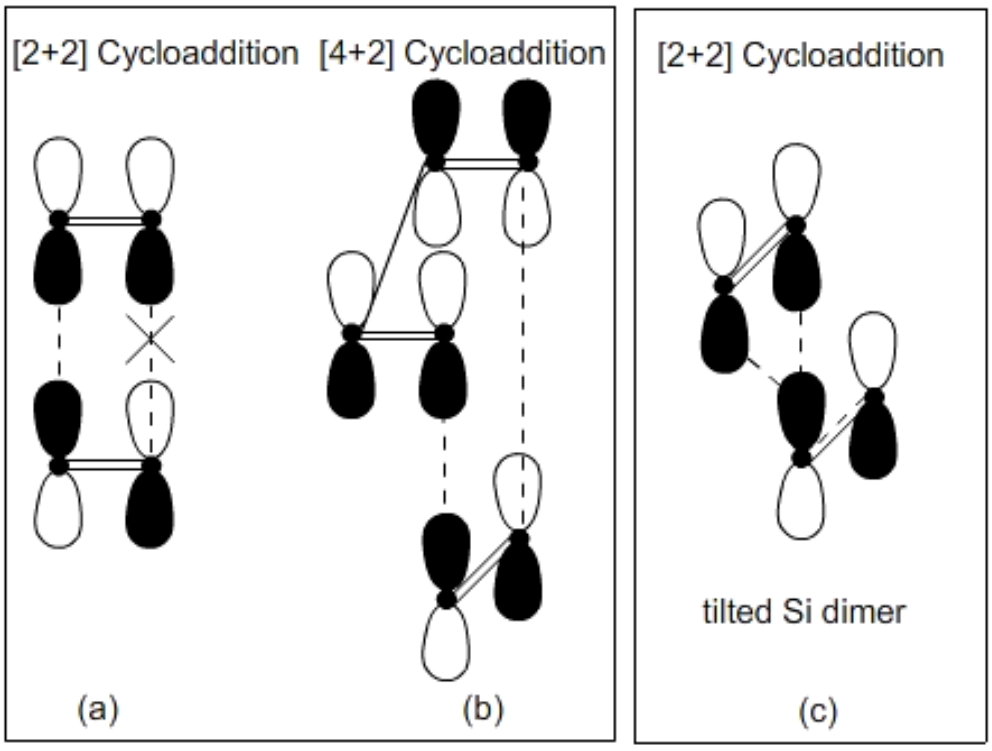

Figure 1.2 Schematic diagram for the cycloaddition reaction.

In addition, the nucleophilic-electrophilic character of the buckled Si dimer has enabled reactions of many other molecules through the dative bonding of the heteroatom (O, N, S), which usually leads to H dissociation on the Si(100)2×1. The buckled up and down Si atoms of the dimer are nucleophilic (electron rich) and electrophilic (electron deficient), respectively, due to donation of significant charge from the down atom to the up atom. A molecule containing a strong nucleophilic atom can easily attack the electrophilic site of the Si dimer to form a dative bond. The subsequent dissociated hydrogen will be bonded to the nucleophilic Si atom of the dimer. Formation of H-dissociation product observed for carboxylic acids, amino acids, alcohols, primary and secondary amines, and thiols belong to this other general class of reaction.[1,2,9,10]

Earlier studies on the surface chemistry of a large number of molecules with a single functional group on Si(100)2×1 show that the nature of the functional group plays an important role in controlling whether cycloaddition or H-dissociation would occur. The study of the competition among different reactive pathways, including [2+2] C=C cycloaddition, [2+2] C=O cycloaddition and O−H dissociation, upon adsorption of multifunctional molecules on Si(100)2×1 represents one of the main goals of the present work.

1.2 Overview of surface analysis techniques

1.2.1 X-ray photoelectron spectroscopy (XPS)

In XPS, also known as electron spectroscopy for chemical analysis (ESCA), an X-ray photon with the energy of $h\nu$ is absorbed by the material, which causes the ejection of an electron from a core shell into vacuum. The energy of the photon should be more than the binding energy (BE) of the electron, which corresponds to the energy needed for the electron to leave from its specific energy level to the vacuum. The relevant notation of nl_j shows the transition of the electron. This notation includes n (the principal quantum number), l (the quantum number describing the orbital angular momentum), and j (spin angular momentum of the electron). The kinetic energy (KE) of the ejected photoelectron is experimentally

measured by the spectrometer. These parameters are related through the equation: EB=*hv*-EK.[18] The schematic diagram of the ejection of an electron from 1s orbital by X-ray can be seen in Figure 1.3.

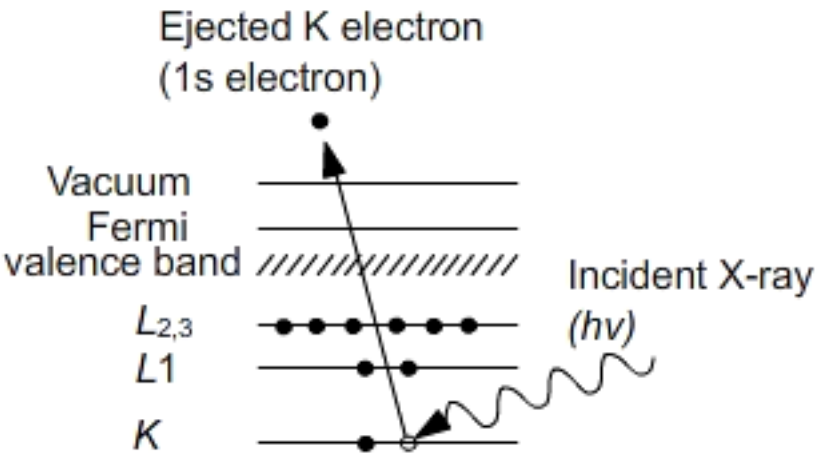

Figure 1.3 Schematic diagram of the XPS process.

XPS generally provides information about the chemical composition of the surface through the determination of the oxidation states of elements at the surface. Change of the chemical environment of the atoms leads to the BE shift of the core shell electrons. The relevant BE shift or chemical shift for the core shell electrons are directly dependent on the charge transfer in the outer electronic level by the redistribution of the charge for the valence electrons. Changing the partial charge for the elements with different chemical environment involved in the chemical bonding causes a chemical shift in the corresponding BE.[19] For the cases that atom keeps its oxidation state in different materials, its core level BE increases while the electronegativity or the electron withdrawing power of the attached atoms or groups increases.[20]

In the present work, XPS was used to initially observe any change of the chemical shifts in the C 1s BEs due to different chemical environment correlating to various adstructures produced by the adsorption of the molecules. Secondly, the sample was

annealed to different temperatures to study the effect of annealing on the disturbance and dissociation of the bonds within the adsorbates resulting in the C 1s chemical shifts for the remaining features before the desorbates are totally eliminated from the surface. The term of "temperature-dependent XPS" is used for the XPS measurements after annealing the surface to different temperatures and re-cooling the sample to the room temperature.

1.2.2 Temperature Programmed Desorption (TPD)

In TPD also known as thermal desorption spectroscopy (TDS), the adsorbate-covered surface is heated with a linear rate and thermally desorbed species are detected with a mass spectrometer. The TPD results give useful information about the nature and the geometry of the adsorbates on the surface. The rate of evolution of the adsorbed molecules is given by the Arrehnius equation:

$$-dN/dt=K_mN^m \exp(-E_d/RT)$$

where N is the number of adsorbed particles per unit area; K_m is the frequency factor; m is desorption reaction rate; E_d is the activation energy for the desorption pathway; T is absolute temperature, and t is the time.[21]

In the present work, TPD was mainly used to qualitatively determine the nature of the desorption features from the surface saturated by the adsorbed molecules. Furthermore, pathways involving bond dissociations required for the formation of various desorbates could be inferred from the TPD profiles. The combined temperature-dependent XPS data with the TPD profiles provide complementary information about the nature of the desorbates and the composition of the remaining adsorbate as a function of annealing temperature which lead to better understanding of the possible desorption pathways.

1.3 Experimental setup

All the experiments were performed in a home-built dual-chamber ultra high vacuum (UHV) system (Figure 1.4) with a base pressure better than 1×10^{-10} Torr. The sample preparation chamber was equipped with an ion-sputtering gun, and a four-grid retarding-field

optics for both reverse-view low energy electron diffraction and Auger electron spectroscopy. The XPS and TPD mass spectrometry studies were carried out in the analysis chamber. A 14×10 mm^2 substrate was cut from a single-side polished, p-type, B-doped Si(100) wafer (0.4 mm thick) with a resistivity of 0.0080-0.0095 Ω cm. The sample mounting and preparation procedures have been described in detail elsewhere. [22] It should be noted that the entire sample holder used in the present work has been rebuilt out of tantalum to further minimize any environmental effects. The surface was cleaned in the preparation chamber by cycles of Ar^+ sputtering (20 mA emission current, 1.5 kV beam energy) for 20 min at room temperature followed by annealing to 900 K for 5 min. The sample was then flash-annealed to 1100 K for 20 sec to obtain the 2×1 reconstructed surface. The cleanliness of the 2×1 surface was further affirmed by the sharpness of the electron diffraction pattern and by our XPS data that showed no significant contamination.

The adsorption of five chemicals, all colorless liquid under ambient condition, used in the present work on the Si(100)2×1 surface was studied. These molecules include three carboxylic acid (acetic acid, 99.9% purity; propanoic acid, 99.5%; and acrylic acid, 99.0%), allyl alcohol (or 2-propenol, 99.0%), and allyl aldehyde (or 2-propenal, 90.0%). Except for acetic acid (Baker), the other four chemicals were purchased from Sigma-Aldrich. All of these chemicals were purified by several freeze-pump-thaw cycles before exposure to the silicon surface through a variable leak valve. The high purity of the exposed chemical was confirmed by its cracking pattern obtained in-situ. All exposures were performed at RT and reported in unit of Langmuir (1 L = 10^{-6} Torr sec), with the pressure monitored by an uncorrected ionization gauge. Studies on a series of exposures have been performed and only TPD and XPS experiments for the low and saturation exposures have been reported, unless stated otherwise.

TPD studies were conducted by using a differentially pumped 1–300 amu quadrupole mass spectrometer (VG Quadrupole SXP Elite). A home-built programmable proportional–integral–differential temperature controller was used to provide linear temperature ramping at an adjustable heating rate. The temperature was measured by using a type-K thermocouple (wrapped in a Ta foil) mechanically placed in good contact with the front face of the sample.

It should be noted that TPD experiments were taken at 3.5 K sec^{-1} for acetic acid, while the heating rate used for the other molecules was 2 K sec^{-1}. The temperature scale was calibrated by the desorption maximum of recombinative H_2 desorption from the monohydrides.[23] To ensure that the selected masses originate only from the species desorbed from the Si surface, the sample was positioned within 1 mm to the entrance (2 mm dia.) of the differentially pumped housing of the mass spectrometer. Unless stated otherwise, the desorption profiles have been smoothed by adjacent averaging for clarity.

XPS experiments were performed by using an electron spectrometer (VG Scientific CLAM-2), consisting of a hemispherical analyser of 100 mm mean radius and a triple-channeltron detector, with a twin-anode X-ray source that supplied unmonochromatic Al K_α radiation at 1486.6 eV photon energy. XPS spectra were collected with an acceptance angle of ±4° at normal emission from the silicon sample, and with a constant pass energy of 50 eV, giving an effective energy resolution of 1.4 eV full-width-at-half-maximum (FWHM) for the Si 2p photopeak. The binding energy scale of the XPS spectra has been calibrated to the Si 2p feature of the bulk at 99.3 eV. Spectral peak fitting based on residual minimization with Gaussian–Lorentzian lineshapes was performed by using the Casa XPS software. For temperature-dependent XPS measurements, the sample was flash-annealed to the preselected temperature and cooled back to RT before collecting the XPS spectra.

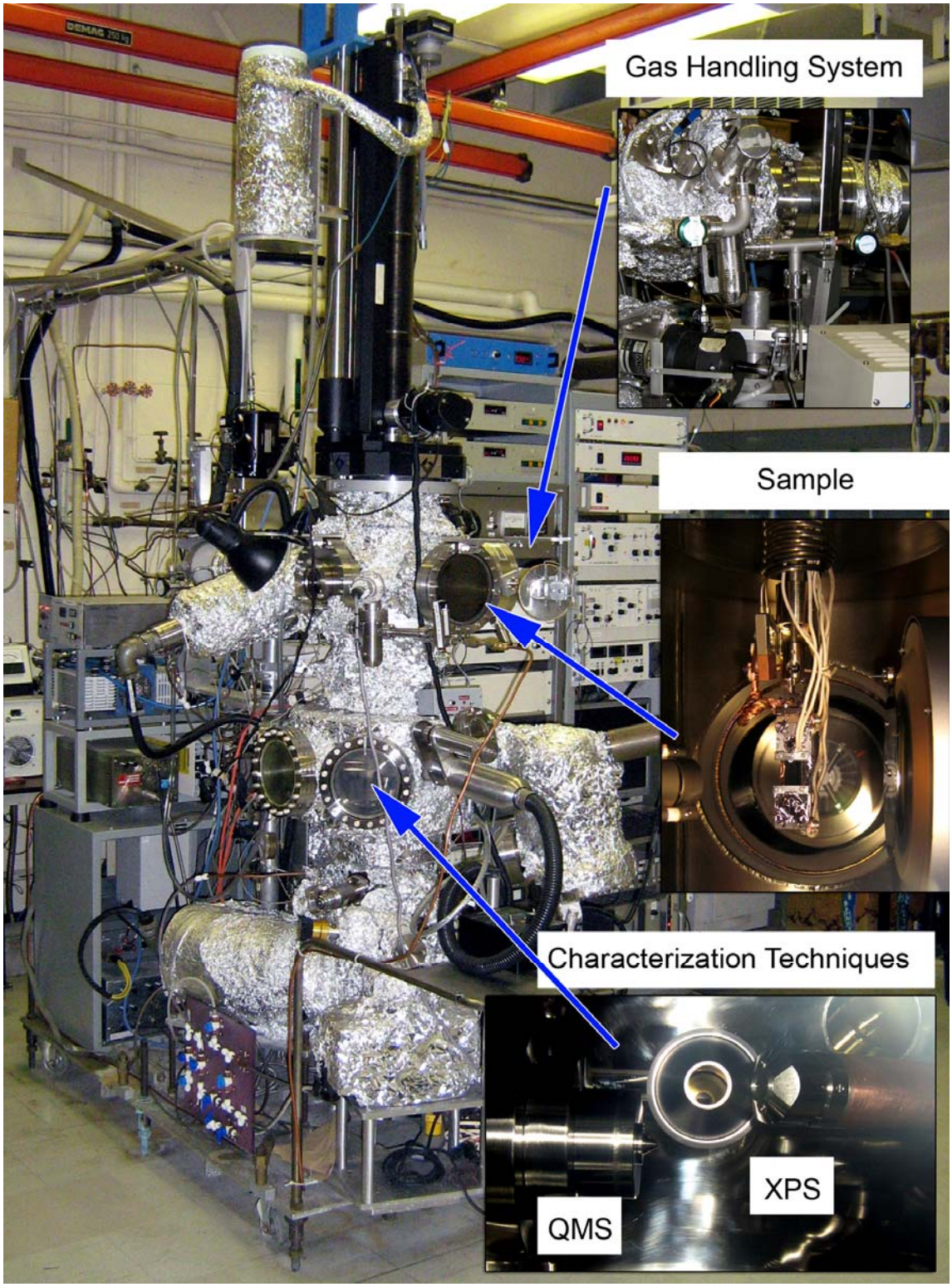

Figure 1.4 Photograph of the Experimental Set up**.**

1.4 Computational Details

Electronic structure calculations were performed by using the density functional theory (DFT) method[24] with the Gaussian 03 software package.[25] The employed hybrid B3LYP functional is composed of Becke's 3-parameter gradient-corrected exchange functional[26] and the Lee-Yang-Parr correlation functional.[27] The DFT/B3LYP method has been shown to provide generally good agreement with the experimental data for the adsorption of many molecular systems on Si(100)2×1.[9] For most of the calculations presented in the present work, four basis sets, including 6-31G(d), 6-31+G(d), 6-31++G(d), and 6-31++G(d,p), were employed unless stated otherwise. All the calculations gave similar results for the optimized geometries and total energies, with the larger basis set generally providing a lower total energy. The interpretation of the results for all the molecules of interest is based on the largest basis set [6-31++G(d,p)]. The Si(100)2×1 surface was simulated by a double-dimer surface of the $Si_{15}H_{16}$ cluster. The adstructures of each molecule were fully optimized without any geometrical constraint on the $Si_{15}H_{16}$ cluster. The corresponding adsorption energy, ΔE, was estimated by the difference between the total energy for the optimized structures of the adsorbate-substrate configurations (ASCs) of the molecule adsorbate on the $Si_{15}H_{16}$ model surface and the sum of the total energies of a free molecule and of a $Si_{15}H_{16}$ cluster. All the total energies were obtained without zero-point correction and no basis set superposition error correction was made to ΔE. Frequency calculation was also performed for all of the optimized geometries, in order to ascertain that the local minima correspond to the equilibrium structures and not transition-state structures.

The free-molecule geometry, along with the calculated energy [in the units of hartree or atomic unit (a.u.)] obtained by DFT for the molecules studies in the present work are presented in Figure 1.5.

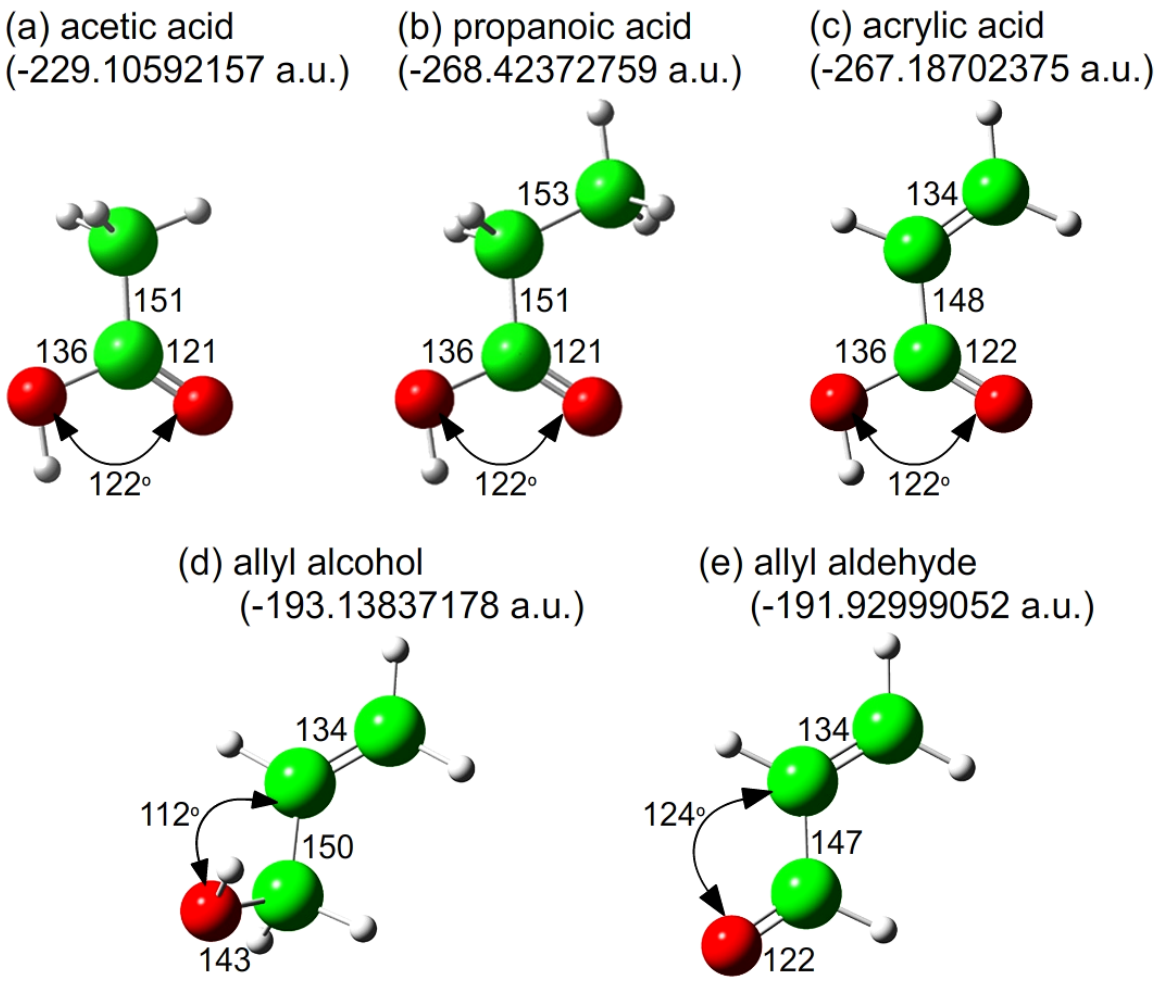

Figure 1.5 Geometry and the total energy calculated by using DFT/B3LYP with 6-31++G(d,p) for (a) acetic acid, (b) propanoic acid, (c) acrylic acid, (d) allyl alcohol, and (d) allyl aldehyde. The energy is reported in units of hartree or atomic unit (a.u.). All the bond lengths are in unit of pm.

1.5 Objectives and scope

The main objective of the present work is the production and characterization of the hybrid organic-inorganic material interface based on the functionalization of Si(100)2×1 with bifunctional carboxylic acid, alcohol, and aldehyde, for potential applications in molecular electronic devices, biosensors, and biomedicine devices. By linking one of functional groups to the Si surface (through the formation of Si−O or Si−C bonds), a multifunctional molecule could utilize the other functional groups to interact with other molecules, in effect changing the reactivity of the prefunctionalized surface. Surface reactions involving a large number of functional groups on Si(100)2×1 have been widely studied and described in the literature.[1,2,9,10] To date, the reactivity of the carboxylic acids, and in general of the bifunctional molecules, has been largely unexplored. This is due to the acidity and high reactivity of these more complicated molecules that could potentially cause the experimental difficulties to the UHV chambers and the equipment. Furthermore, exposing the more complicated molecules, depending on their phase equilibrium at room temperature, in the UHV chamber requires a special dosing system. In addition, formation of many possible reaction products between the multifunctional molecules and the Si(100)2×1 surface complicates the data interpretation.

In the present work, the reactions involving different functional groups are investigated in order to determine the reactivity of these molecules, and the selectivity of the surface for particular functional groups in the molecules of interest. In the case of the carboxylic acids, acetic acid is one of the main constituents of amino acids, the building block of proteins. The study of the surface chemistry of acetic acid on Si(100)2×1 is therefore partially motivated by its biological interest (Chapter 2). To study the selectivity of the surface towards bifunctional carboxylic acid, acrylic acid, as the smallest unsaturated carboxylic acids with C=C and COOH functional groups, was studied. To understand the importance of the C=C bond in the carboxylic acid, propanoic acid, as the saturated form of acrylic acid, was also studied (Chapter 3). In order to compare with the results taken for acrylic acid, the effect of having the hydroxyl (OH) or carbonyl (C=O) group instead of carboxyl group, was further studied by keeping the C=C group in allyl alcohol and allyl

aldehyde . Choosing these two molecules provided the results for studying the competitive reactions of the Si(100) surface with C=C or OH in allyl alcohol, and with C=C or C=O in allyl aldehyde (Chapter 4). The reactions for different functional groups studied in the present thesis, altogether lead to better understanding of the nature of the interfacial bonding between the substrate and the molecular moiety, and of their effects on the electronic properties of the hybrid organic-inorganic material. A thorough characterization by XPS was carried on clean Si(100) surface exposed with these molecules. The observed chemical shifts in the C 1s BEs, together with O 1s BEs, provide the important clues about the understanding plausible geometry of the adstructures at low and high exposures. The geometries of the adstructures calculated by DFT, also provide further support for the chemical environments of the atoms within different proposed adstructures. Moreover, the TPD experiments were used to detect the products evolved from the thermal chemistry of the adstructures. For all of the molecules, several interesting thermal evolution pathways were investigated and presented schematically for a better understanding. The observed thermal desorption products offer a new window into novel chemistry mediated by the 2×1 surface.

By studying the molecules containing one or two functional groups from carboxyl, hydroxyl, carbonyl, and alkenyl functional groups, it is possible to conclude that that the Si(100)2×1 surface is more selective to form O−H dissociation product from carboxyl (for acetic acid, acrylic acid, and propanoic acid) and hydroxyl (for allyl alcohol) groups than other possible reaction products, including [2+2] C=C or C=O cycloaddition products. The preferred formation of [2+2] C=O over C=O cycloaddition product (for allyl aldehyde) was also determined and discussed in detail.

In conclusion, the taken efforts presented the formation of an interfacial Si−O and/or Si−C covalent bond on the surface through one of the functional groups of the adsorbed molecule. In fact, the competition between different functional groups of a molecule determines the preferred reaction with the surface. The unreacted functional group will provide a reactive site for further reaction on the surface, to extend a longer molecular chain for potential application in molecular electronics. As a summary, it was observed that O−H dissociation within carboxylic acids and alcohol is preferred over the other plausible

reactions including [2+2] C=C and C=O cycloadition reactions. Furthermore, the reactivity of the O-containing functional groups including carboxyl, hydroxyl, and carbonyl was investigated to be more reactive than the alkenyl group, in the present work (Chapter 5).

The outline of the following Chapters can be summarized here. All the data chapters (Chapter 2, Chapter 3, and Chapter 4) will include DFT calculations together with XPS and TPD experimental results for different molecules. In particular, the adsorption products and thermal chemistry of acetic acid will be discussed in Chapter 2, while those of acrylic acid and propanoic acid will be presented in Chapter 3. The corresponding results for allyl alcohol and allyl aldehyde will be described in Chapter 4. Finally, the conclusions of the present work together with an outlook on future studies will be briefly noted in Chapter 5.

References

[1] M. A. Filler, S. F. Bent, Prog. Surf. Sci. 73 (2003) 1-56.

[2] S. F. Bent, Surf. Sci. 500 (2002) 879-903.

[3] R. J. Hamers, S. K. Coulter, M. D. Ellison, J. S. Hovis, D. F. Padowitz, M. P. Schwartz, C. M. Greenlief, J. N. Russell Jr., Acc. Chem. Res. 33 (2000) 617-624.

[4] R. A. Wolkow, Annu. Rev. Phys. Chem. 50 (1999) 413-441.

[5] H. N. Waltenburg, J. T. Yates Jr., Chem. Rev. 95 (1995) 1589-1673.

[6] R. J. Hamers, Y. Wang, Chem. Rev. 96 (1996) 1261-1290.

[7] J. M. Buriak, Chem. Commun. 1999, 1051-1060.

[8] J. M. Buriak, Chem. Rev. 102 (2002), 1271-1308.

[9] X. Lu, M. C. Lin, Int. Rev. Phys. Chem. 21 (2002) 137-184.

[10] T. R. Leftwich, A. V. Teplyakov, Surf. Sci. Rep. 63 (2008) 1-71.

[11] N. P. Guisinger, M. E. Greene, R. Basu, A. S. Baluch, M. C. Hersam, NanoLett. 4 (2004) 55-59.

[12] B. Kasemo, Surf. Sci. 500 (2002) 656-677.

[13] J. T. Yates Jr., Science 279 (1998) 335-336.

[14] Z. Lin, T. Strother, W. Cai, X. Cao, L. M. Smith, R. J. Hamers, Langmuir 18 (2002) 788-796.

[15] K. W. Kolasinski, Surface Science Foundations of Catalysis and Nanoscience, John Wiley & Sons Ltd, Chichester, 2002.

[16] R. A. Wolkow, Phys. Rev. Lett. 68 (1992) 2636.

[17] F. A. Carey, Organic Chemistry, 3rd Edition, McGraw-Hill, Toronto, 1996.

[18] J. F. Watts and J. Wolstenholme, An Introduction to Surface Analysis by XPS and AES, John Wiley & Sons Ltd, Chichester, 2003.

[19] G. A. Somorjai, Introduction to Surface Chemistry and Analysis, John Wiley & Sons Ltd, New York, 1994.

[20] D. Briggs, M. P. Seah, Practical Surface Analysis, volume 1, 2nd Edition, John Wiley & Sons Ltd, Chichester, 1990.

[21] J. C. Rivie`re, Surface Analytical Techniques, Oxford University Press, NewYork, 1990.

[22] Q. Li, K. T. Leung, Surf. Sci. 479 (2001) 69-82.

[23] C. C. Cheng, J. T. Yates Jr., Phys. Rev. B 43 (1991) 4041-4045.

[24] W. Kohn, L. J. Sham, Phys. Rev. 140 (1965) A1133-A1138.

[25] M. J. Frisch, G. W. Trucks, H. B. Schlegel, G. E. Scuseria, M. A. Robb, J. R. Cheeseman, J. A. Montgomery Jr., T. Vreven, K. N. Kudin, J. C. Burant, J. M. Millam, S. S. Iyengar, J. Tomasi, V. Barone, B. Mennucci, M. Cossi, G. Scalmani, N. Rega, G. A. Petersson, H. Nakatsuji, M. Hada, M. Ehara, K. Toyota, R. Fukuda, J. Hasegawa, M. Ishida, T. Nakajima, Y. Honda, O. Kitao, H. Nakai, M. Klene, X. Li, J. E. Knox, H. P. Hratchian, J. B. Cross, V. Bakken, C. Adamo, J. Jaramillo, R. Gomperts, R. E. Stratmann, O. Yazyev, A. J. Austin, R. Cammi, C. Pomelli, J. W. Ochterski, P. Y. Ayala, K. Morokuma, G. A. Voth, P. Salvador, J. J. Dannenberg, V. G. Zakrzewski, S. Dapprich, A. D. Daniels, M. C. Strain, O. Farkas, D. K. Malick, A. D. Rabuck, K. Raghavachari, J. B. Foresman, J. V. Ortiz, Q. Cui, A. G. Baboul, S. Clifford, J. Cioslowski, B. B, Stefanov, G. Liu, A. Liashenko, P. Piskorz, I. Komaromi, R. L. Martin, D. J. Fox, T. Keith, M. A. Al-Laham, C. Y. Peng, A. Nanayakkara, M. Challacombe, P. M. W. Gill, B. Johnson, W. Chen, M. W. Wong, C. Gonzalez, J. A. Pople, Gaussian 03, Gaussian, Inc., Wallingford, CT, 2005.

[26] A. D. Becke**,** J. Chem. Phys. 98 (1993) 5648-5652.

[27] C. Lee, W. Yang, R. G. Parr, Phys. Rev. B 37 (1988) 785-789.

Chapter 2

Dissociative adsorption and thermal evolution of acetic acid on Si(100)2×1: Surface-mediated formation of ketene and acetaldehyde from unidentate and bidentate acetate adsorbates

2.1 Introduction

Organic functionalization of semiconductor surfaces such as Si(100)2×1 has attracted a lot of recent attention,[1−10] due to its potential applications in organic-inorganic hybrid semiconductor devices, molecular electronics, chemical and biological sensors, and optical materials.[2,11−15] Understanding the behaviour of organic molecules on Si(100)2×1 surface is fundamentally important, because the electronic and chemical properties and selectivity of the inorganic substrate can be modified by the organic adsorbate.[2] The reactivity of the Si(100) surface comes from the two directional dangling bonds of individual surface atoms. Under appropriate preparation conditions, the Si(100) surface reconstructs to the 2×1 surface, on which the dangling bonds of the adjacent Si atoms pair up to create the surface dimer rows.[1,2,5,6] The dimer bond may be considered as comprising of a full σ bond and a partial π bond, and it provides a unique reactive site for studying organosilicon chemistry. The reactivity of the Si=Si dimer in the pericyclic reactions such as the [2+2] and [4+2] cycloaddition reactions, of which stereochemistry can be predicted by the Woodward-Hoffmann rules,[16] has been demonstrated by many studies.[1,2,3,10] The asymmetric charge distribution in the $Si^{\delta+}$=$Si^{\delta-}$ dimer results in nucleophile and electrophile sites that ultimately control the reactivity and selectivity of the Si(100)2×1 surface.

Surface reactions on Si(100)2×1 have been reported for many organic molecules with single or multiple functional groups, including unsaturated aliphatic hydrocarbons (ethylene,[17−22] acetylene[18,22−24]), aromatic hydrocarbons (benzene[25−27]), halogenated hydrocarbons, [28−33] amines,[34−36] amino acids,[37,38] carbonyl compounds (aldehyde,[39,40] ketone[39,41]), alcohols,[42−46] and aliphatic and aromatic carboxylic acids (formic acid, [47−49]

vinyl acetic acid,[50] benzoic acid,[51,52] and 4-aminobenzoic acid[53]). Among the wide range of organic functional groups, the carboxyl group is one of the key constituents of amino acids, the building blocks of peptides and proteins. The interaction of the carboxyl group with the Si=Si dimers is therefore of special interest to understanding the chemical reactivity and selectivity of biomolecules in general with this widely used semiconductor.

Dissociative reactions of amines[34–36,54] and alcohols[43,44,46] with the dangling bonds of Si(100)2×1 at room temperature (RT) have been discussed in the literature. Formic acid, benzoic acid, and 4-aminobenzoic acid have also been found to dissociate, through the O–H bond to form the unidentate formate, benzoate, and aminobenzoate on the Si(100)2×1 surface. Furthermore, unidentate vinyl acetate adstructure has been proposed by Hwang et al.[50] for the 2×1 surface, upon selective O–H dissociative reaction of vinyl acetic acid (a bifunctional unsaturated carboxylic acid) over the [2+2] C=C or C=O cycloaddition reaction. To date, no experimental study has been reported for the adsorption of acetic acid (the parent carboxylic acid from which glycine or α-amino acetic acid is derived) on Si(100)2×1. Of the two density functional theory (DFT) computational studies for acetic acid on the 2×1 surface, Kim and Cho[55] presented two adsorption pathways to illustrate that both unidentate acetate and the [2+2] C=O cycloaddition reaction product are energetically feasible. However, only the unidentate acetate adstructure is expected to remain on the Si dimers because desorption of the latter adstructure is easily activated at RT. In the other DFT study, Carbone and Cominiti[56] investigated several fragmentation pathways of the adstructures of acetic acid arising from the O–H and C–H bond cleavages. The resulting unidentate adstructure (obtained from O−H bond cleavage) becomes an intra-dimer bidentate acetate after the dissociated H atom has relocated onto a neighbouring dimer site. From the C–H bond breakage, the resulting adstructure could further fragment on the surface to a methyl and a carboxylic acid groups. The adsorption of acetic acid on a sister surface, Ge(100)2×1, at RT has been recently studied by Filler et al.,[57] Kim and coworkers,[58,59] and Kim and Cho.[60] In particular, by using scanning tunneling microscopy (STM)[59] and DFT calculations,[58,59] Kim and coworkers inferred the presence of both unidentate and "end-bridged" bidentate acetates on Ge(100)2×1 at RT, with the "on-top" bidentate acetate becoming feasible only after

annealing to 400 K.* The unidentate and "end-bridged" bidentate acetates have been earlier investigated by Filler et al. by using DFT, XPS, and Fourier transform infrared (FTIR) spectroscopy.[57] They also observed the conversion of bidentate acetate to unidentate acetate upon increasing coverage at RT, while an increase in the bidentate acetate signature was found after annealing the surface to 400 K. These studies highlighted the important role of the semiconductor surface in mediating selective reactions not found in wet chemistry.

In the present work, we investigate the adsorption of acetic acid on Si(100)2×1 and the thermal evolution of the adsorption products by using XPS and TPD. Our results show the formation of bidentate acetate at low exposure and of both unidentate and bidentate acetates at the saturation coverage, upon O–H dissociative adsorption of acetic acid on the 2×1 surface at RT. Our DFT calculations show that of the several energetically possible reaction products arising from [2+2] C=O cycloaddition, C–OH dissociation, and ene formation, the unidentate and bidentate acetates are the most stable adstructures. The adsorption behaviour of acetic acid on the Si(100)2×1 surface observed in the present work is found to be different from that on Ge(100)2×1 reported earlier.[57] Our TPD results further reveal the formation of acetaldehyde and ketene from adsorbed acetate on Si(100)2×1 for the first time. In organic chemistry, the formation of aldehyde from carboxylic acid commonly involves a two-step process: reduction of carboxylic acid to primary alcohol, followed by its oxidation to aldehyde.[16] The development of new methods for producing ketene has also been of considerable interest due to the important role of ketene as a reactive intermediate in many reactions.[61] The present work shows a one-step process of generating acetaldehyde and ketene directly from the acetate adstructures on the Si(100)2×1 surface, suggesting that the 2×1 surface could be used as an important platform for discovering new synthesis methods.

* Kim and coworkers referred the bonding of the carboxyl O atoms to two Ge atoms in two adjacent dimers as "end-bridged" bidentate and that to two Ge atoms in a single dimer as "on-top" bidentate.[58,59] In the present work, we refer to these adstructures, respectively, as inter-dimer bidentate[57] and intra-dimer bidentate.

2.2 Results and Discussion

2.2.1 DFT computational study of adsorbate-substrate configurations

Figure 2.1 shows eight possible adstructures on the double-dimer Si cluster model surface arising from (a, b, c, d) O–H dissociation, (e) C–OH dissociation, (f, g) ene reaction via C_α–H dissociation, and (h) [2+2] C=O cycloaddition, i.e. all with the CCO backbone intact. Frequency calculations for these ASCs (defined here as the optimized geometries for the combined adsorbate-$Si_{15}H_{16}$ structure) confirm their stabilities, with none being a transition state. Evidently, the four ASCs (Figures 2.1e, 2.1f, 2.1g, 2.1h) resulting from the latter reactions are found to have discernibly less negative adsorption energies ΔE (and total energies) than the ASCs (Figures 2.1a, 2.1b, 2.1c) arising from O–H dissociation. In particular, the ΔEs for the inter-dimer bidentate ASC (–280.2 kJ mol^{-1}, Figure 2.1a) and intra-dimer bidentate ASC (–262.5 kJ mol^{-1}, Figure 2.1b) are more negative than the unidentate I ASC (–247.2 kJ mol^{-1}, Figure 2.1c). The formation of an additional Si–O bond in both bidentate ASCs (Figures 2.1a, 2.1b) leads to a more strongly adsorbed structure than the unidentate I ASC (Figure 2.1c). Furthermore, the less stable intra-dimer bidentate ASC, relative to the inter-dimer bidentate ASC, could be due to more strain in the Si–O–C bond angle (120° for the former ASC compared to 135° for the latter ASC, not shown in Figure 2.1). We also obtain a second unidentate II ASC involving the dissociated H atom and acetate bonded to two adjacent Si dimers (Figure 2.1d), instead of a single Si dimer as in unidentate I ASC (Figure 2.1c). This ASC (with ΔE = –154.7 kJ mol^{-1}) is notably less stable, because, unlike the unidentate I ASC, it involves additional energy for relocating the dissociated H-atom to the closest dangling bond site of an adjacent Si dimer. For the optimized geometry of the unidentate I ASC shown in Figure 2.1c, the bond lengths for C–O and C=O are 135 pm and 122 pm, respectively. On the other hand, the bond lengths for both C⋯O bonds within the bidentate ASCs (Figures 2.1a, 2.1b) are ~128 pm, which lies between those of a single and a double bonds. Our frequency calculation also reveals that the wavenumber found for this 1½ C⋯O bond (1437-1560 cm^{-1}) in the bidentate ASCs is between those for the C–O (1265 cm^{-1}) and C=O bonds (1765 cm^{-1}) for the unidentate ASC.

The relevant C–C and O–Si bond lengths and the O–C–O bond angle are also indicated in Figure 2.1. Table 2.1 summarizes the adsorption energies and total energies of the most stable ASCs (Figure 2.1a, 2.1b, 2.1c) obtained with the 6-31G(d), 6-31+G(d), 6-31++G(d), and 6-31++G(d,p) basis sets. It is of interest to compare the present adsorption energies with the corresponding energies for acetic acid on Ge(100) calculated by Kim and Cho.[60] In particular, their result shows that the stability of the calculated ASCs on Ge(100) follows a different order (intra-dimer bidentate > unidentate I > inter-dimer bidentate) than that reported here for Si(100).

Table 2.1 Comparison of the adsorption energies ΔE and total energies (in square parentheses) for the three most stable adsorbate-substrate configurations (ASCs) of acetic acid on Si(100)2×1 obtained by DFT/B3LYP calculations with 6-31G(d), 6-31+G(d), 6-31++G(d), and 6-31++G(d,p) basis sets.

ΔE (kJ mol^{-1}) [Total Energy (a.u.)]	Inter-dimer bidentate	Intra-dimer bidentate	Unidentate I
6-31G(d)	–311.7 [–4581.25958]	–294.7 [–4581.25309]	–274.0 [–4581.24522]
6-31+G(d)	–291.7 [–4581.27918]	–274.1 [–4581.27246]	–258.7 [–4581.26663]
6-31++G(d)	–291.6 [–4581.28073]	–274.0 [–4581.27399]	–258.8 [–4581.26820]
6-31++G(d,p)	–280.2 [–4581.30385]	–262.5 [–4581.29711]	–247.2 [–4581.29129]

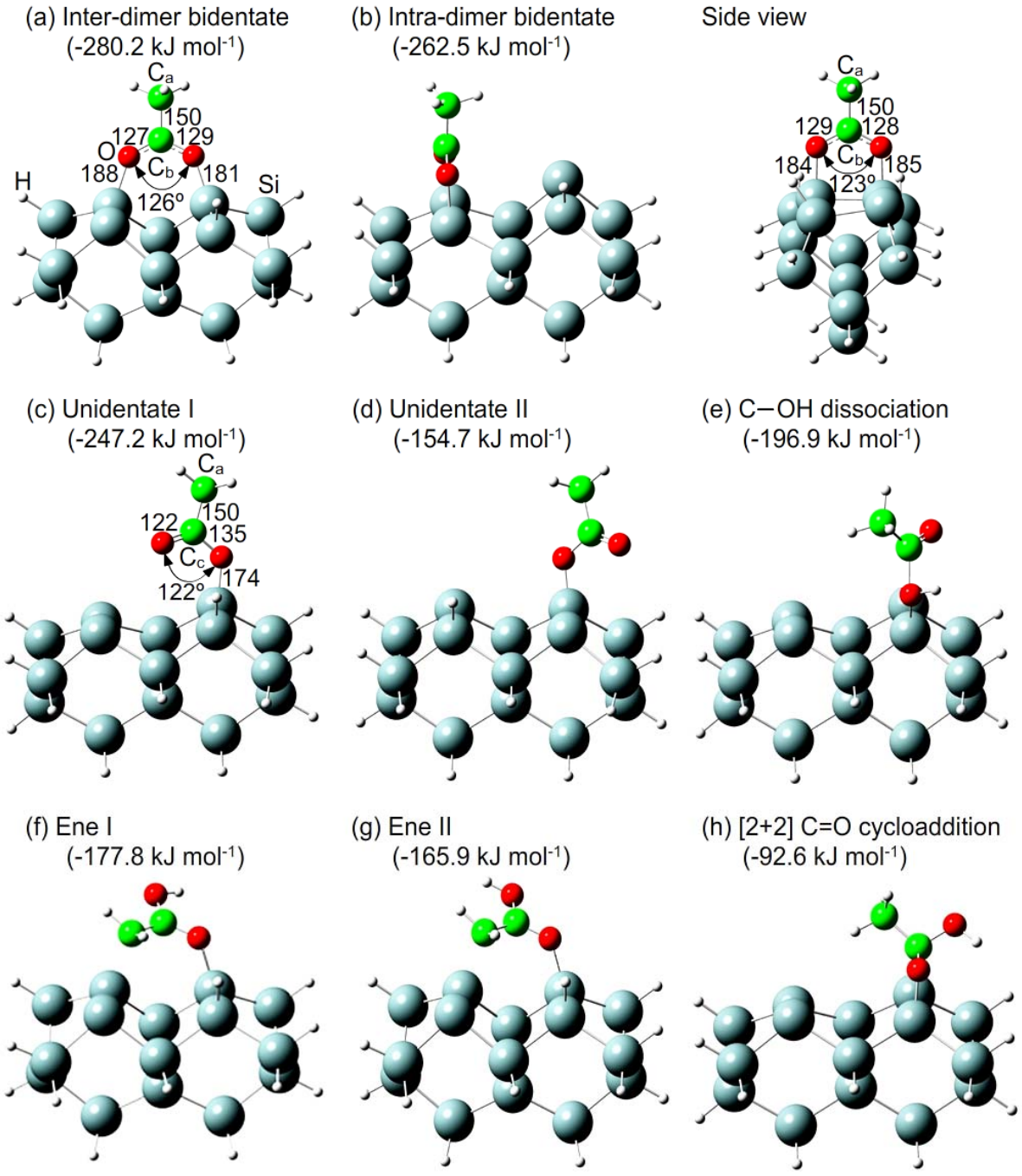

Figure 2.1 Optimized geometries of the adsorption structures of acetic acid on Si(100)2×1: (a) inter-dimer bidentate, (b) intra-dimer bidentate, (c) unidentate I, (d) unidentate II, (e) C–OH dissociation, (f) ene I, (g) ene II , and (h) [2+2] C=O cycloaddition reaction products. The corresponding adsorption energies (ΔE) calculated by 6-31++G(d,p) basis set are given in parentheses. All the bond lengths are in unit of pm.

2.2.2 XPS study of the adspecies at room temperature

Figure 2.2 shows the XPS spectrum of the C 1s region for a saturation exposure of acetic acid as deposited on Si(100)2×1 at RT, along with the more stable unidentate (unidentate I, Figure 2.2a) and bidentate (inter-dimer bidentate, Figure 2.2b) ASCs. The C 1s spectrum for the 100 L (saturation) exposure (Figure 2.2c) exhibits two broad bands. Three Gaussian profiles with an approximate full-width-at-half-maximum of 2.2 eV have been used in our curve-fitting procedure to identify the prominent C local chemical environments. In particular, the C 1s features at binding energies (BEs) of 285.7, 286.9, and 289.8 eV with respective relative intensities of 0.500, 0.247 and 0.253 (or approximately 2:1:1) have been found. It should be noted that the corresponding XPS spectrum for a lower exposure (5 L) of acetic acid reveals only the band at the lower BE, which could be fitted with the first two features (with nearly equal intensities) of the spectrum obtained for the saturation exposure (Figure 2.2c).

In accord with our DFT calculations, the ASCs arising from O–H dissociation (Figure 2.1a, 2.1b, 2.1c) are the most stable (with the most negative ΔE values). Evidently, the chemical environments of the methyl carbon (C_a) in the three ASCs are very similar, while the carboxyl carbon in the bidentate ASCs (C_b, Figure 2.1a, 2.1b) is different from that in the unidentate ASC (C_c, Figure 2.1c). Given that the electronegativity follows the ordering:[16] Si (1.8) < H (2.1) < C (2.5) < O (3.5), the methyl carbon (C_a) is expected to be partially negatively charged and therefore would exhibit a lower C 1s BE than the carboxyl carbons (C_b and C_c). The C 1s feature at 285.7 eV (Figure 2.2c) can therefore be attributed to C_a. The attachment of the carboxyl carbon to the electronegative oxygen atoms through C=O and C–O gives the partial positive charge to C_b and C_c. In order to understand the difference between C_b and C_c, we show a schematic model for the conversion of unidentate ASC (Figure 2.2a) to the resonance structures of the inter-dimer bidentate ASC in Figure 2.2d. An electron located at the O site of the C=O group in the unidentate ASC (Structure I) combines with the electron in the Si dangling bond to form a new Si–O covalent bond, creating the bidentate ASC (Structure IIa). Electron delocalization in the OCO moiety leads to the other two resonance structures (Structures IIb and IIc), giving rise to the resulting hybrid resonance

structure shown as Structure II (Figure 2.2b). Inclusion of the electron from the Si dangling bond in the formation of Structure II in effect reduces the partial positive charge of C_b, therefore lowering the corresponding BE. The C 1s features at 286.9 eV and 289.8 eV can be assigned to C_b and C_c, respectively. The observation of the lower-BE band (containing contributions from C_a and C_b) for the lower exposure indicates the preferred formation of the bidentate ASCs in the early stage of the adsorption process, which is consistent with the more negative adsorption energy (or ΔE) compared to that of the less stable unidentate ASC (Table 2.1).

The observed C 1s features at 285.7, 286.9, and 289.8 eV shown in Figure 2.2c can therefore be assigned to C_a, C_b, and C_c respectively. Given the respective intensity ratio for C_a:C_b:C_c to be approximately 2:1:1, we conclude that the bidentate ASCs (including inter-dimer and/or intra-dimer ASCs) and unidentate I ASC must have nearly equal population. Hwang et al.[50] have also observed a similar double-peak C 1s spectrum for Si(100)2×1 saturated with vinyl acetic acid and assigned the higher-BE feature to the carboxyl C (C_3 in Figure 5 of Ref. 50) of the unidentate vinyl acetate. Furthermore, they attributed the lower-BE feature to the $-CH_2$ (C_1 in Figure 5 of Ref. 50) and $H_2C{=}CH-$ groups (C_2 in Figure 5 of Ref. 50), with the former appeared to have a notably higher fitted intensity than the latter, despite the expected stoichiometric ratio of 1:2. They also assigned the residual intensity in the lower-BE feature (C_4 in Figure 5 of Ref. 50) to the possible requirement for asymmetric line-shapes in the fitting and/or to surface contamination and other decomposition surface products. We believe that their resolved peak at the lower BE could be fitted alternatively such that C_3 and C_4 can be attributed respectively to the carboxyl C of the unidentate and bidentate adstructures. Furthermore, the stoichiometric ratio of 2:1 for C_2:C_1 in the unidentate and bidentate configurations should have been taken into account. In an investigation of the adsorption of formic acid on Si(111), Huang et al.[62] showed that the dissociation of formic acid to unidentate formate adstructure is consistent with the C 1s shift from 290.2 eV to a lower BE of 289.6 eV. Moreover, Baumann et al.[63] have observed a C 1s chemical shift of 2.7 eV for the carboxyl carbon from 290.7 eV for physisorbed acetic acid on Cu(110) also to a lower BE of 288 eV for its chemisorbed bidentate acetate. These latter

studies provide indirect support for our aforementioned C 1s assignment to the carbon atoms in the unidentate and bidentate adstructures.

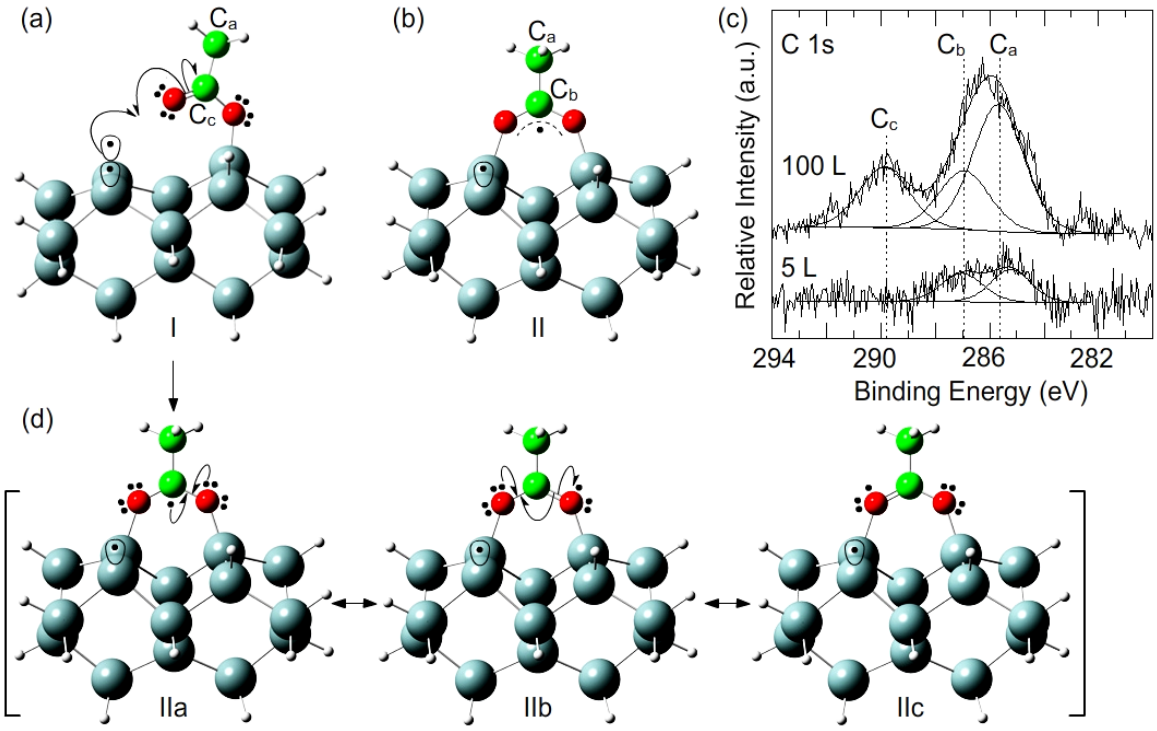

Figure 2.2 Schematic diagrams of (a) unidentate and (b) bidentate adstructures, and (d) the plausible resonance forms of the hybrid resonance structure (b). (c) XPS spectra of the C 1s region for a saturated exposure (100 L) and a 5-L exposure of acetic acid on Si(100)2×1 at 300 K.

2.2.3 XPS and TPD studies of the thermal evolution of adspecies

Figures 2.3 and 2.4 show the corresponding temperature-dependent XPS spectra of the C 1s and O 1s regions of a saturation exposure of acetic acid on Si(100)2×1, respectively. Evidently, the unidentate carboxyl C 1s peak at 289.8 eV (C_c) decreases in intensity upon annealing to 489 K (Figure 2.3b) and disappears completely after annealing to 711 K (Figure 2.3c). Similarly, the intensity of the bidentate carboxyl C 1s feature at 286.9 eV (C_b) also follows a similar decreasing trend and become totally extinguished at the annealing temperature of 933 K (Figure 2.3d). For the methyl C 1s peak at 285.7 eV (C_a), the peak position appears to shift to a lower BE (284.0 eV) while undergoing reduction in intensity upon annealing to 711 K (Figure 2.3c). This is followed by a dramatic reduction at the annealing temperature of 933 K (Figure 2.3d), at which a new feature at 283.3 eV that is commonly attributed to SiC is found to emerge. In Figure 2.3g, we summarize the observed intensity changes of these four C 1s features (C_a, C_b, C_c, and SiC) along with the total C 1s intensity, all relative to the intensity of Si 2p, as a function of the annealing temperature. Thermal evolution of the observed C 1s features therefore indicates that the carboxyl C (C_b, C_c) appears to have been removed from the surface at a temperature (~711 K) lower than the methyl C (C_a), which also suggests a C–C bond cleavage that leads to the direct attachment of the dissociated methyl group to the Si surface. Furthermore, unlike all of the carboxyl C that have apparently been totally removed at 711 K, the methyl group appears to remain on the surface and undergoes further dehydrogenation to eventually become SiC upon further annealing to 933 K. It is of interest to note that nearly half of the total C (corresponding to most of the carboxyl C and some of the methyl C) has left the surface upon annealing to 711 K, with the remaining being converted to SiC that cannot be removed even at an annealing temperature of 1376 K.

In Figure 2.4a, a broad O 1s feature at 532.7 eV is observed for a saturation exposure of acetic acid on Si(100)2×1 at RT. The observed O 1s BE position is in good accord with those of Si–O (531.9 eV) and C=O (532.8 eV) reported for vinyl acetic acid.[50] Upon annealing to 933 K (Figure 2.4d), the O 1s feature is found to undergo a slight reduction in intensity and become sharper, suggesting that the O-containing adspecies are becoming more

homogenous on the surface as other adspecies are desorbed from the surface with increasing annealing temperature. The O 1s feature becomes greatly reduced at 1154 K (Figure 2.4e), which evidently is higher than the temperature at which most of the carboxyl C 1s feature is removed (711-933 K, Figure 2.3g). This suggests that unidentate and bidentate acetates fragment on the surface into adspecies (to be discussed below) that desorb at 489-933 K, and individual O atoms that desorb from the surface above 1000 K (likely as SiO) or diffuse into the bulk. Finally, the residual O 1s intensity above 1154 K likely corresponds to thermal oxides (Figure 2.4g).

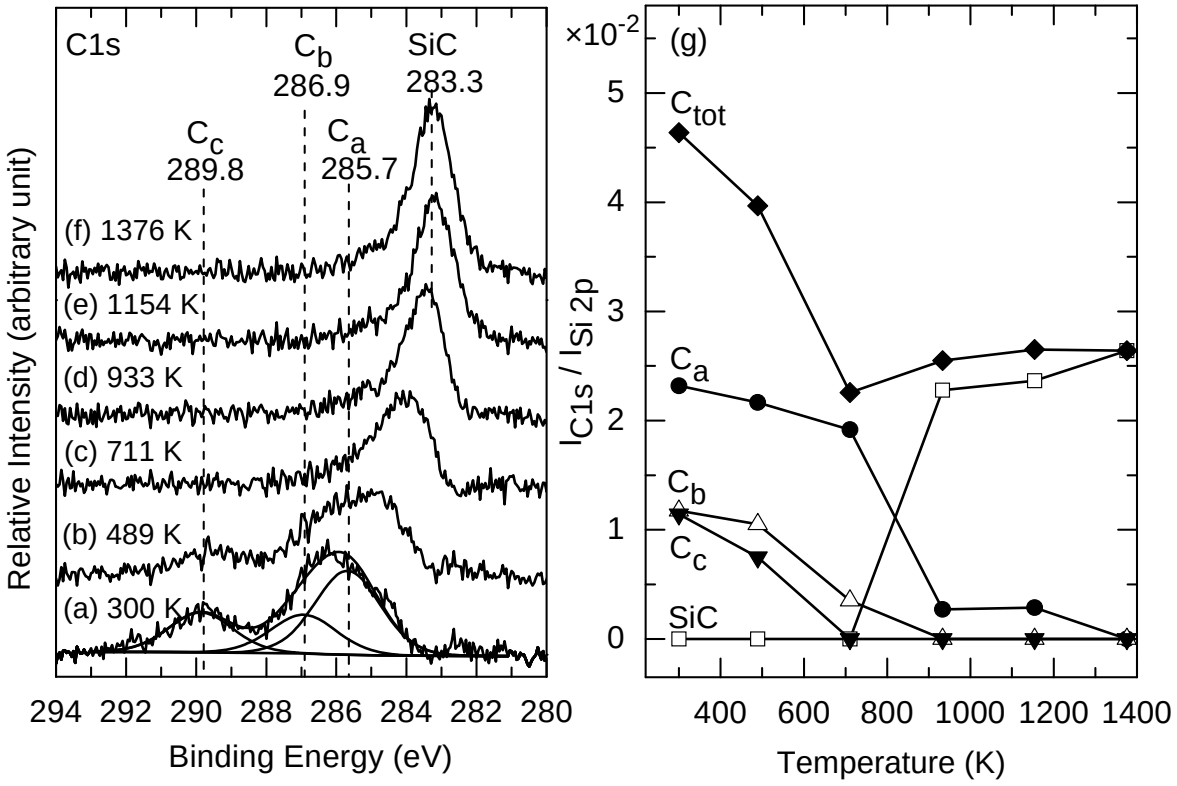

Figure 2.3 XPS spectra of the C 1s region for a saturated exposure of acetic acid on Si(100)2×1 at (a) 300 K, and upon sequential flash-annealing to (b) 489 K, (c) 711 K, (d) 933 K, (e) 1154 K, and (f) 1376 K. (g) shows the corresponding temperature profiles of the C 1s intensities ($I_{C\ 1s}$) for SiC at 283.3 eV, C_a at 284.0-285.7 eV, C_b at 286.9 eV, and C_c at 289.8 eV, along with the total C 1s intensity (C_{tot}), all with respect to the intensity of Si 2p ($I_{Si\ 2p}$).

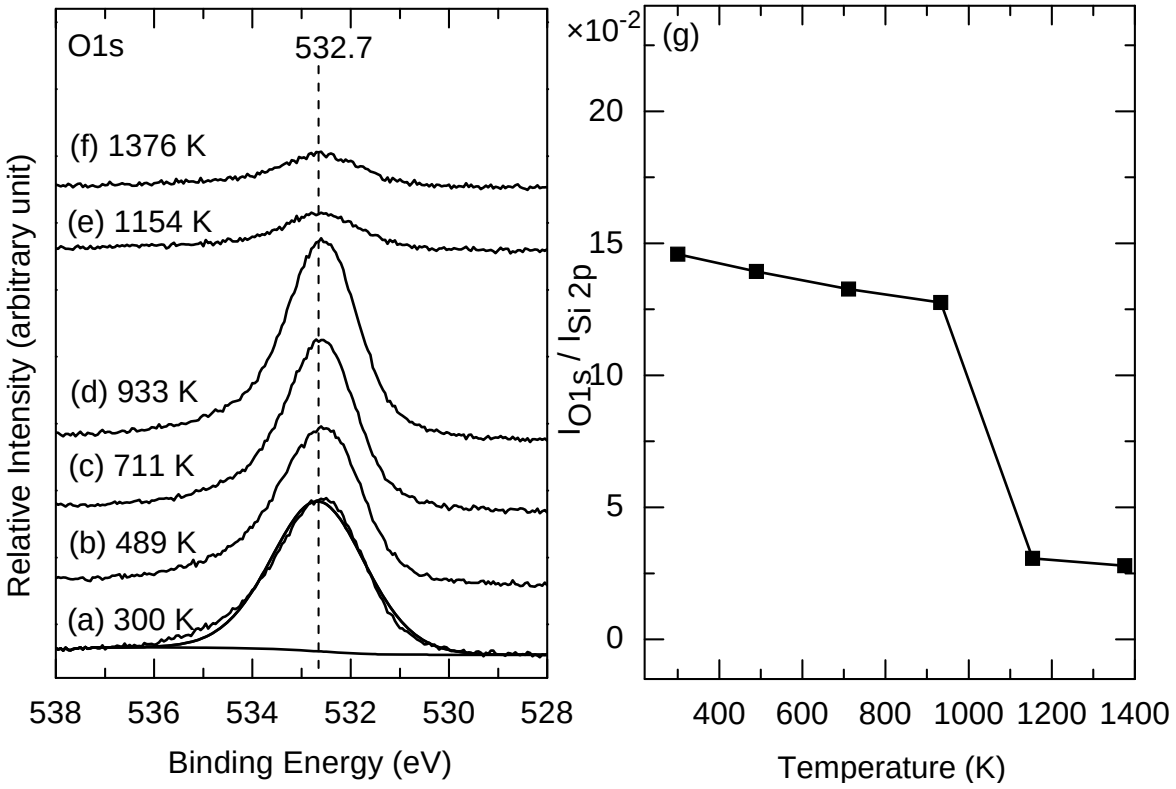

Figure 2.4 XPS spectra of the O 1s region for a saturated exposure of acetic acid on Si(100)2×1 at (a) 300 K, and upon sequential flash-annealing to (b) 489 K, (c) 711 K, (d) 933 K, (e) 1154 K, and (f) 1376 K. (g) shows the corresponding temperature profile of the O 1s intensity ($I_{O\ 1s}$) with respect to the intensity of Si 2p ($I_{Si\ 2p}$).

In addition to the temperature-dependent XPS spectra that show the adspecies remaining on the 2×1 surface after the sample has been annealed to different temperatures, we also perform TPD experiments to investigate the desorption products evolving from the surface as a function of temperature. Figure 2.5 shows the TPD profiles of selected mass fragments with m/z 2, 15, 28, 29, 42, 43, and 44 for a RT saturation exposure of acetic acid on Si(100)2×1. We also monitor other mass fragments, including m/z 60 and 45 corresponding to the parent mass (CH_3COOH^+) and $COOH^+$ fragment of acetic acid [64] respectively, all of which do not exhibit any notable TPD features, suggesting no molecular adsorption of acetic acid at RT. For m/z 2, a large desorption feature at 810 K is observed (Figure 2.5a), which is consistent with the recombinative desorption of H_2 from silicon monohydride.[65] The TPD feature with the next highest intensity is observed at 625 K for m/z 28 (Figure 2.5c), which corresponds to the parent mass of CO. The TPD features for the remaining mass fragments all appear to have notably smaller relative intensities. In particular, m/z 42 corresponds to the parent mass of ketene, CH_2=C=O, the cracking pattern of which also contains m/z 41 and 14 with substantial intensities.[64] The corresponding TPD profile (Figure 2.5e) exhibits a maximum at 580 K. Desorption maxima have been found to be near the same temperature of 565 K for the TPD profiles of m/z 44 (parent mass), 43, 29 (base mass) and 15 (Figure 2.5), all of which correspond to the cracking pattern of acetaldehyde CH_3CHO.[64] Furthermore, m/z 44 could also correspond to the parent/base mass of CO_2.

In Figure 2.6, we show plausible mechanisms for the formation of ketene and acetaldehyde from the unidentate acetate adspecies induced by thermal annealing. In particular, the unidentate acetate (Structure I) undergoes an elimination reaction of CH_2=C=O, upon nucleophilic attack of the bonded O atom on a methyl H atom (Figure 2.6a, Ia), with the resulting surface byproducts of H and OH. The adsorbed unidentate acetate could also thermally evolve to CH_3CHO by elimination of an adsorbed H atom after C−O bond cleavage, leaving the O atom on the surface (Figure 2.6b, Ib). In addition, breakage of C−C and C−O bonds in the acetate could produce dissociated methyl group, O and H atoms on the surface, generating the observed CO desorbate (Figure 2.6c, Ic). On the other hand,

breakage of the C−C and Si−O bonds of the adstructure would also lead to dissociated methyl group and H atoms on the surface and CO_2 as the desorbate (Figure 2.6d, Id). Carbon dioxide could also in principle be generated from breakage of two Si−O bonds, in addition to the C−C bond (Figure 2.6e, IIa), in the adsorbed bidentate acetate (Structure II). The bidentate acetate can also convert to unidentate acetate via a single Si−O bond cleavage (Figure 2.6f, IIb). It should be noted that interconversion among dissociated H, O and OH groups on the surface produced in the proposed pathways (Figures 2.6a, 2.6c) and the Si_2O structure (Figure 2.6b) could also occur.

The desorption maximum for CO or m/z 28 (625 K, Figure 2.5c) is slightly higher than ketene (580 K, Figure 2.5e) and acetaldehyde (565 K, Figure 2.5b, 2.5d, 2.5f, 2.5g). This indicates that there could be an additional desorption state at a higher temperature than 565 K, thus shifting the desorption maximum to 625 K. This observation is consistent with the proposed mechanism for CO formation from the unidentate acetate (Figure 2.6c) that requires nearly the same energy (844 kJ mol^{-1}) to break the necessary bonds, in comparison to those for the formation of ketene (858 kJ mol^{-1}, Figure 2.6a) and acetaldehyde (752 kJ mol^{-1}, Figure 2.6b). It should be noted that the typical bond dissociation energies (in kJ mol^{-1}) are 310 for Si−Si, 800 for Si−O, 447 for Si−C, 293 for Si−H, 459 for C−O, 385 for C−C, 399 for C−H, and 469 for O−H.[66] The considerably stronger intensity observed for the m/z 28 therefore suggests that the pathway for CO formation is kinetically favoured on the 2×1 surface. Despite the discernibly smaller desorption intensities observed for the ketene and acetaldehyde formation, it is important to emphasize that the Si(100)2×1 surface plays a pivotal role in mediating such types of thermally induced surface reactions. The conversion from bidentate to unidentate acetate requires breakage of a Si−O bond (800 kJ mol^{-1}), as depicted in Figure 2.6f, which could occur during the thermal evolution process providing an additional source for unidentate acetate. The latter supply could account for the generally broad TPD profiles (with possible additional desorption state) that are found to extend into higher temperature.

It should be noted that there has been some ambiguity in the observation of CO_2 desorption from unidentate and bidentate organic adstructures. In their EELS and TPD study

of the adsorption of formic acid on Si(100)2×1, Nishijima and coworkers[47] have commented that only 10% of the unidentate formate has dissociated to CO and CO_2. Later, the same group reported strong evidence of desorption of CO but not CO_2 from their TPD data.[48] Recently, a TPD and FTIR study of the adsorption of formaldehyde on Ge(100)2×1 by Filler et al.[67] has reported CO_2 desorption, which led the authors to propose the formation of a bidentate formate adstructure by a "carbon-oxygen coupling" mechanism. Given that the energy required for bond breaking in CO_2 production (1185 kJ mol^{-1}) is higher than that for CO formation, the desorption for m/z 44 is expected to occur at a higher temperature (than 565-625 K) in the present work. However, the observed desorption maximum for m/z 44 occurs at 565 K, essentially identical to those found for m/z 43, 29 and 15 as part of the cracking pattern of acetaldehyde (Figure 2.5). We could therefore rule out the direct CO_2 formation pathway from unidentate acetate (Figure 2.6d) and attribute the observed m/z 44 as part of the acetaldehyde evolution. Furthermore, the formation of CO_2 from bidentate acetate, as proposed in Figure 2.6e, requires additional Si−O bond breaking and therefore an even larger bond breaking energy than the unidentate route (Figure 2.6d), which also makes this pathway improbable.

Our TPD results are consistent with our temperature-dependent XPS data. The reduction of the carboxyl C 1s XPS features in both unidentate and bidentate adstructures at 489-911 K occurs in the same temperature region (400-750 K) as the formation of ketene (Figure 2.6a) and acetaldehyde (Figure 2.6b) as well as CO (Figure 2.6c). For CO, there is evidently a clear shoulder (with substantial intensity) at 750 K in the m/z 28 TPD profile (Figure 2.5c). This suggests the continued production of CO desorbate and the surface methyl C as indicated in Figure 2.6c after the evolution to ketene and acetaldehyde. The observed gradual shift in the methyl C 1s XPS feature to that of SiC supports the gradual dissociation of the methyl group to C and H atoms with increasing temperature above 711 K. With the H atoms so produced undergoing recombinative H_2 desorption at 700-1000 K (Figure 2.5a), the remaining methyl C is being converted to SiC.

In the case of acetic acid on Ge(100)2×1, Filler et al.[57] presented a DFT calculation that showed that the unidentate acetate adstructure is slightly more stable than the bidentate

acetate adstructure (by 2.2 kcal mol^{-1} or 9.2 kJ mol^{-1}), using a $Ge_4Si_{11}H_{16}$ cluster as the model for the Ge(100)2×1 surface. Furthermore, their IR data revealed the presence of both unidentate and bidentate adstructure at RT (while their XPS data could not resolve the C 1s feature for the bidentate), and the conversion of bidentate to unidentate with increasing exposure above 0.03 L. They also concluded that increased conversion of unidentate to bidentate adstructure occurred upon annealing to ~400 K, for a saturation coverage of acetic acid on Ge(100)2×1. In contrast, the present work provides evidence of bidentate acetate (in addition to the unidentate acetate) on Si(100)2×1 from our XPS data for the first time. Our data show adsorption of bidentate acetate at a lower exposure than the unidentate acetate but no direct conversion of bidentate to unidentate adstructure at RT.

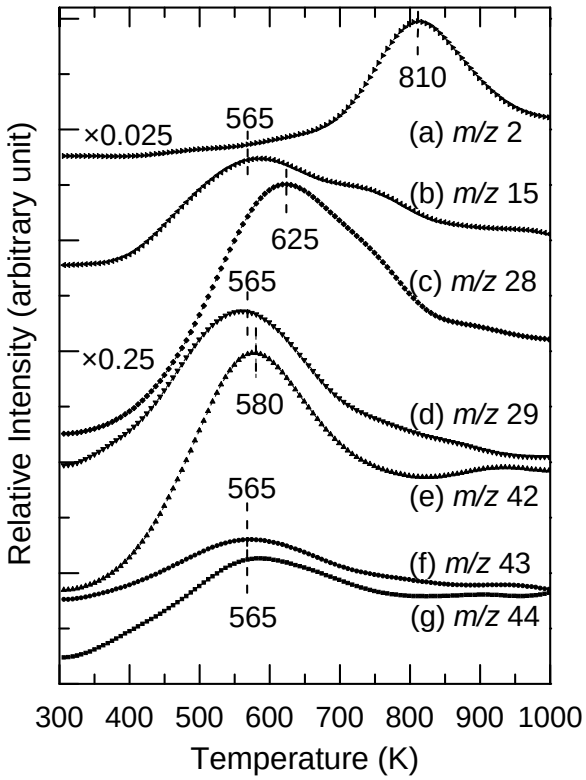

Figure 2.5 TPD profiles of the selected fragments of m/z (a) 2, (b) 15, (c) 28, (d) 29, (e) 42, (f) 43, and (g) 44 for a saturation coverage of acetic acid on Si(100)2×1 at 300 K.

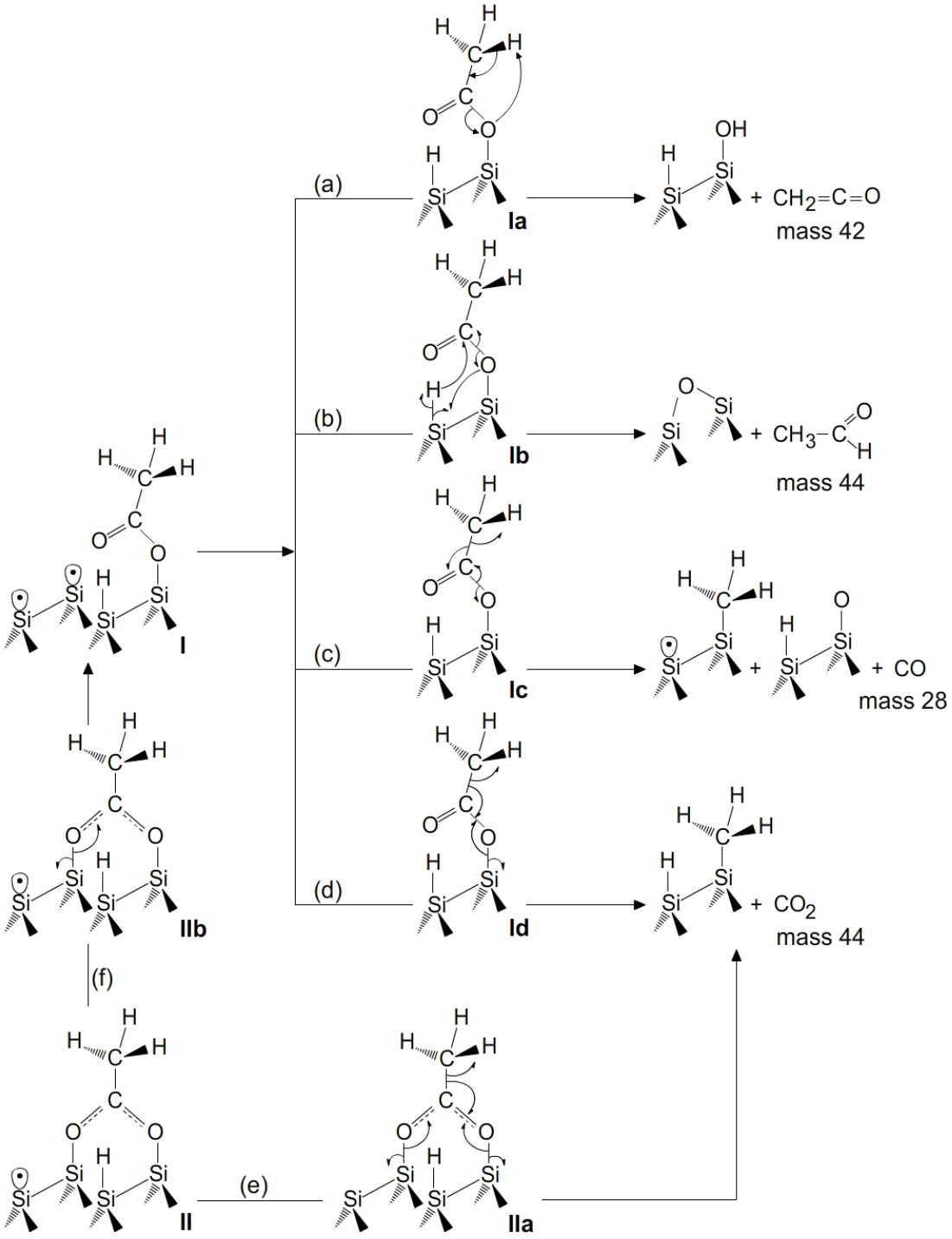

Figure 2.6 Schematic models for thermal evolution of unidentate acetate (structure I) and bidentate acetate (structure II), depicting the formation of (a) ketene, (b) acetaldehyde, (c) CO, and (d,e) CO_2 desorbates, and (f) their interconnection

2.3 Summary

XPS and TPD experiments have been performed for the first time on acetic acid on Si(100)2×1. Of the eight ASCs considered here, DFT calculations show that the bidentate acetate gives the most stable ASCs, followed by the unidentate acetate ASCs. XPS spectra collected at different exposures demonstrate the preferred formation of bidentate ASC at a low exposure, followed by the unidentate ASC formation at a higher exposure, which therefore confirms the relative stabilities of the bidentate and unidentate ASCs. The observation of a more stable bidentate ASC on Si(100)2×1 is in good accord with those observed for metal surface but in contrast to that found for Ge(100)2×1. Furthermore, the combined temperature-dependent XPS and TPD data reveal several plausible thermal evolution pathways that lead to the formation of ketene, acetaldehyde and CO, with almost half of the ASCs dissociated into methyl groups that become SiC with increasing annealing temperature to 933 K. These thermally induced reactions indicate the essential role of the 2×1 surface in mediating the formation of ketene and acetaldehyde. The directional dangling bonds on the Si(100)2×1 surface therefore provide a unique testing ground to investigate novel silicon organic chemistry. As one of the most fundamental biological molecules, acetic acid provides an important reference for studying more complex carboxyl-containing molecules, including amino acids. With the carboxyl group serving as the main anchor to the Si surface, derivatives of acetic acid with multiple functional groups can be used effectively as a linker molecule to further functionalize the Si(100)2×1 surface.

References

[1] M. A. Filler, S. F. Bent, Prog. Surf. Sci. 73 (2003) 1-56.

[2] S. F. Bent, Surf. Sci. 500 (2002) 879-903.

[3] R. J. Hamers, S. K. Coulter, M. D. Ellison, J. S. Hovis, D. F. Padowitz, M. P. Schwartz, C. M. Greenlief, J. N. Russell Jr., Acc. Chem. Res. 33 (2000) 617-624.

[4] R. A. Wolkow, Annu. Rev. Phys. Chem. 50 (1999) 413-441.

[5] H. N. Waltenburg, J. T. Yates Jr., Chem. Rev. 95 (1995) 1589-1673.

[6] R. J. Hamers, Y. Wang, Chem. Rev. 96 (1996) 1261-1290.

[7] J. M. Buriak, Chem. Commun. 1999, 1051-1060.

[8] J. M. Buriak, Chem. Rev. 102 (2002), 1271-1308.

[9] X. Lu, M. C. Lin, Int. Rev. Phys. Chem. 21 (2002) 137-184.

[10] T. R. Leftwich, A. V. Teplyakov, Surf. Sci. Rep. 63 (2008) 1-71.

[11] B. Kasemo, Surf. Sci. 500 (2002) 656-677.

[12] J. T. Yates Jr., Science 279 (1998) 335-336.

[13] Z. Lin, T. Strother, W. Cai, X. Cao, L. M. Smith, R. J. Hamers, Langmuir 18 (2002) 788-796.

[14] M. P. Stewart, J. M. Buriak, Comments Inorg. Chem. 23 (2002) 179-203.

[15] N. P. Guisinger, M. E. Greene, R. Basu, A. S. Baluch, M. C. Hersam, NanoLett. 4 (2004) 55-59.

[16] F. A. Carey, Organic Chemistry, 3rd Edition, McGraw-Hill, Toronto, 1996.

[17] J. Yoshinobu, H. Tsuda, M. Onchi, M. Nishijima, J. Chem. Phys. 87 (1987) 7332-7340.

[18] C. C. Cheng, R. M. Wallace, P. A. Taylor, W. J. Choyke, J. T. Yates Jr., J. Appl. Phys. 67 (1990) 3693-3699.

[19] L. Clemen, R. M. Wallace, P. A. Taylor, M. J. Dresser, W. J. Choyke, W. H. Weinberg,

J.T. Yates Jr., Surf. Sci. 268 (1992) 205-216.

[20] A. J. Mayne, A. R. Avery, J. Knall, T. S. Jones, G. A. D. Briggs, W.H. Weinberg, Surf. Sci. 284 (1993) 247-256.

[21] M. Ikeda, T. Maruoka, N. Nagashima, Surf. Sci. 416 (1998) 240-244.

[22] H. Liu, R. J. Hamers, Surf. Sci. 416 (1998) 354-362.

[23] P. A. Taylor, R. M. Wallace, C. C. Cheng, W. H. Weinberg, M. J. Dresser, W. J. Choyke, J. T. Yates Jr., J. Am. Chem. Soc. 114 (1992) 6754-6760.

[24] M. Nishijima, J. Yoshinobu, H. Tsuda, M. Onchi, Surf. Sci. 192 (1987) 383-397.

[25] T. Y. Taguchi, M. Fujisawa, T. Takaoka, T. Okada, M. Nishijima, J. Chem. Phys. 95 (1991) 6870-6876.

[26] G. P. Lopinski, T. M. Fortier, D. J. Moffatt, R. A. Wolkow, J. Vac. Sci. Technol. A 16 (1998) 1037-1042.

[27] Q. Li, K. T. Leung, Surf. Sci. 479 (2001) 69-82.

[28] X. J. Zhou, Q. Li, Z. H. He, X. Yang, K. T. Leung, Surf. Sci. 543 (2003) L668-L674.

[29] F. Y. Naumkin, J. C. Polanyi, D. Rogers, Surf. Sci. 547 (2003) 335-348.

[30] X. J. Zhou, K. T. Leung, Surf. Sci. 600 (2006) 3285-3296.

[31] X. J. Zhou, Q. Li, K. T. Leung, J. Phys. Chem. B 110 (2006) 5602-5610.

[32] X. J. Zhou, K. T. Leung, J. Phys. Chem. B 110 (2006) 9601-9607.

[33] X. J. Zhou, Z. H. He, K. T. Leung, Surf. Sci. 600 (2006) 468-477.

[34] E. K. Hlil, L. Kubler, J. L. Bischoff, D. Bolmont, Phys. Rev. B 35 (1987) 5913-5916.

[35] F. Bozso, Ph. Avouris, Phys. Rev. B 38 (1988) 3937-3942.

[36] J.-B. Wu, Y.-W.Yang, Y.-F. Lin, H.-T. Chiu, J. Phys. Chem. B 108 (2004) 1677-1685.

[37] A. Lopez, T. Heller, T. Bitzer, N. V. Richardson, Chem. Phys. 277 (2002) 1-8.

[38] A. C. Ferraz, R. Miotto, Brazilian J. Phys. 36 (2006) 309-312.

[39] J. L. Armstrong, J. M. White, M. Langell, J. Vac. Sci. Technol. A 15 (1997) 1146-1154.

[40] X. Lu, Q. Zhang, M. C. Lin, Phys. Chem. Chem. Phys. 3 (2001) 2156-2161.

[41] A. C. Ferraz, R. Miotto, Appl. Surf. Sci. 234 (2004) 185-189.

[42] C. Shannon, A. Campion, Surf. Sci. 227 (1990) 219-223.

[43] M. P. Casaletto, R. Zanoni, M. Carbone, M. N. Piancastelli, L. Aballe, K. Weiss, K. Horn, Surf. Sci. 505 (2002) 251-259.

[44] J. Eng Jr., K. Raghavachari, L. M. Struck, Y. J. Chabal, B. E. Bent, G. W. Flynn, S. B. Christman, E. E. Chaban, G. P. Williams, K. Radermacher, S. Mantl, J. Chem. Phys. 106 (1997) 9889-9898.

[45] P. L. Silvestrelli, Surf. Sci. 552 (2004) 17-26.

[46] M. P. Casaletto, R. Zanoni, M. Carbone, M. N. Piancastelli, L. Aballe, K. Weiss, K. Horn, Surf. Sci. 447 (2000) 237-244.

[47] S. Tanaka, M. Onchi, M. Nishijima, J. Chem. Phys. 91 (1989) 2712-2725.

[48] T. Kubo, N. Minami, T. Aruga, N. Takagi, M. Nishijima, J. Phys. Chem. B 101 (1997) 7007-7011.

[49] H. Ikeura-Sekiguchi, T. Sekiguchi, Surf. Sci. 433-435 (1999) 549-553.

[50] H.-N. Hwang, J. Y. Baik, K.-S. An, S. S. Lee, Y. Kim, C. C. Hwang, B. Kim, J. Phys. Chem. B 108 (2004) 8379-8384.

[51] T. Bitzer, T. Alkunshalie, N. V. Richardson, Surf. Sci. 368 (1996) 202-207.

[52] T. Bitzer, N. V. Richardson, Surf. Sci. 427-428 (1999) 369-373.

[53] A. Lopez, T. Bitzer, T. Heller, N. V. Richardson, Surf. Sci. 480 (2001) 65-72.

[54] C. Mui, J. H. Han, G. T. Wang, C. B. Musgrave, S. F. Bent, J. Am. Chem. Soc. 124 (2002) 4027-4038.

[55] H.-J. Kim, J.-H. Cho, Phys. Rev. B 72 (2005) 195305-1-195305-5.

[56] M. Carbone, R. Caminiti, Surf. Sci. 602 (2008) 852-858.

[57] M. A. Filler, J. A. Van Deventer, A. J. Keung, S. F. Bent, J. Am. Chem. Soc. 128 (2006) 770-779.

[58] D. H. Kim, E. Hwang, S. Hong, S. Kim, Surf. Sci. 600 (2006) 3629-3632.

[59] E. Hwang, D. H. Kim, Y. J. Hwang, A. Kim, S. Hong, S. Kim, J. Phys. Chem. C 111 (2007) 5941-5945.

[60] H.-J. Kim, J.-H. Cho, J. Phys. Chem. C 112 (2008) 6947-6952.

[61] H. R. Seikaly, T. T. Tidwell, Tetrahedron 42 (1986) 2587-2613.

[62] J. Y. Huang, H. G. Huang, K. Y. Lin, Q. P. Liu, Y. M. Sun, G. Q. Xu, Surf. Sci. 549 (2004) 255-264.

[63] P. Baumann, H. P. Bonzel, G. Pirug, J. Werner, Chem. Phys. Lett. 260 (1996) 215-222.

[64] NIST Mass Spec Data Center, S.E. Stein (director), "Mass Spectra" in NIST Chemistry WebBook, NIST Standard Reference Database Number 69, edited by P.J. Linstrom and W.G. Mallard, June 2005, National Institute of Standards and Technology, Gaithersburg (http://webbook.nist.gov).

[65] C. C. Cheng, J. T. Yates Jr., Phys. Rev. B 43 (1991) 4041-4045.

[66] "Bond Dissociation Energies" by Y.-R. Luo, in CRC Handbook of Chemistry and Physics, 88th Edition (Internet Version 2008), edited by D. R. Lide, CRC Press/Taylor and Francis, Boca Raton.

[67] M. A. Filler, C. B. Musgrave, S. F. Bent, J. Phys. Chem. C 111 (2007) 1739-1746.

Chapter 3

Selective adsorption and thermal evolution of bifunctional carboxylic acids: Competition of O−H dissociation and other reaction products in acrylic acid and propanoic acid on Si(100)2×1

3.1 Introduction

The surface chemistry of organic molecules with multiple functional groups on the Si(100)2×1 surface is of fundamental interest and also provides the key to selective organic functionalization of Si in many potential applications, particularly in molecular electronics.[1−7] Selective reactions of one of the functional groups with the Si dimers will leave the others intact for further reactions with other molecules, which offers a versatile approach to modifying the surface reactivity of the (functionalized) Si(100)2×1 surface. The reactivity of a pristine Si(100)2×1 surface is directly related to the localized, directional dangling bonds of the Si dimer rows. A large number of studies have focused on [2+2] and [4+2] cycloaddition reactions with the Si dimer.[1,2,6] These studies treated the Si=Si bond in the Si dimer analogously as the C=C bond, with the partial π bond in the Si dimer making the Si=Si bond weaker than its C=C analog.[8,9] Although thermal [2+2] cycloaddition reactions are symmetry-forbidden by the Woodward-Hoffman selection rules,[10] the [2+2] cycloaddition products of many alkenes can be readily formed on Si(100)2×1 at room temperature (RT),[11] due to the existence of asymmetrically tilted dimers in the Si dimer rows, as revealed by low-temperature scanning tunneling microscopy (STM) studies.[12,13] It is well-known that unsaturated hydrocarbons including ethylene,[6,14−20] acetylene,[6,15,19−21] and many other aliphatic, cyclic, and aromatic hydrocarbons containing C=C [6] can readily form [2+2] and [4+2] cycloaddition products with the Si dimers. However, the mechanisms of these surface reactions are not well understood.[1,6] In addition, the nucleophilic-electrophilic character of the buckled Si dimer has made surface reactions of carboxylic acids, alcohols, and amines possible through the dative bonding of the heteroatom followed by H

dissociation.[1,10] Depending on the functional groups of the incoming molecule, competition between cycloaddition reactions and reactions involving dative bonds could lead to markedly different functionalized Si surfaces. The nature of the functionalized Si surface can therefore be controlled by judicious choice of the functional groups in the multifunctional molecules.

The surface chemistry of carboxylic acids on a single-crystal semiconductor surface such as Si(100)2×1[22−30] and Ge(100)2×1 [31−33] has continued to attract much recent attention. These studies focused on the essential role of the semiconductor surface in mediating selective reactions not found in wet chemistry. Similar to (primary and secondary) amines [34−37] and alcohols,[38−42] of which respective N–H and O–H dissociation are found upon adsorption, exclusive O–H dissociative adsorption is observed experimentally in aliphatic and aromatic carboxylic acids. In particular, the formation of unidentate carboxylate for formic acid,[22−24] acetic acid (CH_3–COOH),[25,26] vinyl acetic acid (CH_2=CH–CH_2–COOH),[27] benzoic acid,[28] and 4-aminobenzoic acid [30] on Si(100)2×1, and for acetic acid [31−33] on Ge(100)2×1 was reported to be the predominant process. Richardson and co-workers have shown that benzoic acid and 4-aminobenzoic acid also form bidentate carboxylates on a Si(100)2×1 surface modified by Na.[29,30] However, our recent work on the adsorption of acetic acid on Si(100)2×1[26] indicated that the formation of the more thermodynamically stable bidentate acetate always occurs at a low exposure before that of unidentate acetate at a higher exposure, both upon O–H dissociative adsorption on the clean Si(100)2×1. This observation is also in marked contrast to its bifunctional homolog of vinyl acetic acid, for which Hwang et al.[27] concluded from their photoemission data that the formation of only unidentate vinyl acetate on the 2×1 surface, upon O–H dissociative reaction, is preferred over the [2+2] C=C or C=O cycloaddition reactions.

Like vinyl acetic acid, acrylic acid (CH_2=CH–COOH) contains a C=C double-bond and a carboxyl functional groups. Despite this apparent similarity, acrylic acid has an electron delocalized backbone of C_β···C_α···C···O, with the C_β-to-O line-of-sight distance of 2.9 Å compatible with the Si-Si dimer bond length (2.3 Å). Acrylic acid therefore offers an alternating double bond structure (not found in vinyl acetic acid) essential for providing electron conduction in molecular electronics applications. The delocalized backbone can be

considered as a special type of functional group that enables the formation of dative bonds between C_β and O and the Si dimer (referred to here as [O, C] bidentate), in direct competition with O−H dissociation. Conversely, should O−H dissociation prevail as the preferred route, the "unreacted" backbone would facilitate new bonding possibilities with incoming molecules, including, e.g. [2+2] and [4+2] cycloaddition reactions, and nucleophilic addition reaction at C_β. The electrophilic site (C_β) in the "enoate" ($-C_\beta=C-COO-$) provides a reactive site for nucleophile reaction. This nucleophile reaction could promote further reactions to build an extended molecular chain on the functionalized surface. In contrast, an adsorbed vinyl acetic acid molecule could not facilitate this type of reactions due to the lack of a similar electrophilic site, leaving only the unreacted C=C group to undergo alkene-related reactions. To date, no experimental study has been reported for the adsorption of acrylic acid on Si(100)2×1. Only one recent DFT computational study involving pseudo-potential has been reported by Favero et al.,[43] who concluded that O−H dissociation of both acrylic acid and vinyl acetic acid occurs on Si(100).

In the present work, we investigate the RT adsorption of acrylic acid on Si(100)2×1 and follow the thermal evolution of the adsorption products by X-ray photoelectron spectroscopy (XPS) and thermal programmed desorption (TPD) mass spectrometry. These results are compared with those of its saturated homolog, propanoic acid (CH_3-CH_2-COOH), i.e. without the C=C double bond. Our data shows the formation of bidentate acrylate at a low exposure, followed by that of unidentate acrylate at a higher exposure, resembling that found for propanoic acid (and acetic acid)[26] on Si(100)2×1. In addition to the bidentate and unidentate O−H dissociation products (acrylates) observed experimentally, our DFT calculations reveal several other less energetically stable reaction products arising from [O, C] bidentate formation, C−OH dissociation, [2+2] C=C and C=O cycloaddition, as well as ene formation. Our TPD results indicate the evolution of CO, ethylene, acetylene, and propene from the adsorbed acrylate on Si(100)2×1. Despite the plausible dative bonding provided by the delocalized $C_\beta\cdots C_\alpha\cdots C\cdots O$ backbone, O−H dissociation of the carboxyl group remains the preferred adsorption pathway for acrylic acid on Si(100)2×1, which in turn

allows the delocalized backbone free to react (link) with other incoming molecules to provide further functionalization.

3.2 Results and Discussion

3.2.1 DFT computational study of adsorbate-substrate configurations

Figure 3.1 shows eight possible ASCs on the $Si_{15}H_{16}$ model surface arising from (a, b, c) O–H dissociation, (d) [O,C] bidentate, (e) C–OH dissociation, (f) [2+2] C=C cycloaddition, (g) [2+2] C=O cycloaddition, and (h) ene reaction via C_α–H dissociation. Frequency calculations for these ASCs confirm their stabilities, with none being a transition state. Evidently, the five ASCs (Figure 3.1d, 3.1e, 3.1Figure 3.1f, 3.1g, 3.1h) resulting from the latter reactions are found to have discernibly less negative adsorption energies ΔE (and total energies) than the ASCs arising from O–H dissociation (Figures 3.1a, 3.1b, 3.1c). In particular, the ΔEs for the inter-dimer bidentate ASC (–284.9 kJ mol^{-1}, Figure 3.1a) and intra-dimer bidentate ASC (–266.4 kJ mol^{-1}, Figure 3.1b) are more negative than the unidentate ASC (–248.8 kJ mol^{-1}, Figure 3.1c). The formation of an additional Si–O bond in both bidentate ASCs (Figures 3.1a, 3.1b) leads to a more strongly adsorbed structure than the unidentate ASC (Figure 3.1c). Furthermore, the greater strain in the Si–O–C bond angle (120°, not shown in Figure 3.1) for the intra-dimer bidentate ASC compared to that of inter-dimer bidentate ASC (135°) accounts for the former ASC being less stable than the latter ASC. The formation of an additional Si–O bond in the same dimer as in the intra-dimer bidentate ASC (Figure 3.1b) from the unidentate ASC (Figure 3.1c) would require relocation of hydrogen from one dimer to its neighboring dimer, contributing to the less negative ΔE for the intra-dimer ASC than the inter-dimer ASC. Figure 3.2 shows the three most stable ASCs resulting from O−H dissociative adsorption of propanoic acid on Si(100)2×1, with the inter-dimer bidentate (with ΔE of −281.2 kJ mol^{-1}) being more stable than the intra-dimer bidentate (−262.8 kJ mol^{-1}) and unidentate (−247.8 kJ mol^{-1}) ASCs. The other three less stable ASCs, including C−OH dissociation, ene, and [2+2] C=O cycloaddition products, are

also depicted in Figure 3.2. Table 3.1 summarizes the adsorption energies and total energies of the most stable ASCs for acrylic acid (Figures 3.1a, 3.1b, 3.1c) and propanoic acid (Figures 3.2a, 3.2b, 3.2c) obtained with the 6-31G(d), 6-31+G(d), and 6-31++G(d,p) basis sets.

For the optimized geometries of the acrylate (Figure 3.1c) and propanoate unidentate ASCs (Figure 3.2c), the bond lengths for C–O and C=O are 135 pm and 122 pm, respectively. On the other hand, the bond lengths for both C···O bonds within the corresponding bidentate ASCs (Figures 3.1a, 3.1b, and 3.2a, 3.2b) are 127-129 pm, which lie between those of a single and a double bonds. Our frequency calculation also reveals that the wavenumber found for this 1½ C···O bond in the acrylate bidentate (1390-1534 cm^{-1}) and propanoate bidentate ASCs (1402-1558 cm^{-1}) is between those for the C–O (1200-1212 cm^{-1}) and C=O bonds (1742-1762 cm^{-1}) for the respective unidentate ASC. The C–C and C=C bond lengths for the three acrylate ASCs are 146-148 pm and 134 pm, respectively, while the respective C−C and C=C bond lengths for gas-phase acrylic acid are 148 pm and 134 pm, which suggests that the ethenyl (CH_2=CH–) group is not directly affected by the dissociative adsorption. Not surprisingly, the bond lengths for the CH_3–CH_2 (153-155 pm) and CH_2–CO bonds (150-151 pm) for the three propanoate ASCs (Figure 3.2) are found to be different from the corresponding bond lengths for the CH_2=CH (134 pm) and CH–CO bonds (146-148 pm) for the respective acrylate ASCs (Figure 3.1), while the bond lengths and bond angles in the carboxyl groups are found to be essentially the same between the respective propanoate and acrylate ASCs. It is also not surprising that for the bond lengths for the CH_3–CH_2 (153 pm), and CH_2–CO (151 pm) [as well as C=O bonds (121 pm)] for the gas-phase propanoic acid molecule are almost the same as the corresponding bonds in the bidentate (and unidentate) propanoate ASC (Figure 3.2c).

Table 3.1 Comparison of the adsorption energies ΔE and total energies (in square parentheses) for the three most stable adsorbate-substrate configurations (ASCs) of acrylic acid and of propanoic acid on Si(100)2×1 obtained by DFT/B3LYP calculations with 6-31G(d), 6-31+G(d), and 6-31++G(d,p) basis sets.

	ΔE (kJ mol^{-1}) [Total Energy (a.u.)]		
Acrylic Acid	Inter-dimer bidentate	Intra-dimer bidentate	Unidentate
6-31G(d)	–315.7 [–4619.34005]	–298.2 [–4619.33336]	–274.8 [–4619.32445]
6-31+G(d)	–296.5 [–4619.36154]	–278.0 [–4619.35449]	–260.2 [–4619.34771]
6-31++G(d,p)	–284.9 [–4619.38676]	–266.4 [–4619.37968]	–248.8 [–4619.37298]
Propanoic Acid	Inter-dimer bidentate	Intra-dimer bidentate	Unidentate
6-31G(d)	–311.7 [–4620.57444]	–294.3 [–4620.56778]	–274.2 [–4620.56012]
6-31+G(d)	–292.7 [–4620.59467]	–274.7 [–4620.58780]	–259.3 [–4620.58195]
6-31++G(d,p)	–281.2 [–4620.62205]	–262.8 [–4620.61504]	–247.8 [–4620.60934]

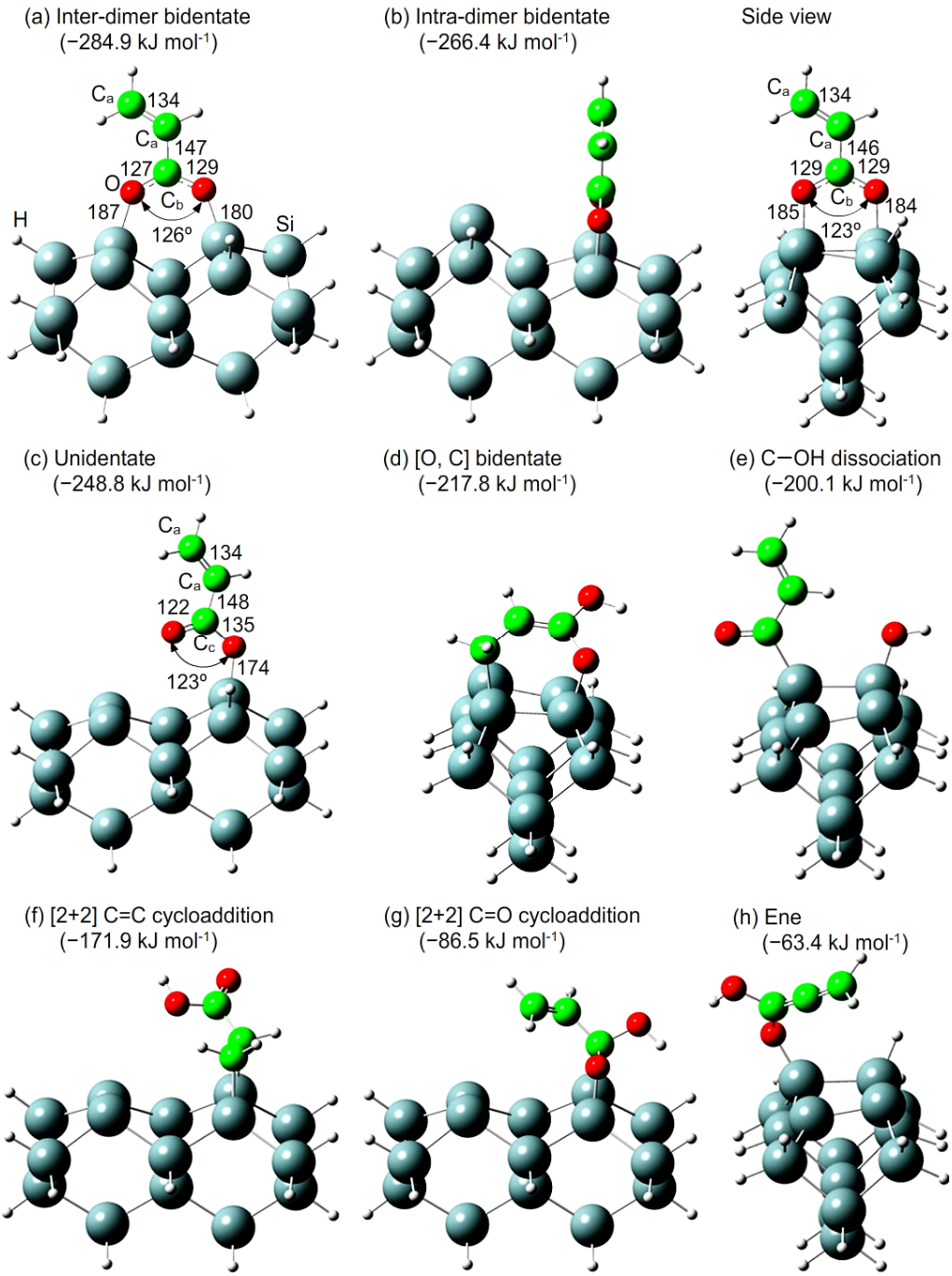

Figure 3.1 Optimized geometries of the adsorbate-substrate configurations of acrylic acid on Si(100)2×1: (a) inter-dimer bidentate, (b) intra-dimer bidentate, (c) unidentate, (d) [O,C] bidentate, (e) C–OH dissociation, (f) [2+2] C=C cycloaddition reaction, (g) [2+2] C=O cycloaddition reaction, and (h) ene products. The corresponding adsorption energies (ΔE) calculated with a 6-31++G(d,p) basis set are given in parentheses. All the bond lengths are given in unit of pm.

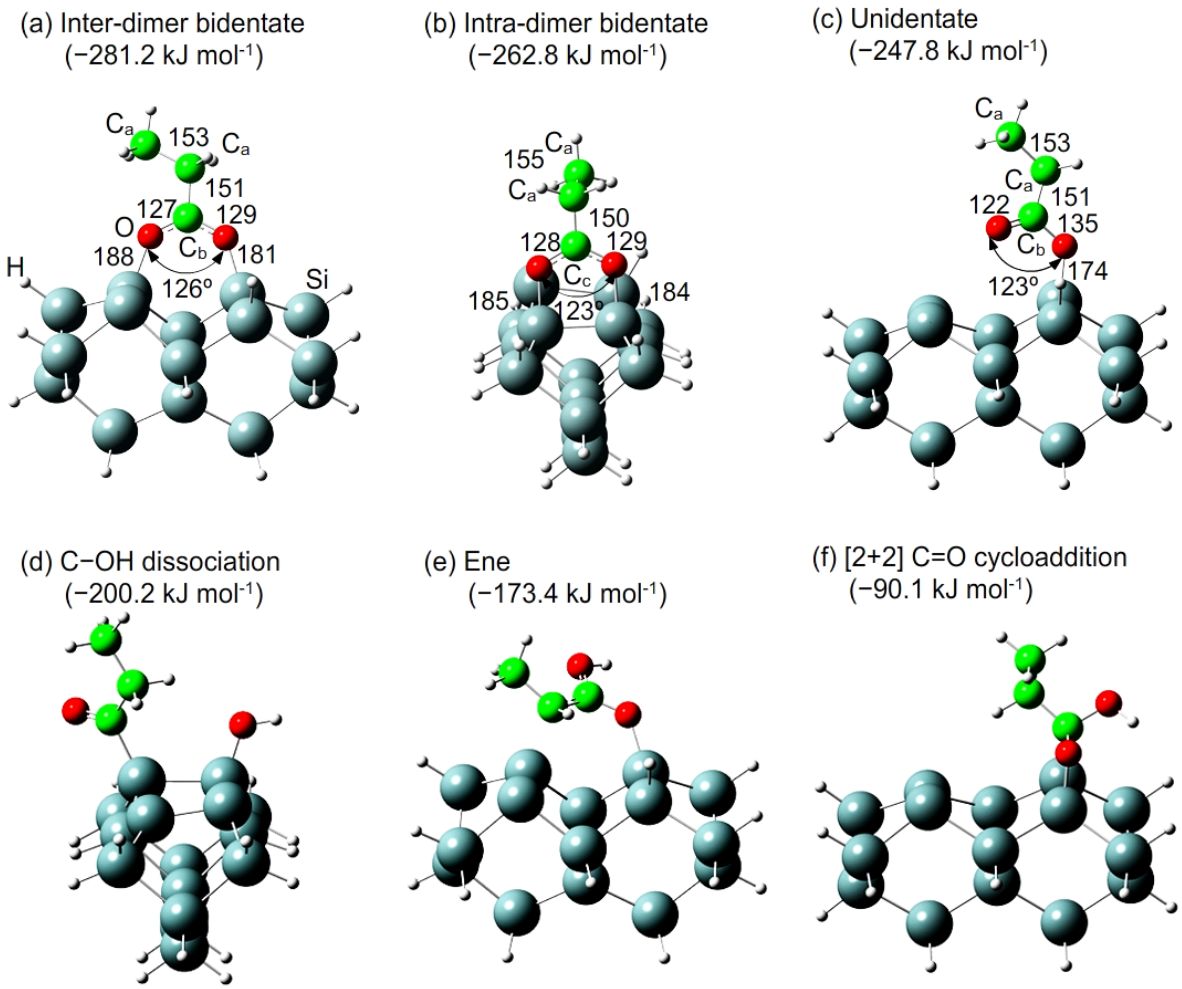

Figure 3.2 Optimized geometries of the adsorbate-substrate configurations of propanoic acid on Si(100)2×1: (a) inter-dimer bidentate, (b) intra-dimer bidentate, (c) unidentate, (d) C–OH dissociation, (e) ene, and (f) [2+2] C=O cycloaddition reaction products. The corresponding adsorption energies (ΔE) calculated with a 6-31++G(d,p) basis set are given in parentheses. All the bond lengths are given in unit of pm.

3.2.2 XPS study of room-temperature adsorption of acrylic acid and propanoic acid

In the present work, we have carried out XPS measurements for a number of exposures of acrylic acid and propanoic acid on Si(100)2×1, ranging from 1 L to 500 L. Figure 3.3 shows the XPS spectra (Figure 3.3c) of the C 1s and O 1s regions for a low exposure (2 L) and a saturation exposure (130 L) of acrylic acid on Si(100)2×1 at RT, along with the unidentate (Figure 3.3a) and (inter-dimer) bidentate ASCs (Figure 3.3b). Evidently, two C 1s bands for the 130 L exposure while only one broad band at the lower binding energy (BE) for the 2 L exposure are observed (Figure 3.3c). This observation would suggest that different adstructures are being formed at the low and high exposures. Three Gaussian profiles, each with an approximate full-width-at-half-maximum of 2.0 eV, have been used in our curve-fitting procedure to identify the prominent C local chemical environments. In particular, the C 1s features at 285.0, 286.8, and 289.3 eV BE with respective relative integrated intensities of 0.674, 0.153, and 0.172 (or approximately 4:1:1) have been found. The corresponding XPS spectrum for the lower exposure (2 L) was fitted with the first two features with the relative intensities of 2:1 at the same BEs as that obtained for the saturation exposure (Figure 3.3c).

In accord with our DFT calculations, the ASCs arising from O–H dissociation (Figures 3.1a, 3.1b, 3.1c) are the most stable (i.e., with the most negative ΔE values). Evidently, the chemical environments of the ethenyl carbons (CH_2=CH–, designated as C_a) in the three most stable ASCs are different from the carboxyl carbons, whereby the carboxyl carbon in the bidentate ASCs (C_b, attached to O through two C···O bonds, Figures 3.1a, 3.1b) is different from that in the unidentate ASC (C_c, attached to O through a C=O and a C–O bonds, Figure 3.1c). Given that the electronegativity of C (2.5) is less than that of O (3.5),[16] the carboxyl carbons (C_b and C_c) are expected to be partially positively charged and therefore should exhibit a higher C 1s BE than the ethenyl carbons (C_a). The C 1s feature at the lowest BE (285.0 eV, Figure 3.2c) can therefore be attributed to the ethenyl C_a atoms. For the two C 1s features at the higher BEs, we have previously attributed them to the

bidentate and unidentate carboxyl carbons for the adsorption of acetic acid on Si(100)2×1.[26] Following this recent work on acetic acid, we show a similar schematic model for the conversion of unidentate ASC (Figure 3.3a) to the resonance structures of the inter-dimer bidentate ASC in Figure 3.3d. Combining one electron from the C=O group in the unidentate ASC (Structure I) with the electron in the Si dangling bond produces a new Si–O covalent bond, creating the inter-dimer bidentate ASC (Structure IIa). Electron delocalization in the OCO moiety leads to Structures IIa, IIb, and IIc, while participation of the ethenyl group in the electron delocalization in the C_β···C_α···C···O backbone gives rise to Structure IId. These four resonance structures altogether correspond to the hybrid resonance structure shown as Structure II (Figure 3.3b). Inclusion of the electron from the Si dangling bond in the formation of Structure II in effect reduces the partial positive charge of C_b, therefore "lowering" the corresponding BE. Consequently, the C 1s features at 286.8 eV and 289.3 eV can be assigned to C_b and C_c, respectively. The observation of only the lower-BE band (containing contributions from C_a and C_b) for the lower exposure (Figure 3.3c, lower panel) indicates the preferred formation of the bidentate ASCs in the early stage of the adsorption process, which is consistent with the more negative adsorption energy (or ΔE) compared to that of the less stable unidentate ASC (Table 3.1). The observed C 1s features at 285.0, 286.8, and 289.3 eV shown in Figure 3.3c can therefore be assigned to C_a, C_b, and C_c respectively. Given the respective intensity ratio for C_a:C_b:C_c to be approximately 4:1:1 for the saturation exposure, we conclude that the bidentate ASCs (including inter-dimer and/or intra-dimer ASCs) and unidentate ASC must have nearly equal population.

It is of interest to compare the C 1s spectra of acrylic acid to that of acetic acid reported by us recently.[26] Like acrylic acid, the bidentate and unidentate ASCs are observed for acetic acid.[26] However, replacement of the methyl group in acetic acid by the ethenyl group in acrylic acid is not expected to affect the respective XPS features of the bidentate carboxyl C (C_b), because it is the participation of the electron from the neighbouring Si dimer [from Structure I (Figure 3.3a) to Structure II (Figure 3.3b)] and its delocalization that reduces the partial positive charge of this carbon (Figure 3.3d). The presence of the ethenyl group will only increase the number of resonance forms (to 4 in acrylic acid from 3 in acetic

acid)[26] and the delocalization within the larger C_{β}···C_{α}···C···O backbone. On the other hand, this replacement will affect the BE position of the C 1s feature of the carboxyl carbon (C_c) for the unidentate acrylate ASC by changing the partial positive charge of C_c relative to that of acetate ASC.[26] The free C=O group in the unidentate acrylate ASC can be represented as C^{+}–O^{-} in Structure Ic (Figure 3.3e), of which the positive charge on C is shared with Structure Ib (Figure 3.3e) due to electron delocalization. This delocalization in effect reduces the average partial positive charge on the C_c atom, resulting in a lower C 1s BE for unidentate acrylate ASC (289.3 eV) than that of acetate (289.8 eV).[26] It should be noted that delocalization of the π electrons in the C=C and C=O bonds of unidentate acrylate ASC reduces the double-bond character of the C=C and C=O bonds in the hybrid resonance form (Structure I', Figure 3.3e), which in turn reduces the C=O stretching mode by 23 cm^{-1} from our calculated wavenumber for unidentate acetate (1765 cm^{-1}) [26] to that for unidentate acrylate (1742 cm^{-1}). Similar reduction has also been observed experimentally[44] and found in our frequency calculation for gas-phase acetic acid (1822 cm^{-1}) [26] relative to acrylic acid (1799 cm^{-1}).

Figure 3.3h shows the C 1s and O 1s XPS spectra for a low (2 L) and a saturation exposures (30 L) of propanoic acid at RT on Si(100)2×1. Similar to the spectra for acrylic acid (Figure 3.3c), the C 1s band at the lower-BE observed for the low exposure (lower panel) can be attributed to bidentate propanoate (Figure 3.3g), while the additional band at the higher BE observed for the higher exposure (upper panel) can be assigned to unidentate propanoate (Figure 3.3f). The C 1s features at 285.3 eV, 286.8 eV and 289.2 eV, obtained after appropriate curve fitting, can therefore be assigned to C_a, C_b and C_c. There is only a slight difference between the C_a 1s BE of the ethyl group (CH_3–CH_2–) of the propanoate (285.3 eV, Figure 3.3h) and the ethenyl group (CH_2=CH–) of acrylate (285.0 eV, Figure 3.3c). This small difference is not surprising because the conjugation effect reduces the double-bond character of C_a in the unidentate and bidentate acrylate ASCs. Furthermore, the C_b 1s and C_c 1s BEs for propanoate ASCs (Figure 3.3h) are found to be essentially the same as the corresponding BEs for acrylate ASCs (Figure 3.3c). We have attributed the similarity in the BE between C_b 1s of bidentate acrylate ASCs and that of bidentate acetate to electron

delocalization within the OCO moiety. This delocalization is essentially the same also for bidentate propanoate, which therefore leads to similar C_b 1s BE. Moreover, as discussed above, the difference in the C_c 1s BE between the unidentate acrylate and unidentate acetate is due to the smaller partial positive charge produced by the conjugation effect in the acrylate. In the case of unidentate propanoate, however, the difference in the C_c 1s BE (289.2 eV) from that of unidentate acetate (289.8 eV) is caused by the greater electron donating character of the ethyl group (relative to the methyl group) that also reduces the partial positive charge of the C_c atom.

It is of interest to note that the earlier studies on vinyl acetic acid[27] and acetic acid[25] on Si(100)2×1 by other workers have also reported a double-band profile for the C 1s spectra, but concluded the formation of only unidentate carboxylates on the surface. In our recent work, we discussed in detail our observation for acetic acid on Si(100)2×1[26] and compared with the result reported for vinyl acetic acid.[27] The present work on acrylic acid and propanoic acid on Si(100)2×1 has provided further support for our analysis for acetic acid. By presenting a model for the formation and the resonance structures of the bidentate carboxylate for the first time, we attribute the differences in the C 1s spectra observed for acetic acid, acrylic acid and propanoic acid on Si(100)2×1 to the formation of bidentate carboxylate at a lower exposure followed by that of unidentate carboxylate at a higher exposure.

Figure 3.3c also shows the corresponding O 1s spectra for the 2 L and 130 L RT exposures of acrylic acid on Si(100)2×1. In particular, a broad feature at 532.8 eV is observed, with the width and the intensity for the 130 L exposure discernibly larger than those for the 2 L exposure. Similar observations can be made for the corresponding O 1s spectra of propanoic acid on Si(100)2×1 shown in Figure 3.3h. The observed O 1s BE position is in good accord with those of Si–O (531.9 eV) and C=O (532.8 eV) reported for vinyl acetic acid[27] and acetic acid,[26] which supports that the carboxylates are the preferred ASCs in accord with the C 1s data. It should be noted that due to the large natural linewidths of the O 1s transitions it is generally difficult to resolve the underlying features.

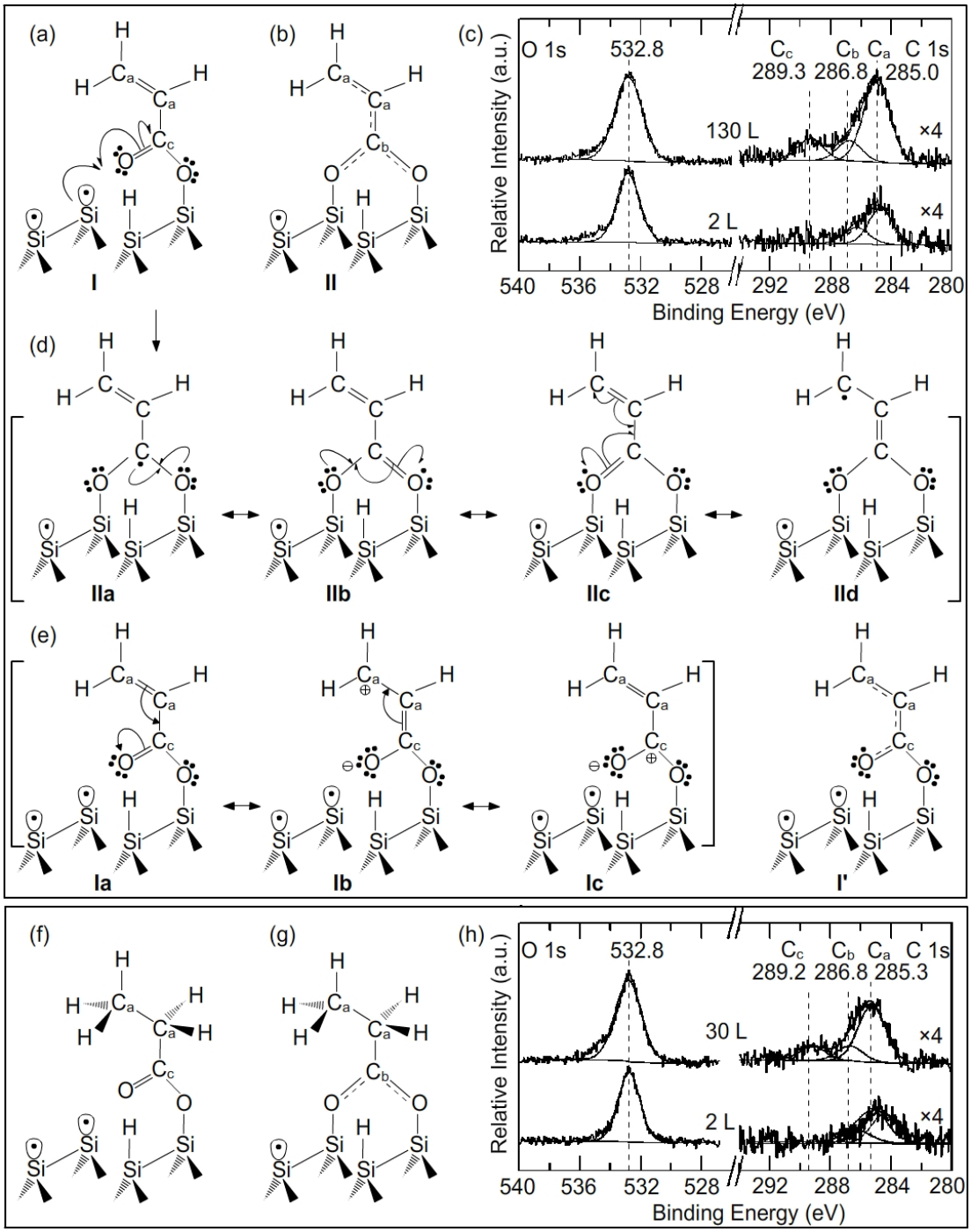

Figure 3.3 Schematic diagrams of (a) unidentate and (b) bidentate acrylate adstructures, and the plausible resonance structures of (d) bidentate and (e) unidentate acrylate, and of (f) unidentate and (g) bidentate propanoate. XPS spectra of the C 1s and O 1s regions for (c) a saturation exposure (130 L) and a 2-L exposure of acrylic acid and (h) a saturation exposure (30 L) and a 2-L exposure of propanoic acid, all on Si(100)2×1 at 300 K.

3.2.3 XPS and TPD studies of the thermal evolution of acrylate adspecies

Figures 3.4 and 3.5 show the respective XPS spectra of the C 1s and O 1s regions of a saturation exposure (130 L) of acrylic acid as deposited on Si(100)2×1 and after successive flash-annealing up to 1350 K. Evidently, the unidentate carboxyl C 1s peak at 289.3 eV (C_c) decreases in intensity upon annealing to 525 K (Figure 3.4b) and disappears completely after annealing to 770 K (Figure 3.4c). The intensity of the bidentate carboxyl C 1s feature at 286.8 eV (C_b) follows a similar decreasing trend and becomes totally extinguished at 1050 K (Figure 3.4d). For the ethenyl C 1s peak at 285.0 eV (C_a), the peak position appears to shift to a lower BE (284.0 eV) while undergoing reduction in intensity, indicative of desorption of adspecies (to be discussed below), upon annealing to 525-770 K (Figure 3.4c). This is followed by a marked reduction in its intensity upon annealing to 1050 K (Figure 3.4d), and the emergence of a new feature at 283.3 eV commonly attributed to SiC. This SiC feature remains unchanged upon annealing above 1185 K (Figure 3.4e) to 1350 K (Figure 3.4f). In Figure 3.4g, we summarize the observed intensity changes as a function of the annealing temperature for these four C 1s features (C_a, C_b, C_c, and SiC) along with the total C 1s intensity, all relative to the intensity of the Si 2p peak at 99.3 eV. A more gradual removal of the observed carboxyl C (C_b, C_c) 1s features from the surface is observed over the 525 K-1050 K region. Meanwhile, the intensity of the ethenyl C (C_a) undergoes first a gradual reduction from 525 K to 770 K, followed by an abrupt reduction at 1050 K. Unlike all of the carboxyl C that have apparently been totally removed near 770 K, some of the ethenyl group appears to remain on the surface, as represented by the "intermediate" feature near 284.0 eV (Figure 3.4c), and undergoes further dehydrogenation to eventually become SiC upon further annealing to 1050 K.[19] It is of interest to note that 33% of the total C (corresponding to most of the carboxyl C and some of the ethenyl C) has left the surface upon annealing to 770 K, with the remaining C being converted to SiC that cannot be removed even at an annealing temperature of 1350 K.

In Figure 3.5, the broad O 1s feature at 532.8 eV observed for the saturation exposure of acrylic acid on Si(100)2×1 is found to undergo a slight reduction in intensity upon annealing to 770 K (Figure 3.5c). Apparently, the O 1s feature also becomes sharper with a

small shift to a lower BE, suggesting that one of the oxygen atoms (C=O) of the adspecies with the higher BE has dissociated from the ASC, leaving the other O with the lower BE bounded to Si (Si–O) at a higher annealing temperature. The O 1s feature becomes greatly reduced at 1050 K (Figure 3.5d), which evidently is higher than the temperature at which most of the carboxyl C 1s feature is removed (770-1050 K, Figure 3.4g). This suggests that the adsorbed acrylates dissociate on the surface to adspecies (to be discussed below) that desorb at 525-1050 K, and to individual O atoms that desorb from the surface above 1000-1350 K (likely as SiO) or diffuse into the bulk. The O 1s intensity is completely removed above 1350 K (Figure 3.5g).

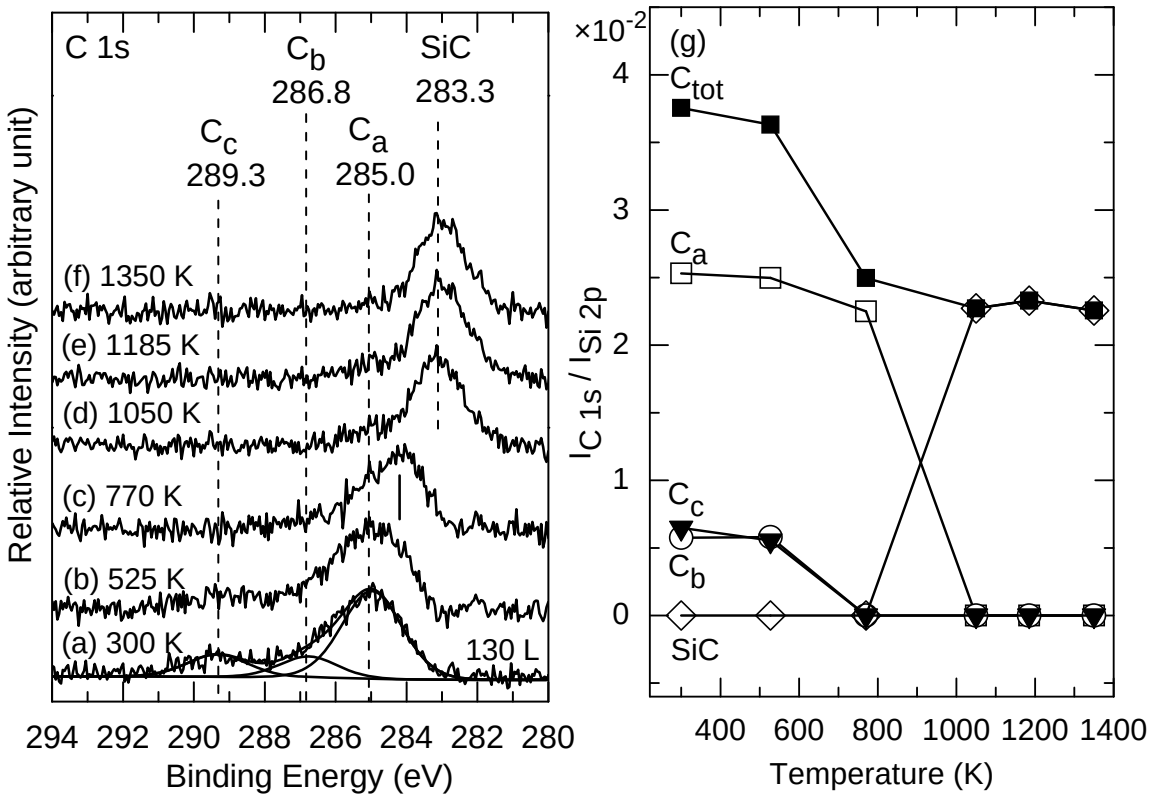

Figure 3.4 XPS spectra of the C 1s region for (a) a saturated exposure (130 L) of acrylic acid on Si(100)2×1 at 300 K, and upon sequential flash-annealing to (b) 525 K, (c) 770 K, (d) 1050 K, (e) 1185 K, and (f) 1350 K. (h) shows the corresponding temperature profiles of the C 1s intensities ($I_{C\ 1s}$) for SiC at 283.3 eV, C_a at 284.0-285.0 eV, C_b at 286.8 eV, and C_c at 289.3 eV, along with the total C 1s intensity (C_{tot}), all with respect to the intensity of Si 2p ($I_{Si\ 2p}$).

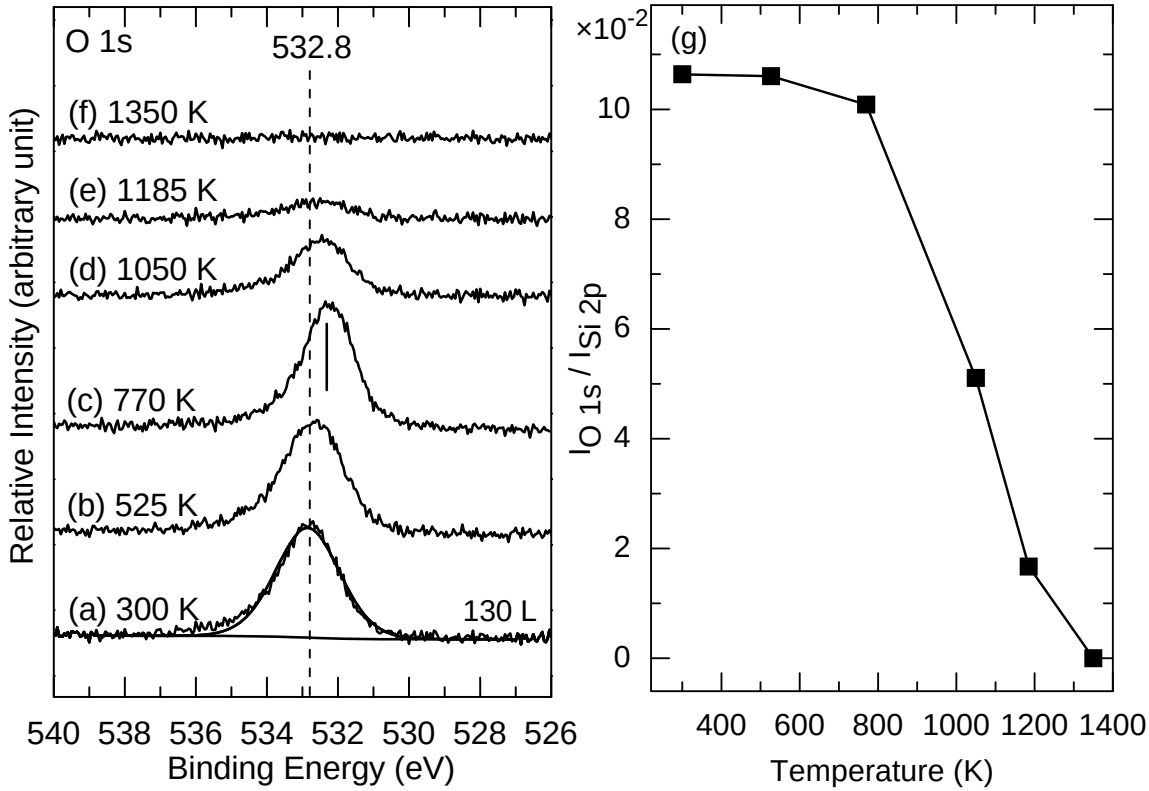

Figure 3.5 XPS spectra of the O 1s region for (a) a saturated exposure (130 L) of acrylic acid on Si(100)2×1 at 300 K, and upon sequential flash-annealing to (b) 525 K, (c) 770 K, (d) 1050 K, (e) 1185 K, and (f) 1350 K. (g) shows the corresponding temperature profile of the O 1s intensity ($I_{O\ 1s}$) with respect to the intensity of Si 2p ($I_{Si\ 2p}$).

In addition to the temperature-dependent XPS spectra that show the adspecies remaining on the 2×1 surface after the sample has been annealed to different preselected temperatures, we also performed TPD experiments to investigate the desorption products evolved from the surface as a function of temperature. Figure 3.6A shows the TPD profiles of selected mass fragments with m/z 2, 26, 27, 28, 39, 41 and 42 for a RT saturation exposure (130 L) of acrylic acid on Si(100)2×1. We also monitored other mass fragments, including m/z 45, 55, and 72 corresponding to $COOH^+$, CH_2=CH–CO^+, and the parent mass (CH_2=CH–$COOH^+$) of acrylic acid, respectively.[45] No notable TPD features of these latter two mass fragments are found, which indicates no molecular adsorption of acrylic acid. Furthermore, the lack of TPD feature for m/z 45 provides further support that any adsorption process that keeps the COOH group intact (i.e. not directly involved in bonding with the surface), such as the [2+2] C=C cycloaddition product, does not occur. For m/z 2, a strong desorption feature at 810 K is observed (Figure 3.6Aa), which is consistent with the recombinative desorption of H_2 from silicon monohydride.[46] The next strongest desorption feature is observed at 595 K for m/z 28 (Figure 3.6Ad), which corresponds to the parent mass of CO. The TPD features for the remaining mass fragments all appear to have considerably smaller relative intensities. In particular, the TPD profile for m/z 26 exhibits two peaks (Figure 3.6Ab). The first m/z 26 peak at 595 K, together with the corresponding m/z 27 (Figure 3.6Ac) and 28 features (Figure 3.6Ad) found at the same temperature, can be assigned to the desorption of ethylene (CH_2=CH_2), with the parent/base mass of m/z 28. The second m/z 26 peak observed at a higher temperature of 760 K corresponds to the parent mass of acetylene (HC≡CH).[45] The very weak profile for m/z 42 (Figure 3.6Ag) is correlated with desorption of propene (CH_2=CH–CH_3),[45] the cracking pattern of which also contains m/z 27 (Figure 3.6Ac), 39 (Figure 3.6Ae), and 41 (Figure 3.6Af), all with desorption maxima occurring at the same temperature of 595 K. Our TPD results for acrylate acid are consistent with our temperature-dependent XPS data. The reduction of the carboxyl (C_b, C_c) and ethenyl (C_a) C 1s features in both unidentate and bidentate ASCs at 525-800 K occurs over essentially the same temperature range as the formation of ethylene and acetylene as well as CO (Figure 3.6A).

Figure 3.6B shows the TPD profiles of selected mass fragments with m/z 2, 25, 26, 27, and 28 for a saturation exposure (30 L) of propanoic acid on Si(100)2×1. Similar to acrylic acid, the lack of TPD features of the parent mass (m/z 74) and m/z 45 ($COOH^+$) and m/z 29 ($CH_3–CH_2^+$) indicates no molecular adsorption. Furthermore, the intense m/z 2 feature at 805 K again indicates recombinative desorption of H_2 (Figure 3.6Ba). The other masses m/z 25, 26, 27, and 28 (Figure 3.6B) with desorption maxima all appearing at 700 K correspond to desorption of ethylene (with the parent mass of m/z 28). The m/z 28 desorption profile could also have some contribution from CO (which also has a parent mass of m/z 28). Although it is possible that m/z 28 could also come from desorption of ethane ($CH_3–CH_3$), the TPD profiles for m/z 29 and m/z 30, belonging to the cracking pattern of ethane, did not show any notable feature. This maybe because the formation of ethane requires pre-dissociation of C–C leading to the formation of the unstable $CH_3–CH_2$ ethyl radical.

Figure 3.7A shows plausible mechanisms for the formation of CO, ethylene, and acetylene from the unidentate and bidentate acrylate adspecies induced by thermal annealing. The mechanism for the formation of propene (mass 42) inferred from the TPD data is unclear and will not be discussed further. It should be noted that although the mechanisms likely involve multi-step reaction processes, we only present a simple model for bond dissociation to illustrate the formation pathways of these desorbates. In particular, the unidentate acrylate (Structure I) undergoes a C−C and C−O bond cleavage (Structure Ia) to produce CO (Figure 3.7A, pathway a). The dissociated ethenyl radical group (CH_2=$CH^•$) stays on the surface (Structure Ibc) to subsequently abstract a H atom from Si−H, forming the ethylene desorbate (Structure Ib) via pathyway b (Figure 3.7A). Furthermore, at a higher temperature (760 K, Figure 3.6Ab), the surface ethenyl radical could itself also undergo H abstraction (Structure Ic), producing the acetylene desorbate via pathway c. From the typical bond dissociation energies (in kJ mol^{-1}) for Si−Si (310), Si−O (800), Si−C (447), Si−H (293), C−O (459), C−C (385), C−H (399), and O−H (469),[47] we estimate the energy required for the formation of the observed desorbates. In particular, the energy needed to break a C−C and a C−O bonds for the formation of CO from Structure Ia (Figure 3.7A) is 844 kJ mol^{-1}. Furthermore, the

subsequent formation of ethylene from the ethenyl radical requires additional energy to break a Si−H bond (293 kJ mol^{-1}) while the formation of acetylene needs to cleave a C−H bond, with a higher bond dissociation energy (399 kJ mol^{-1}). This energy consideration is therefore consistent with the observation of the desorption maxima for the CH_2=CH_2 fragments (m/z 26, 27, 28) at a lower temperature (595 K, Figure 3.6A) than the corresponding HC≡CH fragments (m/z 26) at 760 K, Figure 3.6A). The broad profile for m/z 28 (Figure 3.6Ad) suggests plausible contributions from more than one feature desorbed at different temperatures, which is in accord with our schematic model depicting the formation of CO before ethylene (Figure 3.7A, pathways a and b).

The dissociation of C−C bond in the bidentate acrylate (Structure IId) could also produce the surface ethenyl radical through pathway d (Figure 3.7A), which leads to the formation of ethylene and acetylene (pathway e). Fragmentation of the remaining OCO radical (Structure IIe) could also produce CO (pathway e'). It should be noted that conversion from bidentate acrylate (Structure II) to unidentate acrylate (Structure I) could also occur during the thermal evolution process. Finally, in addition to the main CO, CH_2=CH_2, and HC≡CH desorbates, dissociated O, H, and OH stay on the surface as byproducts that can be removed from the surface at the higher annealing temperatures.
It is of interest to note that the desorption maxima for the CO and ethylene related masses appear at a higher temperature (700 K) for propanoic acid (Figure 3.6B) than those for acrylic acid (595 K, Figure 3.6A), suggesting different dissociation pathways for the propanoates. Figure 3.7B shows the proposed mechanisms involving fragmentation of unidentate (Structure IIIf) and bidentate propanoates (Structure IVg) to CO and ethylene, both with m/z 28. Apparently, simultaneous breakage of C−C, C−O and C−H bonds in propanoates (to produce CO and ethylene) requires more energy (1243 kJ mol^{-1}) than that to produce CO (844 kJ mol^{-1}) and ethylene (1137 kJ mol^{-1}) from acrylates, which would lead to higher desorption temperatures for the desorbates from propanoates, as observed in our TPD experiments.

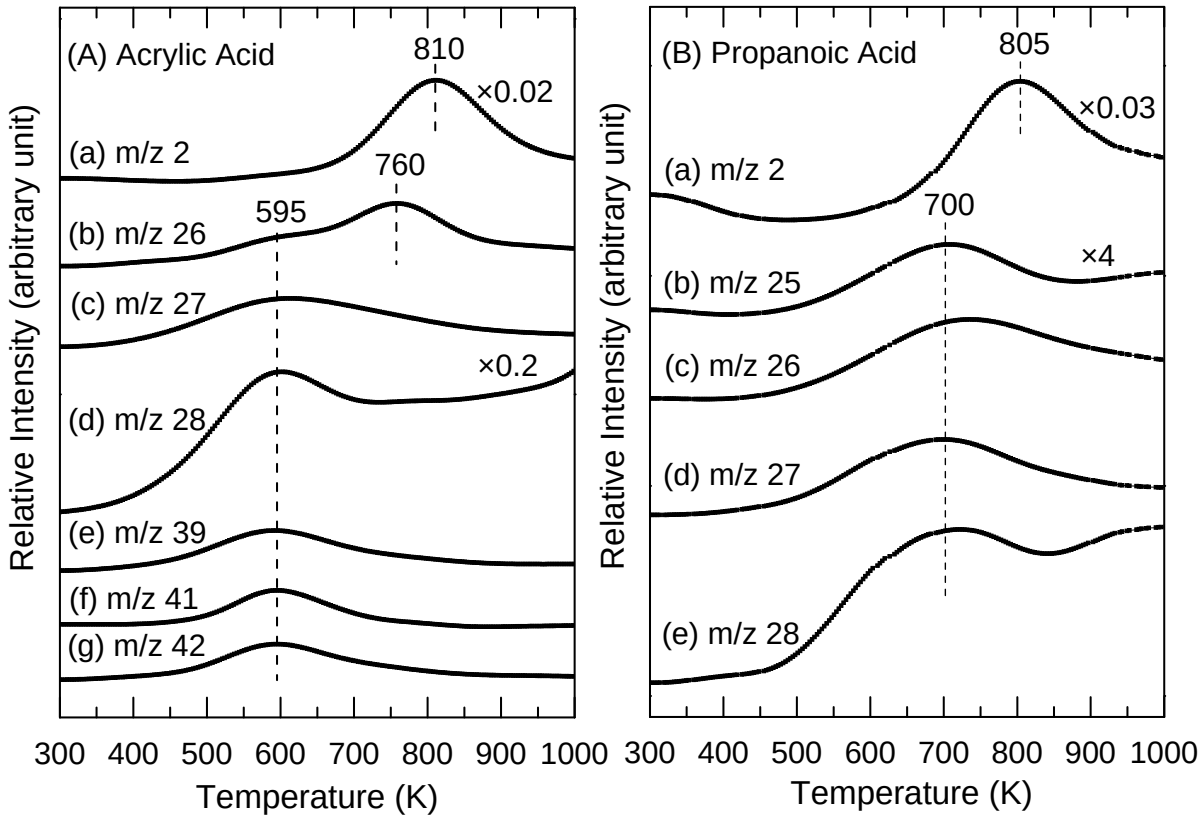

Figure 3.6 TPD profiles of selected fragments of (A) m/z (a) 2, (b) 26, (c) 27, (d) 28, (e) 39, (f) 41, and (g) 42 for a saturation coverage (130 L) of acrylic acid, and (B) m/z (a) 2, (b) 25, (c) 26, (d) 27, and (e) 28 for a saturation coverage (30 L) of propanoic acid, on Si(100)2×1 at 300 K.

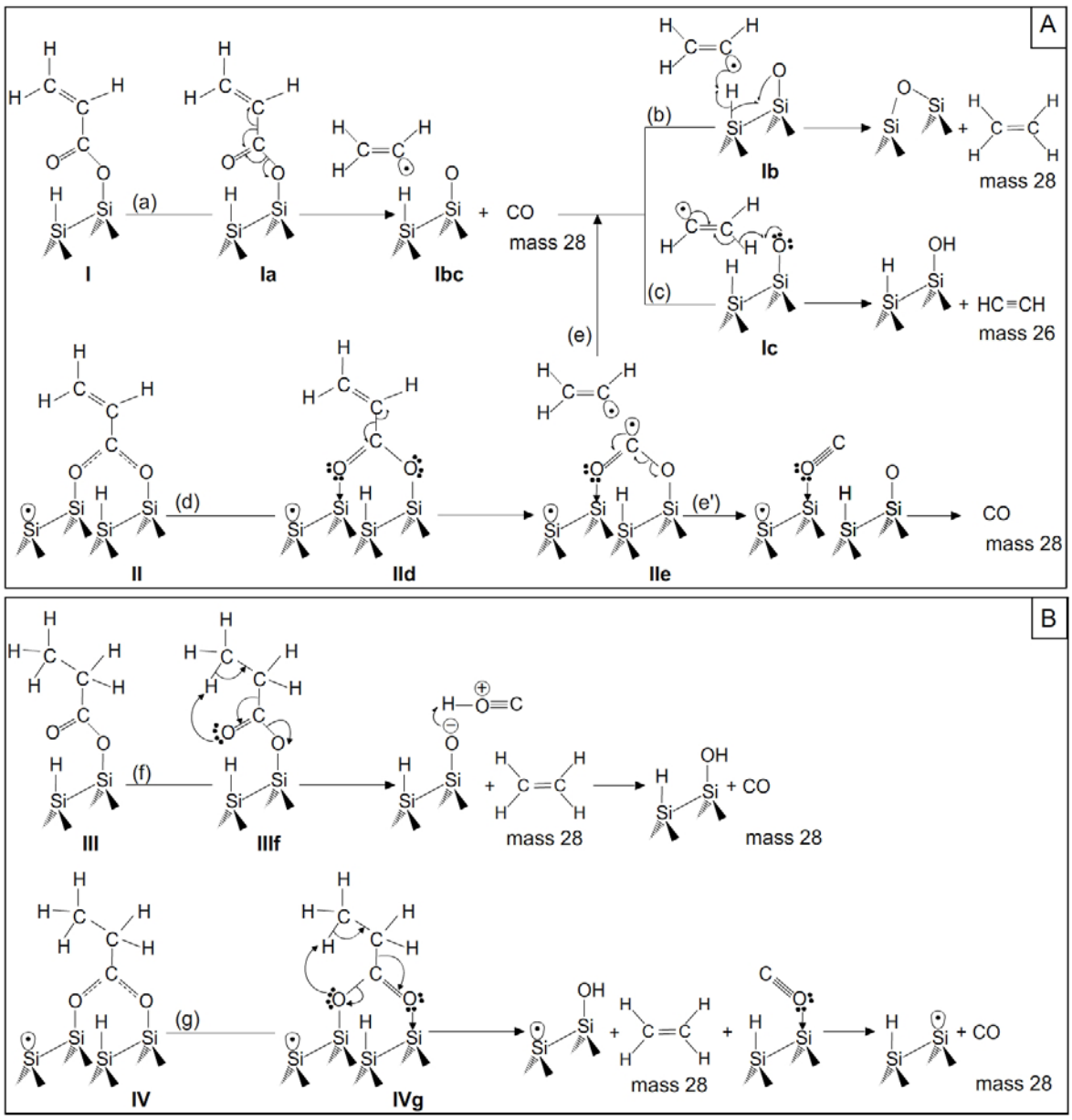

Figure 3.7 Schematic models for thermal evolution of unidentate and bidentate (A) acrylate and (B) propanoate on Si(100)2×1, depicting the formation of CO, ethylene, and acetylene, and of CO and ethylene, respectively.

3.3 Summary

XPS and TPD experiments have been performed, for the first time, on acrylic acid and propanoic acid on Si(100)2×1. Of the calculated ASCs for acrylic acid and propanoic acid, the bidentate ASCs are found to be more stable than the unidentate ASCs, both of which are more stable than the other calculated ASCs. In accord with our recent study on acetic acid,[26] the present XPS data provides evidence for the formation of bidentate acrylate and propanoate at a lower exposure than the corresponding unidentate carboxylate on Si(100)2×1. At the saturation coverage, both the bidentate and unidentate ASCs are present in equal population. The presence of the bidentate and unidentate ASCs reflects the selectivity of the 2×1 surface in mediating the formation of the O–H dissociation products over other possible reaction products (e.g., cycloaddition reactions, ene formation and C–OH dissociation). Furthermore, the combined temperature-dependent XPS and TPD data for acrylic acid reveal several plausible thermal evolution pathways that lead to the formation of CO, ethylene, and acetylene, with 90% of the dissociated ethenyl group (or nearly 60% of the total C) converting to SiC with increasing annealing temperature to above 770 K. The formation of ethylene and acetylene provides further evidence for the selectivity of the surface towards O–H dissociation, which leaves the ethenyl group intact for subsequent thermally induced production of these desorbates. For propanoic acid on Si(100)2×1, only CO and ethylene were observed in the TPD experiment. The lack of any detectable CO_2 feature for acrylic acid and propanoic acid in our TPD experiments is consistent with the thermal evolution of acetic acid on Si(100)2×1.[26] The selectivity of the directional dangling bonds on the Si(100)2×1 surface therefore preferentially enables the linkage through the carboxyl group while leaving the other functional groups intact for further functionalization of the 2×1 surface. As a bifunctional molecule, acrylic acid provides an important reference for studying molecules containing carboxyl and alkenyl groups. The delocalized C_β···C_α···C···O backbone serves as a special reactive site for further nucleophilic reactions on the surface pre-functionalized with acrylic acid. Further studies comparing the selectivity of the Si(100)2×1 towards other multifunctional molecules will lead to further insight into the surface organosilicon chemistry and molecular electronics.

References

[1] M. A. Filler, S. F. Bent, Prog. Surf. Sci. 73 (2003) 1-56.

[2] S. F. Bent, Surf. Sci. 500 (2002) 879-903.

[3] J. M. Buriak, Chem. Commun. (1999) 1051-1060.

[4] J. M. Buriak, Chem. Rev. 102 (2002) 1271-1308.

[5] X. Lu, M. C. Lin, Int. Rev. Phys. Chem. 21 (2002) 137-184.

[6] T. R. Leftwich, A. V. Teplyakov, Surf. Sci. Rep. 63 (2008) 1-71.

[7] J. T. Yates Jr., Science 279 (1998) 335-336.

[8] R. J. Hamers, Y. Wang, Chem. Rev. 96 (1996) 1261-1290.

[9] R. J. Hamers, S. K. Coulter, M. D. Ellison, J. S. Hovis, D. F. Padowitz, M. P. Schwartz, C. M. Greenlief, J. N. Russell Jr., Acc. Chem. Res. 33 (2000) 617-624.

[10] F. A. Carey, "Organic Chemistry", 3rd Edition, McGraw-Hill, Toronto, 1996.

[11] R. A. Wolkow, Annu. Rev. Phys. Chem. 50 (1999) 413-441.

[12] R. A. Wolkow, Phys. Rev. Lett. 68 (1992) 2636.

[13] H. N. Waltenburg, J. T. Yates Jr., Chem. Rev. 95 (1995) 1589-1673.

[14] J. Yoshinobu, H. Tsuda, M. Onchi, M. Nishijima, J. Chem. Phys. 87 (1987) 7332-7340.

[15] C. C. Cheng, R. M. Wallace, P. A. Taylor, W. J. Choyke, J. T. Yates Jr., J. Appl. Phys. 67 (1990) 3693-3699.

[16] L. Clemen, R. M. Wallace, P. A. Taylor, M. J. Dresser, W. J. Choyke, W. H. Weinberg, J.T. Yates Jr., Surf. Sci. 268 (1992) 205-216.

[17] A. J. Mayne, A. R. Avery, J. Knall, T. S. Jones, G. A. D. Briggs, W.H. Weinberg, Surf. Sci. 284 (1993) 247-256.

[18] M. Ikeda, T. Maruoka, N. Nagashima, Surf. Sci. 416 (1998) 240-244.

[19] H. Liu, R. J. Hamers, Surf. Sci. 416 (1998) 354-362.

[20] H. W. Yeom, S. Y. Baek, J. W. Kim, H. S. Lee, H. Koh, Phys. Rev. B 66 (2002) 115308-1-115308-6.

[21] P. A. Taylor, R. M. Wallace, C. C. Cheng, W. H. Weinberg, M. J. Dresser, W. J. Choyke, J. T. Yates Jr., J. Am. Chem. Soc. 114 (1992) 6754-6760.

[22] S. Tanaka, M. Onchi, M. Nishijima, J. Chem. Phys. 91 (1989) 2712-2725.

[23] T. Kubo, N. Minami, T. Aruga, N. Takagi, M. Nishijima, J. Phys. Chem. B 101 (1997) 7007-7011.

[24] H. Ikeura-Sekiguchi, T. Sekiguchi, Surf. Sci. 433-435 (1999) 549-553.

[25] H.-K. Lee, K.-J. Kim, J.-H. Han, T.-H. Kang, J. W. Chung, B. Kim, Phys. Rev. B 77 (2008) 115324.

[26] M. Ebrahimi, J. F. Rios, K. T. Leung, J. Phys. Chem. C (2009) in press; and references therein.

[27] H.-N. Hwang, J. Y. Baik, K.-S. An, S. S. Lee, Y. Kim, C. C. Hwang, B. Kim, J. Phys. Chem. B 108 (2004) 8379-8384.

[28] T. Bitzer, T. Alkunshalie, N. V. Richardson, Surf. Sci. 368 (1996) 202-207.

[29] T. Bitzer, N. V. Richardson, Surf. Sci. 427-428 (1999) 369-373.

[30] A. Lopez, T. Bitzer, T. Heller, N. V. Richardson, Surf. Sci. 480 (2001) 65-72.

[31] M. A. Filler, J. A. Van Deventer, A. J. Keung, S. F. Bent, J. Am. Chem. Soc. 128 (2006) 770-779.

[32] D. H. Kim, E. Hwang, S. Hong, S. Kim, Surf. Sci. 600 (2006) 3629-3632.

[33] E. Hwang, D. H. Kim, Y. J. Hwang, A. Kim, S. Hong, S. Kim, J. Phys. Chem. C 111 (2007) 5941-5945.

[34] E. K. Hlil, L. Kubler, J. L. Bischoff, D. Bolmont, Phys. Rev. B 35 (1987) 5913-5916.

[35] F. Bozso, Ph. Avouris, Phys. Rev. B 38 (1988) 3937-3942.

[36] J.-B. Wu, Y.-W.Yang, Y.-F. Lin, H.-T. Chiu, J. Phys. Chem. B 108 (2004) 1677-1685.

[37] C. Mui, J. H. Han, G. T. Wang, C. B. Musgrave, S. F. Bent, J. Am. Chem. Soc. 124 (2002) 4027-4038.

[38] C. Shannon, A. Campion, Surf. Sci. 227 (1990) 219-223.

[39] M. P. Casaletto, R. Zanoni, M. Carbone, M. N. Piancastelli, L. Aballe, K. Weiss, K. Horn, Surf. Sci. 505 (2002) 251-259.

[40] J. Eng Jr., K. Raghavachari, L. M. Struck, Y. J. Chabal, B. E. Bent, G. W. Flynn, S. B. Christman, E. E. Chaban, G. P. Williams, K. Radermacher, S. Mantl, J. Chem. Phys. 106 (1997) 9889-9898.

[41] M. P. Casaletto, R. Zanoni, M. Carbone, M. N. Piancastelli, L. Aballe, K. Weiss, K. Horn, Surf. Sci. 447 (2000) 237-244.

[42] J. Kim, K. Kim, K. Yong, J. Vac. Sci. Technol. A 20 (2002) 1582-1.

[43] P. P. Favero, A. C. Ferraz, R. Miotto, Phys. Rev. B 77 (2008) 085304-1-085304-7.

[44] D. L. Pavia, G. M. Lampman, G. S. Kriz, Introduction to Spectroscopy, 2nd Edition, Saunders Golden Sunburst Series, Harcourt Brace College Publishers, USA, 1996.

[45] NIST Mass Spec Data Center, S.E. Stein (director), "Mass Spectra" in NIST Chemistry WebBook, NIST Standard Reference Database Number 69, edited by P.J. Linstrom and W.G. Mallard, June 2005, National Institute of Standards and Technology, Gaithersburg (http://webbook.nist.gov).

[46] C. C. Cheng, J. T. Yates Jr., Phys. Rev. B 43 (1991) 4041-4045.

[47] "Bond Dissociation Energies" by Y.-R. Luo, in CRC Handbook of Chemistry and Physics, 88th Edition (Internet Version 2008), edited by D. R. Lide, CRC Press/Taylor and Francis, Boca Raton.

Chapter 4

Selective surface chemistry of allyl alcohol and allyl aldehyde on Si(100)2×1: Competition of [2+2] C=C cycloaddition with O−H dissociation and with [2+2] C=O cycloaddition in bifunctional molecules

4.1 Introduction

Surface chemistry of multifunctional organic molecules on Si(100)2×1 has attracted a lot of attention in the past decade.[1−7] The electrophile-nucleophile character of the buckled silicon dimers[8,9] on the Si(100)2×1 surface provides unique control of how this surface reacts with different functional groups. The buckling of the Si dimers enables the [2+2] cycloaddition reaction with alkene at room temperature (RT), which is normally symmetry-forbidden in classical chemistry by the Woodward-Hoffman selection rules.[10] To date, surface reactions of alkenes (with the C=C functional group), [6,11−24] aldehydes[25,26] and ketones (both with the C=O functional group)[25,27,28] on Si(100)2×1 have been reported to form [2+2] and [4+2] cycloaddition products, while those of alcohols (with the OH functional group), [29−34] carboxylic acids (with the COOH functional group),[35−44] and primary and secondary amines have resulted in H dissociation products.[1,5,6] These studies illustrate the critical role of the silicon surface in mediating selective chemical reactions largely involving a single functional group.

In order to investigate the selectivity of the 2×1 surface toward the aforementioned functional groups, we employ a molecule that contains multiple functional groups as the adsorbate, and study its thermal surface chemistry by using X-ray photoelectron spectroscopy (XPS) and temperature-programmed desorption (TPD), along with density functional theory (DFT) calculations. In our recent work on acrylic acid,[44] the simplest unsaturated carboxylic acid containing two functional groups, we compared the reactivity of the carboxyl group and ethenyl group in this bifunctional molecule with those of saturated carboxylic acids: acetic acid[43] and propanoic acid, both containing just the carboxyl group.[44] In particular, we

showed that the Si(100)2×1 surface selectively favours O–H dissociation of the carboxyl group over [2+2] C=C cycloaddition of the ethenyl group and other possible reaction products in acrylic acid. As was also found for acetic acid[43] and propanoic acid,[44] O–H dissociation in acrylic acid also leads to bidentate and unidentate carboxylate adspecies.

Using the ethenyl group as the "reference" functional group, we now extend our study of relative reactivity and selectivity of the carboxyl group[44] to other functional groups in a bifunctional molecule on Si(100)2×1. In particular, allyl alcohol (or 2-propenol, CH_2=CH–CH_2OH) and allyl aldehyde (or 2-propenal, CH_2=CH–CHO) offer the hydroxyl group (OH) and carbonyl group (C=O), respectively, as the second functional group, in addition to the common ethenyl group (CH_2=CH−). In acrylic acid[43] (and carboxylic acids in general), the carboxyl group itself could be considered as consisting of two smaller functional groups, the OH and C=O. The present work, in effect, compares the competition of the ethenyl group with each of these smaller functional groups individually in their reactions with the 2×1 surface. To date, no experimental study has been reported for the adsorption of allyl alcohol and allyl aldehyde on Si(100)2×1. Only one DFT computational study [using the B3LYP/6-31G(d) method] of allyl alcohol on model Si(100) and Ge(100) cluster surfaces has been reported by Li et al.[45] Their calculations showed that O–H dissociation results in more thermodynamically favourable products than [2+2] C=C cycloaddition products.

In the present work, we present XPS and TPD studies to follow the thermal evolution of the adsorption products of allyl alcohol and allyl aldehyde on Si(100)2×1. Together with our DFT calculations, these experimental results show that for allyl alcohol O−H dissociation is preferred over [2+2] C=C cycloaddition, as was proposed by Li et al.[45] and was also observed for other carboxylic acids.[41,44] For allyl aldehyde, [2+2] C=O cycloaddition is found to be more favourable than [2+2] C=C cycloaddition by our XPS measurement, in spite of the less negative calculated adsorption energy obtained for the former product than that for the latter by our DFT calculation. The present work therefore further affirms the remarkable stability of the ethenyl group relative to any of the following functional groups: OH, C=O (this work), COOH,[44] and Cl[46,47] as well as other heteroatom-containing groups,[6]

on the 2×1 surface. These latter functional groups (except Cl) can therefore be used as the linkage to connect the molecule to the 2×1 surface, leaving the ethenyl group free for further reactions. Furthermore, the present experimental result also shows that multiple linkages through simultaneous interactions of two functional groups with the surface (such as the [O, C, C] tridentate and the [O, C] bidentate adstructures) do not occur, despite the considerably more negative adsorption energy calculated for these multiply bonded adstructures. The formation of ethylene, acetylene, and propene fragments found in our TPD experiments for both allyl alcohol and allyl aldehyde adspecies further supports that the common unreacted moiety (the ethenyl group) remains intact and free to undergo further thermal chemistry upon adsorption on Si(100)2×1.

4.2 Results and Discussion

4.2.1 DFT computational study of adsorbate-substrate configurations

Figure 4.1 shows four plausible adstructures on the double-dimer model surface of the $Si_{15}H_{16}$ cluster, involving O–H dissociation (ASC I) and [2+2] C=C cycloaddition (ASC II) for allyl alcohol, and [2+2] C=O cycloaddition (ASC IV) and [2+2] C=C cycloaddition (ASC V) for allyl aldehyde. Table 4.1 summarizes the calculated adsorption energies and total energies of the four ASCs obtained with four different basis sets: 6-31G(d), 6-31+G(d), 6-31++G(d), and 6-31++G(d,p). Evidently, all four basis sets provide very similar values, with the larger basis set generally giving a lower total energy but a less negative adsorption energy. There is a more notable change in the adsorption energy between the 6-31G(d) and the next larger basis set [6-31+G(d)] than that between the larger basis sets. The change between the 6-31++G(d) and the largest 6-31++G(d,p) basis sets appears to be more noticeable for ASC I, likely due to the improved modeling of the diffuse bonding involving O−H dissociation. The results obtained with the largest 6-31++G(d,p) basis set will be used for the following discussion.

Evidently for allyl alcohol, the adsorption energy (and total energy) for the O–H dissociation product (–249.4 kJ mol^{-1}, Figure 4.1a) is considerably more negative than that

for the [2+2] C=C cycloaddition product (−169.1 kJ mol^{-1}, Figure 4.1b). The dative bonding between O and the electron-deficient site of the Si dimer leads to the attachment of allyl alcohol to Si through O followed by O–H dissociation to eventually form ASC I. For the less stable ASC II, the reduction of the π bond results in the formation of two Si−C bonds in the cycloaddition reaction, which is expected to give a lower C 1s binding energy (BE) than that in C−C and C=C. For allyl aldehyde, the calculated adsorption energy of the [2+2] C=O cycloaddition product (−164.7 kJ mol^{-1}, Figure 4.1d) is found to be less negative than that of [2+2] C=C cycloaddition product (−174.8 kJ mol^{-1}, Figure 4.1e). However, the similarity of these values indicates that both ASCs IV and V are equally probable thermodynamically. The presence of C=C only in ASC IV should give rise to a notable difference in the C 1s BE between ASCs IV and V, which would allow us to distinguish these structures from our XPS measurement (to be discussed below).

Our frequency calculations show that the wavenumbers for C−O (1071 cm^{-1}) and C=C stretching vibrations (1715 cm^{-1}) for ASC I are slightly higher than the corresponding calculated values for isolated allyl alcohol molecule (1045 cm^{-1} and 1708 cm^{-1}, respectively). Similarly, the wavenumber for C=C stretch (1692 cm^{-1}) for ASC IV is also essentially the same as the corresponding calculated value for isolated allyl aldehyde molecule (1683 cm^{-1}). The similarity in the wavenumbers for C=C vibrations in ASC I and ASC IV to those of their respective isolated allyl alcohol and allyl aldehyde molecules is not surprising, because the ethenyl group is not directly involved in binding to the surface. On the other hand, no corresponding calculated wavenumber for C=C is found for ASC II and ASC V due to the formation of C−C bonding as a result of [2+2] cycloaddition.

Our DFT calculation also reveals two unique, multiply bonded ASCs, including an [O, C, C] tridentate $\underline{C}H_2-\underline{C}H-CH_2-\underline{O}$ complex obtained from [2+2] C=C cycloaddition and O–H dissociation of allyl alcohol (Figure 4.1c), and an [O, C] bidentate $\underline{C}H_2-CH=CH-\underline{O}$ complex derived from the delocalized form ($CH_2\cdots CH\cdots CH\cdots O$) of allyl aldehyde (Figure 4.1f). Despite having the most negative adsorption energies, these ASCs are improbable due to kinetic effects and the need for additional molecular motions to facilitate the required multiple attachments to the Si(100)2×1 surface. As discussed below, these ASCs can be

ruled out by our XPS measurement.

Table 4.1 Comparison of the adsorption energies, ΔE, and total energies (in square parentheses) for plausible adsorbate-substrate configurations (ASCs) of allyl alcohol and allyl aldehyde on Si(100)2×1 obtained by DFT/B3LYP calculations with 6-31G(d), 6-31+G(d), 6-31++G(d), and 6-31++G(d,p) basis sets.

ΔE (kJ mol^{-1}) [Total Energy (hartree)]	6-31G(d)	6-31+G(d)	6-31++G(d)	6-31++G(d,p)
O–H dissociation ASC I	–276.7 [–4545.27532]	–261.0 [–4545.29652]	–261.1 [–4545.29823]	–249.4 [–4545.32457]
[2+2] C=C cycloaddition ASC II	–175.6 [–4545.23682]	–169.3 [–4545.26162]	–169.7 [–4545.26340]	–169.1 [–4545.29397]
[2+2] C=O cycloaddition ASC IV	–173.1 [–4545.03698]	–163.8 [–4545.05824]	–163.9 [–4545.05981]	–164.7 [–4545.08393]
[2+2] C=C cycloaddition ASC V	–185.2 [–4545.04158]	–174.9 [–4545.06246]	–174.9 [–4545.06401]	–174.8 [–4545.08776]

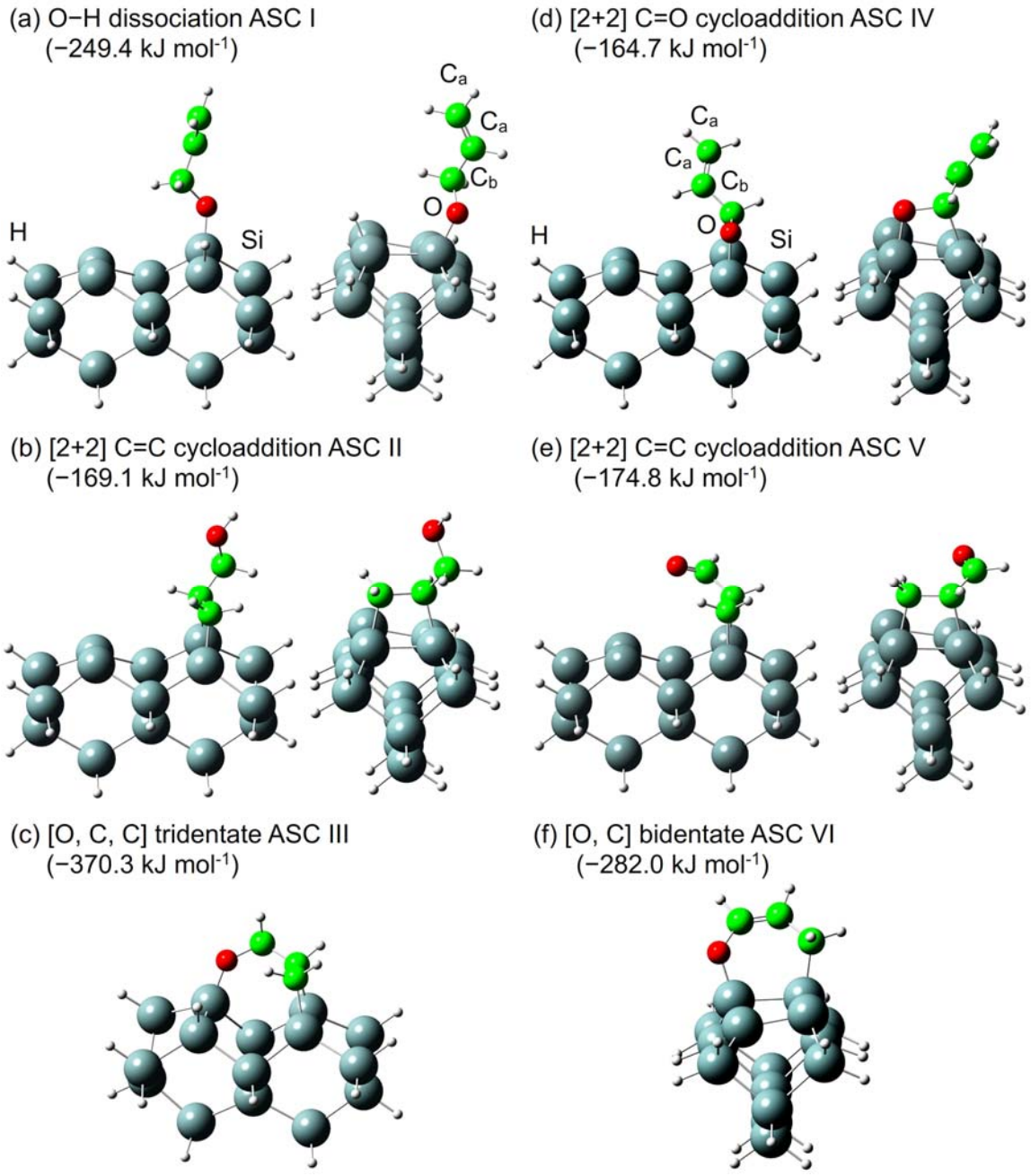

Figure 4.1 Optimized geometries of the adsorbate-substrate configurations (ASCs): (a) O–H dissociation ASC I, (b) [2+2] C=C cycloaddition ASC II, and (c) [O, C, C] tridentate ASC III products of allyl alcohol, and (d) [2+2] C=O cycloaddition ASC IV, (e) [2+2] C=C cycloaddition ASC V and (f) [O, C] bidentate ASC VI products of allyl aldehyde, all on Si(100)2×1. The corresponding adsorption energies calculated with the 6-31++G(d,p) basis set are given in parentheses.

4.2.2 Room-temperature adsorption of allyl alcohol and allyl aldehyde on Si(100)2×1

In the present work, we have carried out XPS measurements for a number of exposures of allyl alcohol and of allyl aldehyde on Si(100)2×1, ranging from 0.1 L to 120 L. The saturation exposure for allyl aldehyde (60 L) is found to be discernibly lower than that for allyl alcohol (106 L), in good agreement with the generally higher reactivity of aldehyde relative to alcohol.

Figure 4.2 shows the XPS spectra of the C 1s and O 1s regions for a low exposure (0.45 L) and a saturation exposure (106 L) of allyl alcohol deposited on Si(100)2×1 at RT. The C 1s spectra for both exposures exhibit a single broad band, which we appropriately fitted with two Gaussian profiles, each with an approximate width of 1.8 eV full-width-at-half-maximum (FWHM), in order to identify the prominent C local chemical environments. In marked contrast to the XPS results for acetic acid,[43] acrylic acid and propanoic acid,[44] similar features are obtained at both low and high RT exposures for allyl alcohol on Si(100)2×1, suggesting the presence of adstructures with similar C 1s environments for both low and high exposures. In particular, the C 1s features at BEs of 284.8 eV and 286.4 eV are found to have, respectively, relative integrated intensities of 0.031 and 0.014 (with an approximate intensity ratio of 2:1) with respect to the intensity of Si 2p for both low (Figure 4.2Aa) and saturation exposures (Figure 4.2Ab). The C 1s BEs for the C=O, C−O, C=C, C−C, C−Si bonds are generally found at 287.8-288.5 eV,[25−27] 285.4-286.9 eV,[25−27,34] 284.8-285 eV,[14,17,20] 284.4 eV,[17,20] and 283.7-284.3,[14,17,20,27] respectively. The absence of the C−Si feature below 284.3 eV in our C 1s spectra could therefore be used to rule out the existence of ASC II (Figure 4.1b) and ASC III (Figure 4.1c). The observation of the C 1s features at 284.8 eV (C_a) and 286.4 eV (C_b) attributed to C=C and C−O moieties, respectively, indicates the predominant formation of ASC I. Given the higher electronegativity of O (3.5, Pauling scale) with respect to C (2.5),[16] C_b (with an O atom attached) should be partially positively charged and it should therefore exhibit a higher C 1s BE than the ethenyl (CH_2=CH–) carbons (C_a), as observed in Figure 4.2Aa. The nearly constant C 1s intensity ratio of C_a:C_b with respect to exposure (Figures 4.2Aa, 4.2Ab) suggests that no new ASC (other than ASC

I) is formed at a higher exposure. The C_a:C_b value of 2:1 is also in excellent accord with the stoichoimetric ratio of C_a to C_b in ASC I. In the case of O 1s, the corresponding BE observed at 532.7 eV (Figures 4.2Ba, 4.2Bb) is not very useful for identifying the adstructures (i.e. between ASC I and ASC II/III) because of the similarity in the electronegativities of Si (1.8) and H (2.1) and the generally broad widths found for the O 1s peaks.

The XPS spectra of the C 1s and O 1s regions for a low exposure (0.2 L) and a saturation exposures (60 L) of allyl aldehyde on Si(100)2×1 at RT, shown in Figure 4.3, are found to be remarkably similar to those of allyl alcohol (Figure 4.2). In particular, two Gaussian profiles at 284.7 eV and 286.3 eV, each with a width of 1.6 eV FWHM, can be fitted to the broad C 1s bands observed for both exposures, giving relative integrated intensities of 0.037 and 0.019 with an approximate intensity ratio of 2:1. As with the allyl alcohol case (Figure 4.2), the BE positions of the observed C 1s peaks at 284.7 eV (C_a) and 286.3 eV (C_b) (Figure 4.3) correspond to the C=C and C−O bonds, consistent with the [2+2] C=O cycloaddition product (ASC IV). It should be noted that, despite the difference in the local chemical environment of C_b between ASC IV (bonded to Si) and ASC I (bonded to H), the corresponding BEs are found to be essentially the same because of the similar electronegativities for Si (1.8) and H (2.1). The observed C 1s BE positions for C_a and C_b also rule out the formation of [2+2] C=C cycloaddition product (ASC V), because no signatures of C−Si (expected at 283.7-284.3 eV)[14,17,20,27] and C=O (at 287.8-288.5 eV)[25−27] are observed in the C 1s spectra (Figure 4.3). Despite the discernibly more negative adsorption energy for ASC V (Figure 4.1e) than that for ASC IV (Figure 4.1d) obtained in the DFT calculations, the present XPS measurement is therefore instrumental in identifying the adsorption structures. In contrast to the C=C bond, the asymmetric electron density of the C=O bond is more compatible with the electrophile-nucleophile character of the Si=Si dimer, which favours the formation of [2+2] C=O cycloaddition product. Furthermore, we can also rule out the formation of [O, C] bidentate ASC VI (Figure 4.1f), because three distinct C 1s features corresponding to C−Si, C=C, and C−O (with equal intensity) expected for this structure are not observed. In addition, the O 1s feature at 532.6 eV shown in Figures 4.3Ba and 4.3Bb for allyl aldehyde is also found at the similar position to that of allyl alcohol

(532.7 eV, Figures 4.2Ba, 4.2Bb). This similarity is not surprising because the O atom is attached to a Si and a C_b atoms in both ASC I (Figure 4.1a) and ASC IV (Figure 4.1d).

4.2.3 Thermal evolution of allyl alcohol and allyl aldehyde adspecies on Si(100)2×1

Figures 4.2 and 4.3 also show the C 1s and O 1s XPS spectra for RT saturation exposures of allyl alcohol and allyl aldehyde, respectively, on Si(100)2×1 upon successive flash-annealing to selected temperatures. Evidently, the C_b 1s peak for O–H dissociation product (ASC I) of allyl alcohol (Figure 4.1a) at 286.4 eV decreases in intensity gradually upon annealing to 545 K (Figure 4.2Ad) and disappears completely after annealing to 800 K (Figure 4.2Ae). For the ethenyl C_a 1s peak at 284.8 eV, little change to the intensity is observed up to the annealing temperature of 545 K. Upon further annealing to 800 K, the C_a 1s peak position appears to shift to a lower BE (284.3 eV) and undergoes a small reduction in intensity due to possible fragmentation and desorption of the smaller fragments. Continued annealing to 1090 K completely removes the C_a 1s feature (Figure 4.2Af), and introduces a new feature at 283.1 eV, commonly attributed to SiC, the intensity of which remains unchanged at the highest annealing temperature of 1390 K (Figure 4.2Ag). The latter could be due to dehydrogenation of the remaining C_a containing fragments and its conversion to SiC on the surface in this temperature range. In Figure 4.2Ah, we summarize the observed intensity changes of these three C 1s features (C_a, C_b, and SiC) along with the total C 1s intensity, all relative to the intensity of Si 2p, as a function of the annealing temperature. The temperature profiles clearly indicate the presence of a transition region between 545 K and 1090 K, where thermal desorption and fragmentation occur. It is of interest to note that nearly 45% of the total C (corresponding to almost all of the C_b and some of the C_a) has been eliminated from the surface upon annealing to 800 K, with the remaining converted to SiC that cannot be removed even at the annealing temperature of 1390 K. The corresponding temperature profile for the O 1s feature, shown in Figure 4.2Bh, depicts a gradual reduction in intensity up to 800 K, followed by a marked decrease upon further annealing to 1390 K.

Between the annealing temperature of 545 K and 800 K, the O 1s feature has evidently become sharper and shifted from 532.7 eV (Figure 4.2Bd) to a slightly lower BE of 532.1 eV (Figure 4.2Be). This spectral change suggests that part of the O-containing moiety has undergone dissociation and/or desorption from the surface, producing Si−O on the surface with a lower O 1s BE. The reduction in the O 1s intensity above 800 K is likely due to desorption of SiO fragments or O diffusion into the bulk.

For a saturation exposure of allyl aldehyde on Si(100)2×1, the corresponding spectral changes in the C 1s and O 1s features as a function of annealing temperature (Figure 4.3) appear to be similar to those found for allyl alcohol (Figure 4.2). In particular, the C_a 1s temperature profile for allyl aldehyde (Figure 4.3Ah) closely follows that of for allyl alcohol (Figure 4.2Ah), with minimal reduction in intensity upon annealing to 800 K followed by complete extinction after further annealing to 1090 K. A notable difference observed in the C_b 1s temperature profile for allyl aldehyde (Figure 4.3Ah) from that for allyl alcohol (Figure 4.2Ah) is that the temperature of its complete extinction occurs at a higher annealing temperature (1090 K) for the former than that for the latter (800 K). The C 1s spectrum for the 800 K annealing temperature (Figure 4.3Ae) appears to have shifted to the lower BE side. The small shift to the lower BE found for C_a 1s (284.3 eV) is consistent with the attachment of an ethenyl group (with the C 1s peak commonly found at 283.9 eV),[46] after dissociation from the C̲H−O̲ moiety attached to the Si surface (Figure 4.1d) at 800 K. The dissociation removes the effectively electron withdrawing ethenyl group and reduces the partial positive charge on the C of the remaining di-σ bonded C̲H−O̲ moiety, causing the C_b 1s peak to shift to a lower BE (285.5 eV). For allyl aldehyde, the related peak for SiC at 283.0 eV (Figure 4.3Ae) is found at a similar annealing temperature (1090 K) (Figure 4.3Af) as that for allyl alcohol (Figure 4.2Af). In accord with the allyl alcohol case, SiC begins to form above 800 K (Figure 4.3Af) and the spectral intensity becomes slightly reduced upon further annealing from 1090 K to 1390 K. Furthermore, nearly 80% of the total C of the adsorbed allyl aldehyde has been converted to SiC, in marked contrast to allyl alcohol where only 55% of the C remains as SiC. This difference in the SiC formation indicates more C-containing desorbates for allyl alcohol than allyl aldehyde, which suggests limited desorption channels

for the C-containing species for allyl aldehyde on Si(100)2×1. For the O 1s temperature profile, there is virtually no change in the O 1s intensity for allyl aldehyde up to 800 K (Figure 4.3Bh), in contrast to the early onset of the gradual reduction in O 1s intensity at 425 K for allyl alcohol (Figure 4.2Bh). This difference in the onset temperature suggests that more energy is required for the dissociation or formation of O-containing fragments for allyl aldehyde than allyl alcohol. Above 800 K, the O 1s intensities for both allyl aldehyde and allyl alcohol evidently undergo marked reduction, with total removal at 1390 K.

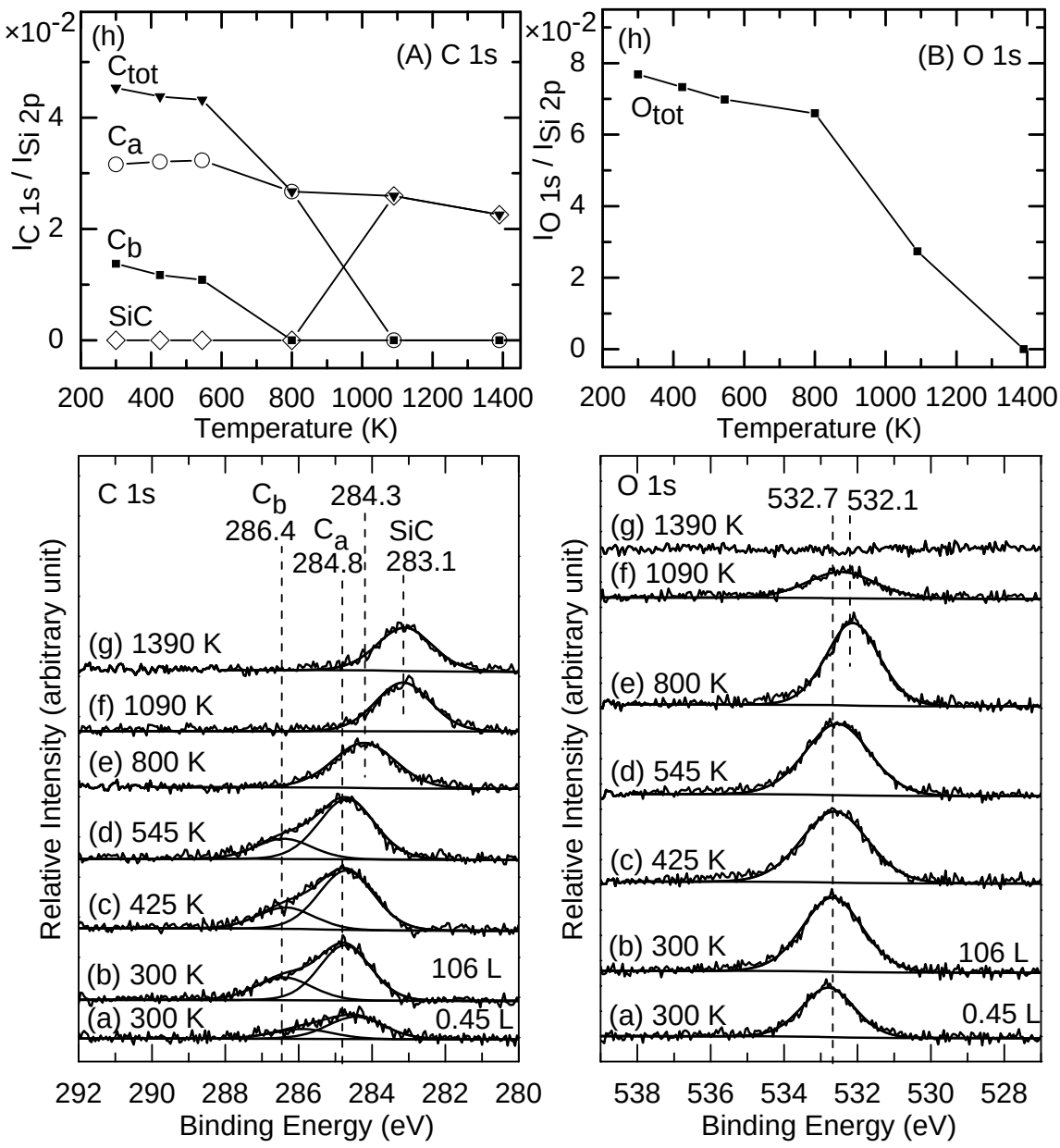

Figure 4.2 XPS spectra of the C 1s (left column) and O 1s regions (right column) for (a) a 0.45 L and (b) a saturated exposures (106 L) of allyl alcohol deposited on Si(100)2×1 at 300 K, and for sample (b) upon sequential flash-annealing to (c) 425 K, (d) 545 K, (e) 800 K, (f) 1090 K, and (g) 1390 K. (h) Corresponding temperature profiles of the C 1s intensities ($I_{C\ 1s}$) for SiC at 283.1 eV, C_a at 284.3-284.8 eV, and C_b at 286.4 eV, along with the total intensity for C 1s (C_{tot}), and of the total O 1s intensity ($I_{O\ 1s}$), all with respect to the intensity of Si 2p ($I_{Si\ 2p}$).

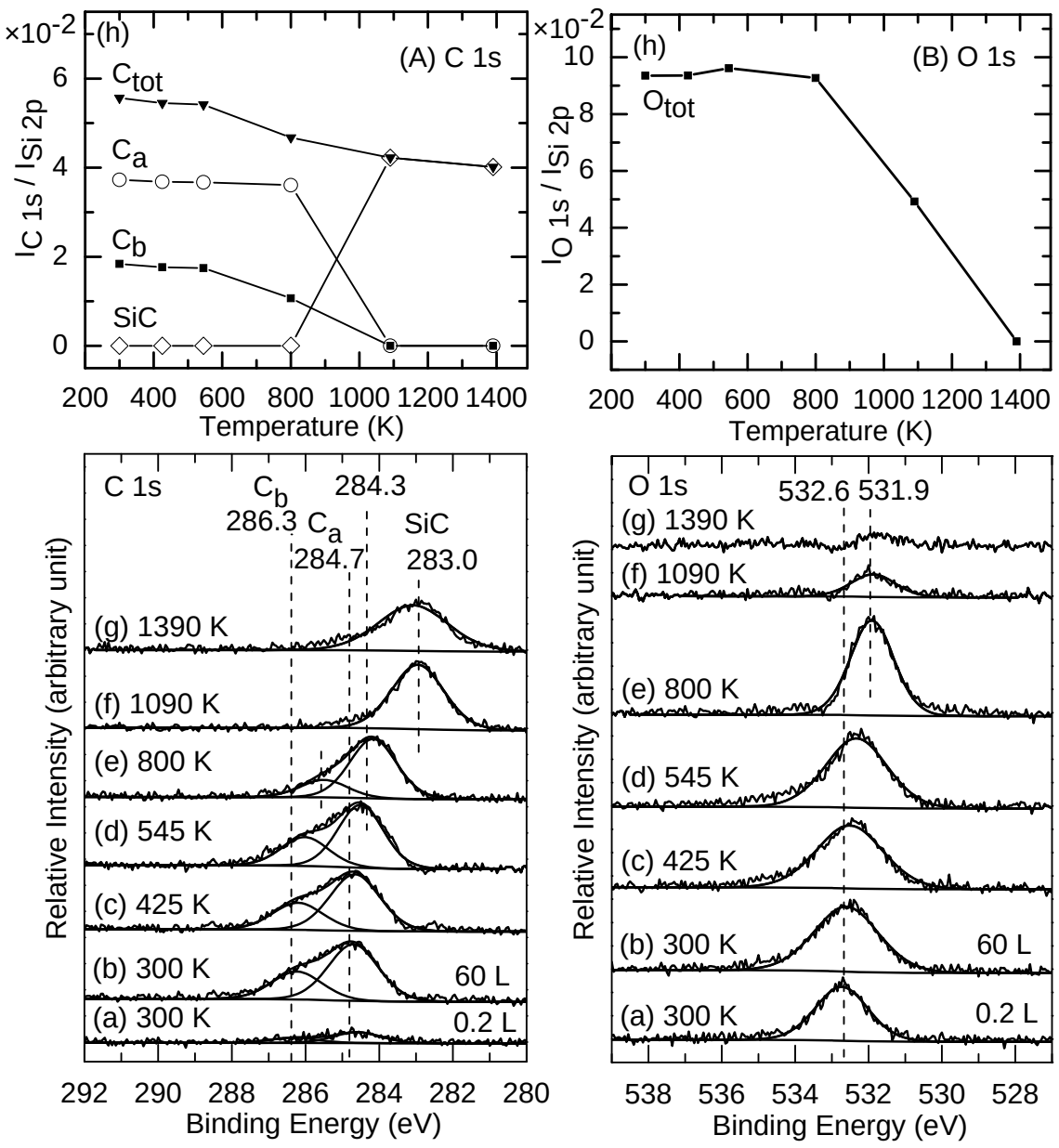

Figure 4.3 XPS spectra of the C 1s (left column) and O 1s regions (right column) for (a) a 0.2 L and (b) a saturated exposures (60 L) of allyl aldehyde deposited on Si(100)2×1 at 300 K, and for sample (b) upon sequential flash-annealing to (c) 425 K, (d) 545 K, (e) 800 K, (f) 1090 K, and (g) 1390 K. (h) Corresponding temperature profiles of the C 1s intensities ($I_{C\ 1s}$) for SiC at 283.0 eV, C_a at 284.3-284.7 eV, and C_b at 286.3 eV, along with the total intensity for C 1s (C_{tot}), and of the total O 1s intensity ($I_{O\ 1s}$), all with respect to the intensity of Si 2p ($I_{Si\ 2p}$).

In addition to the temperature profiles obtained from our XPS measurements that depict the thermal evolution of the adspecies remaining on the 2×1 surface, we also performed TPD experiments to follow the desorption products that evolve from the surface as a function of temperature. Figure 4.4 compares the TPD profiles of selected mass fragments with m/z 2, 26, 27, 28, 39, 40, 41, and 42 for a RT saturation exposure of allyl alcohol and of allyl aldehyde on Si(100)2×1. We also monitored other mass fragments, including m/z 30 ($CH{=}OH^+$), and m/z 31 ($CH_2{=}OH^+$), and m/z 57 ($CH_2{=}CH{-}CH{=}OH^+$ or the parent mass) of allyl alcohol, as well as m/z 55 ($CH_2{=}CH{-}C{\equiv}O^+$) and m/z 56 ($CH_2{=}CH{-}CHO^+$ or the parent mass) of allyl aldehyde.[48] Except for the observed TPD profiles of the masses shown in Figure 4.4, none of the other monitored masses exhibit any TPD features, which suggests that neither allyl alcohol nor allyl aldehyde adsorbs molecularly on Si(100)2×1 at RT. For both allyl alcohol and allyl aldehyde, the most intense desorption feature is observed for m/z 2 at 810 K (Figures 4.4Aa, 4Ba), which corresponds to recombinative desorption of H_2 from silicon monohydrides.[49]

For allyl alcohol on Si(100)2×1, the TPD profile for m/z 26 exhibits two peaks at 585 K and 770 K (Figure 4.4Ab). Given that the cracking pattern of propene ($CH_2{=}CH{-}CH_3$) contains m/z 26 ($C_2H_2^+$), m/z 27 ($C_2H_3^+$), m/z 39 ($C_3H_3^+$), m/z 40 ($C_3H_4^+$), m/z 41 ($C_3H_5^+$, base mass) and m/z 42 ($C_3H_6^+$, parent mass),[48] the weak m/z 26 peak found at the same temperature as those of these other mass fragments (585 K, Figure 4.4A) therefore supports the molecular desorption of propene. The stronger m/z 26 peak at 770 K corresponds to desorption of acetylene (with m/z 26 as its parent and base masses), in accord with similar desorption temperature found in earlier work.[46,47] Furthermore, the TPD profiles of m/z 28 ($C_2H_4^+$, parent and base masses) and m/z 27 ($C_2H_3^+$), corresponding to the cracking pattern of ethylene, also reveal a peak maximum at 770 K, suggesting that the desorption of both acetylene and ethylene fragments comes from a common source. (It should be noted that the cracking pattern of ethylene also includes m/z 26, present as a minor component.) The broad TPD profile of m/z 28, with a significant desorption intensity over 450-850 K not accountable in the TPD profile of m/z 27, therefore suggests additional contribution from CO (with parent mass of m/z 28), in good accord with our temperature-dependent XPS data

(Figure 4.2Ah, 4.2Bh), which shows intensity reduction of both C_b 1s and O 1s upon annealing in this temperature range.

Similar to allyl alcohol, allyl aldehyde also exhibits TPD profiles with desorption maxima at 700 K for m/z 39, m/z 40, m/z 41 and m/z 42 (Figures 4.4Be-h), but with considerably weaker intensities. These desorption features can be attributed to propene desorption, and the observed higher desorption temperature (700 K, compared to that found for allyl alcohol, 585 K) suggests that propene production requires a higher energy pathway for allyl aldehyde than that for allyl alcohol. The rather weak desorption intensity of the base mass, m/z 41, for propene desorption also indicates that the corresponding contributions to m/z 26 and m/z 27 from propene desorption cannot account for the strong desorption intensities found for these two masses, suggesting additional sources. The strong desorption features at 700 K found for m/z 26, m/z 27, and m/z 28 all correspond to the desorption of ethylene. However, given that the desorption maximum for m/z 26 (Figure 4.4Bb) is almost the same as that of m/z 28 (the parent and base masses of ethylene), additional contribution likely from acetylene (with its parent and base masses at m/z 26) must be present. Unlike allyl alcohol (Figure 4.2Bh), no loss of O 1s intensity over the 425-800 K annealing temperature range is observed for allyl aldehyde (Figure 4.3Bh), which therefore suggests that the observed TPD profile for m/z 28 (Figure 4.4Bd) does not have any contribution from CO desorption.

It is also of interest to note that the absolute desorption intensity (not shown) for any selected mass fragment observed for allyl aldehyde is found to be considerably smaller than that for allyl alcohol (by at least a factor of 20). This observation indicates that the adspecies of allyl aldehyde prefer dissociation over desorption, in good agreement with the corresponding higher total C 1s XPS signal after annealing to 1390 K found for allyl aldehyde (Figures 4.3Ah) than that for allyl alcohol (Figure 4.2Ah).

Figure 4.5 shows the schematic pathways proposed for the formation of ethylene, acetylene, and propene as well as CO from the O−H dissociation product ASC I (Structure I) for allyl alcohol, and for the formation of ethylene, acetylene, and propene from the [2+2] C=O cycloaddition product ASC III (Structure II) for allyl aldehyde. It should be noted that

the actual mechanisms likely follow more complicated reaction steps than that presented here, to only show the necessary bond dissociation involved in the formation of these desorbates. In particular, we present a similar model for the formation of ethylene and acetylene from the respective allyl alcohol and allyl aldehyde adstructures on the 2×1 surface. For both Structure I (Figure 4.5A) and Structure II (Figure 4.5B), a C−C bond cleavage produces a dissociated ethenyl radical (CH_2=CH•) that stays on the surface, generating the respective intermediates. The Ibc intermediate (Figure 4.5A) subsequently abstracts a H atom likely from Si−H (Structure Ib) through pathway b or undergoes C−H dissociation in the cleaved surface ethenyl radical (Structure Ic) through pathway c, producing ethylene and acetylene, respectively. The remaining O−CH_2 fragment singly bonded to the surface could undergo total dissociation, producing the observed CO desorbate (and dissociated H atoms). Similarly, the IIfg intermediate (Figure 4.5B) also abstracts a H atom from the surface (Structure IIf) through pathway f, producing ethylene, or undergoes C−H dissociation in the surface ethenyl radical (Structure IIg) through pathway g, producing acetylene. With the dissociated H_2C−O fragment firmly di-σ bonded to the Si surface, it is not surprising that CO cannot be released as a desorbate.

For the formation of propene desorbates from allyl alcohol (Figure 4.5A), Structure I could undergo C−O dissociation (Structure Id) through pathway d to produce a propenyl radical (CH_2=CH−CH_2•), which becomes propene through abstraction of a H atom from the surface (Structure Id'). For allyl aldehyde, the formation of propene from Structure II (Figure 4.5B) likely proceeds through pathway h involving C−O dissociation and double H abstraction, the mechanism of which is unclear. The generally higher temperature of the desorption maxima (700 K) observed for propene-related mass fragments (m/z 27, 39, 40, 41, and 42) from allyl aldehyde (Figure 4.4B) relative to that (585 K) from allyl alcohol (Figure 4.4A) is consistent with the higher energy required for the multi-step process expected from pathway h relative to that required for pathway d.

For m/z 26, 27 and 28, considerable desorption intensities are found over the 600-800 K range for both allyl alcohol and allyl aldehyde, in good accord with the similar bond dissociation energies required for the production of ethylene and acetylene. As depicted in

Figure 4.5, both Structure I and II involve C−C bond dissociation (with a typical bond dissociation energy of 385 kJ mol^{-1})[50] to generate the ethenyl radical as the precursor, followed by Si−H (293 kJ mol^{-1}) and C−H dissociation (399 kJ mol^{-1}) to produce ethylene and acetylene, respectively. These pathways require rather similar energies, therefore giving rise to desorption intensities in the observed similar temperature range. In addition, for allyl alcohol on Si(100)2×1, the desorption maxima for propene desorption (585 K) have been found to be lower than those for ethylene and acetylene (770 K) (Figure 4.4A). This observation is consistent with the preferred formation of the more stable propenyl radical in pathway d over the ethenyl radical in pathway a (Figure 4.5A), which also accounts for the stronger desorption intensities found for the propene-related fragments than those for ethylene and acetylene.

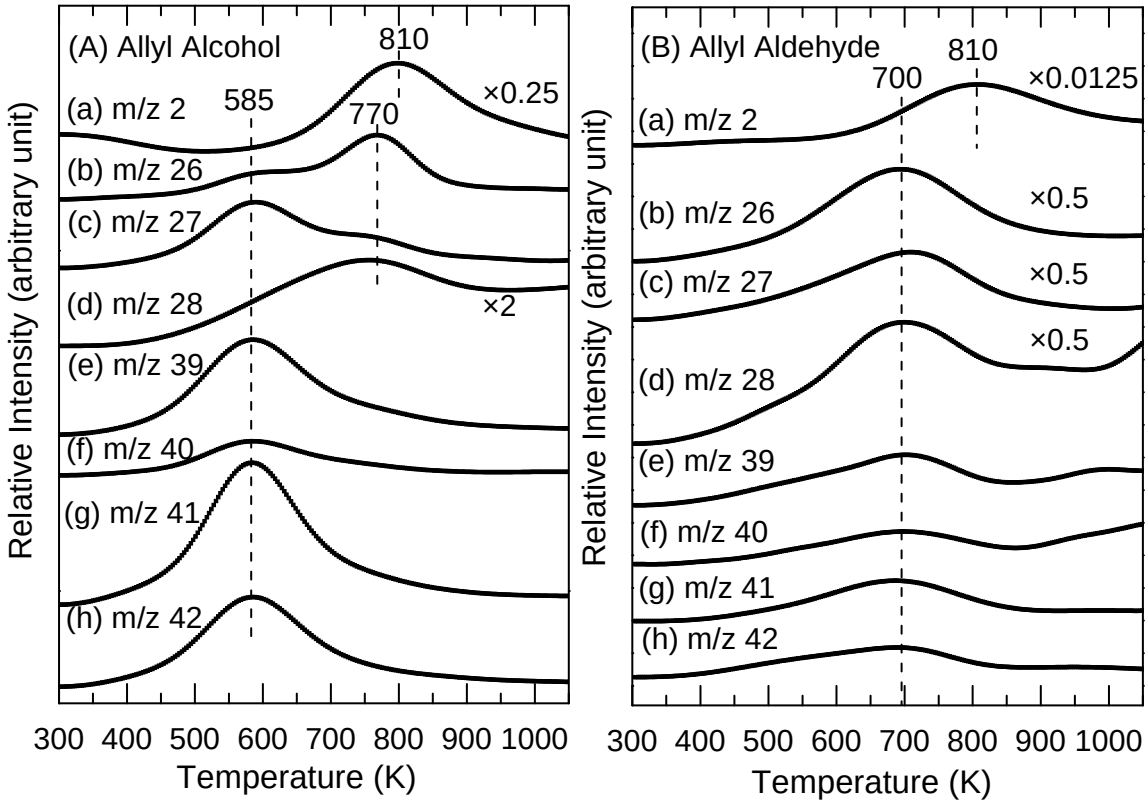

Figure 4.4 TPD profiles of selected fragments of m/z (a) 2, (b) 26, (c) 27, (d) 28, (e) 39, (f) 40, (g) 41, and (h) 42 for a saturation exposure of (A) allyl alcohol and (B) allyl aldehyde on Si(100)2×1 deposited at 300 K.

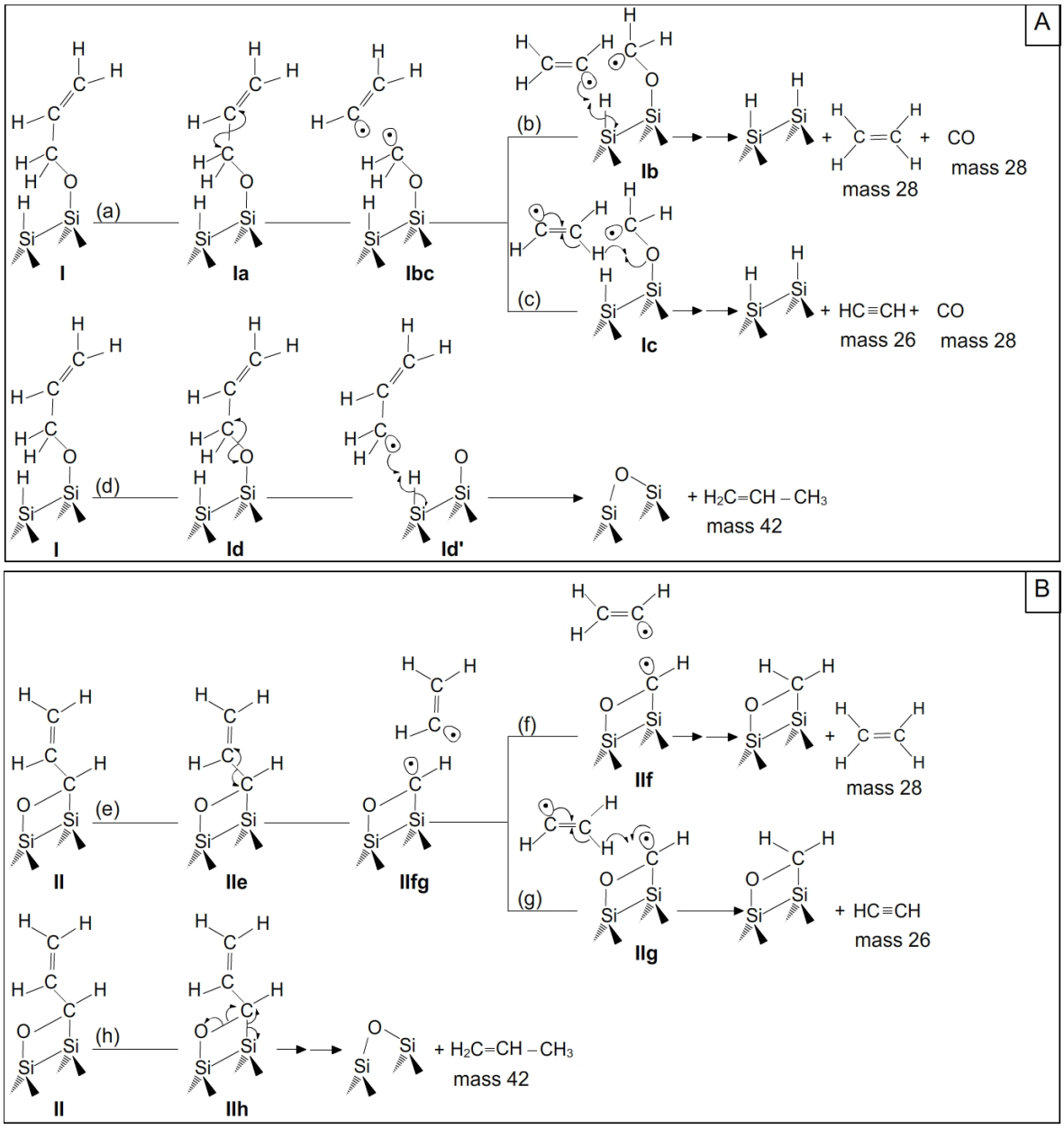

Figure 4.5 Schematic models for thermal evolution of the O−H dissociation and [2+2] C=O cycloaddition products to ethylene, acetylene, and propene for (A) allyl alcohol and (B) allyl aldehyde, respectively, on Si(100)2×1, and to additional CO desorption for allyl alcohol.

4.3 Summary

XPS and TPD experiments have been performed for the first time on allyl alcohol and allyl aldehyde on Si(100)2×1. The C 1s and O 1s spectra of allyl alcohol show that the O–H dissociation product is preferred over the [2+2] C=C cycloaddition product, in agreement with the DFT calculation. For allyl aldehyde, even though DFT calculation shows that the adsorption energy for the [2+2] C=C cycloaddition product is more negative than the C=O cycloaddition product, our XPS data supports the formation of the C=O cycloaddition product. These results are consistent with the efficacy of the electrophilic O in allyl alcohol and of the electrophilic-nucleophilic C=O bond in allyl aldehyde in establishing direct interactions with the Si buckled dimer on the 2×1 surface. Furthermore, the combined temperature-dependent XPS and TPD data can be used to infer plausible thermal evolution pathways that lead to the observed formation of ethylene, acetylene, and propene, resulting from the O−H dissociation product of allyl alcohol and the [2+2] C=O cycloaddition product of allyl aldehyde. The formation of these desorption products reflects the selectivity of the directional dangling bonds on the Si(100)2×1 surface for preferred reactions with the hydroxyl and carbonyl groups over the ethenyl group. Desorption of CO is also observed from the former and not the latter, while the formation of SiC from the dissociated ethenyl group above 1050 K indicates the remarkable stability of the C=C bond. As bifunctional molecules that leave the ethenyl group intact upon adsorption on the 2×1 surface, allyl alcohol and allyl aldehyde, like acrylic acid, therefore serve as viable linker molecules to provide further functionalization of this important semiconductor surface.

References

[1] M. A. Filler, S. F. Bent, Prog. Surf. Sci. 73 (2003) 1-56.

[2] S. F. Bent, Surf. Sci. 500 (2002) 879-903.

[3] J. M. Buriak, Chem. Commun. (1999) 1051-1060.

[4] J. M. Buriak, Chem. Rev. 102 (2002) 1271-1308.

[5] X. Lu, M. C. Lin, Int. Rev. Phys. Chem. 21 (2002) 137-184.

[6] T. R. Leftwich, A. V. Teplyakov, Surf. Sci. Rep. 63 (2008) 1-71.

[7] R. A. Wolkow, Annu. Rev. Phys. Chem. 50 (1999) 413-441.

[8] R. A. Wolkow, Phys. Rev. Lett. 68 (1992) 2636.

[9] H. N. Waltenburg, J. T. Yates Jr., Chem. Rev. 95 (1995) 1589-1673.

[10] F. A. Carey, "Organic Chemistry" 3rd Edition, McGraw-Hill, Toronto, (1996).

[11] C. C. Cheng, R. M. Wallace, P. A. Taylor, W. J. Choyke, J. T. Yates Jr., J. Appl. Phys. 67 (1990) 3693-3699.

[12] L. Clemen, R. M. Wallace, P. A. Taylor, M. J. Dresser, W. J. Choyke, W. H. Weinberg, J.T. Yates Jr., Surf. Sci. 268 (1992) 205-216.

[13] A. J. Mayne, A. R. Avery, J. Knall, T. S. Jones, G. A. D. Briggs, W.H. Weinberg, Surf. Sci. 284 (1993) 247-256.

[14] M. Ikeda, T. Maruoka, N. Nagashima, Surf. Sci. 416 (1998) 240-244.

[15] J. S. Hovis, H. B. Li, R. J. Hamers, J. Phys. Chem. B 102 (1998) 6873-6879.

[16] M. J. Kong, A. V. Teplyakov, J. Jagmohan, J. G. Lyubovitsky, C. Mui, S. F. Bent, J. Phys. Chem. B 104 (2000) 3000-3007.

[17] H. Liu, R. J. Hamers, Surf. Sci. 416 (1998) 354-362.

[18] M. Kiskinova, J. T. Yates Jr., Surf. Sci. 325 (1995) 1-10.

[19] H. B. Liu, R. J. Hamers, J. Amer. Chem. Soc. 119 (1997) 7593-7594.

[20] J. S. Hovis, R. J. Hamers, J. Phys. Chem. B 101 (1997) 9581-9585.

[21] L. C. Teague, J. J. Boland, J. Phys. Chem. B 107 (2003) 3820-3823.

[22] H. S. Kato, M. Wakatsuchi, M. Kawai, J. Yoshinobu, J. Phys. Chem. C 111 (2007) 2557-2564.

[23] R. J. Hamers, Y. Wang, Chem. Rev. 96 (1996) 1261-1290.

[24] R. J. Hamers, S. K. Coulter, M. D. Ellison, J. S. Hovis, D. F. Padowitz, M. P. Schwartz, C. M. Greenlief, J. N. Russell Jr., Acc. Chem. Res. 33 (2000) 617-624.

[25] J. L. Armstrong, J. M. White, M. Langell, J. Vac. Sci. Technol. A 15 (1997) 1146-1154.

[26] H. G. Huang, Y. P. Zhang, Y. H. Cai, J. Y. Huang, K. S. Yong, G. Q. Xu, J. Chem. Phys. 123 (2005) 104702-1-104702-6.

[27] J. L. Armstrong, E. D. Pylant, J. M. White, J. Vac. Sci. Technol. A 16 (1998) 123-130.

[28] G. T. Wang, C. Mui, C. B. Musgrave, S. F. Bent, J. Am. Chem. Soc. 124 (2002) 8990-9004.

[29] C. Shannon, A. Campion, Surf. Sci. 227 (1990) 219-223.

[30] J. Eng Jr., K. Raghavachari, L. M. Struck, Y. J. Chabal, B. E. Bent, G. W. Flynn, S. B. Christman, E. E. Chaban, G. P. Williams, K. Radermacher, S. Mantl, J. Chem. Phys. 106 (1997) 9889-9898.

[31] M. P. Casaletto, R. Zanoni, M. Carbone, M. N. Piancastelli, L. Aballe, K. Weiss, K. Horn, Surf. Sci. 447 (2000) 237-244.

[32] M. P. Casaletto, R. Zanoni, M. Carbone, M. N. Piancastelli, L. Aballe, K. Weiss, K. Horn, Surf. Sci. 505 (2002) 251-259.

[33] J. Kim, K. Kim, K. Yong, J. Vac. Sci. Technol A 20 (2002) 1582-1586.

[34] J. W. Kim, M. Carbone, M. Tallarida, J. H. Dil, K. Horn, M. P. Casaletto, R. Flammini, M. N. Piancastelli, Surf. Sci. 559 (2004) 179-185.

[35] S. Tanaka, M. Onchi, M. Nishijima, J. Chem. Phys. 91 (1989) 2712-2725.

[36] T. Bitzer, T. Alkunshalie, N. V. Richardson, Surf. Sci. 368 (1996) 202-207.

[37] T. Kubo, N. Minami, T. Aruga, N. Takagi, M. Nishijima, J. Phys. Chem. B 101 (1997) 7007-7011.

[38] H. Ikeura-Sekiguchi, T. Sekiguchi, Surf. Sci. 433-435 (1999) 549-553.

[39] T. Bitzer, N. V. Richardson, Surf. Sci. 427-428 (1999) 369-373.

[40] A. Lopez, T. Bitzer, T. Heller, N. V. Richardson, Surf. Sci. 480 (2001) 65-72.

[41] H.-N. Hwang, J. Y. Baik, K.-S. An, S. S. Lee, Y. Kim, C. C. Hwang, B. Kim, J. Phys. Chem. B 108 (2004) 8379-8384.

[42] H.-K. Lee, K.-J. Kim, J.-H. Han, T.-H. Kang, J. W. Chung, B. Kim, Phys. Rev. B 77 (2008) 115324.

[43] M. Ebrahimi, J. F. Rios, K. T. Leung, J. Phys. Chem. C (2009) in press.

[44] M. Ebrahimi, J. M. Chong, K. T. Leung, submitted (2009).

[45] J. Li, Y.-Q. Qu, K.-L. Han, G.-Z. He, Surf. Sci. 586 (2005) 45-55.

[46] X. J. Zhou, Z. H. He, K. T. Leung, Surf. Sci. 600 (2006) 468-477.

[47] X. J. Zhou, Q. Li, K. T. Leung, J. Phys. Chem. B 110 (2006) 5602-5610.

[48] NIST Mass Spec Data Center, S.E. Stein (director), "Mass Spectra" in NIST Chemistry WebBook, NIST Standard Reference Database Number 69, edited by P.J. Linstrom and W.G. Mallard, June 2005, National Institute of Standards and Technology, Gaithersburg (http://webbook.nist.gov).

[49] C. Lee, W. Yang, R. G. Parr, Phys. Rev. B 37 (1988) 785-789.

[50] "Bond Dissociation Energies" by Y.-R. Luo, in CRC Handbook of Chemistry and Physics, 88th Edition (Internet Version 2008), edited by D. R. Lide, CRC Press/Taylor and Francis, Boca Raton.

Chapter 5
Conclusion

Dry functionalization of Si(100)2×1 under ultra-high vacuum condition by a number of bifunctional organic molecules has been investigated in the present thesis. The main goal was to study the competition between several possible reaction pathways that result in selective formation of desirable adsorption products on the surface of Si(100)2×1. The preferred products are formed through the attachment of one of the functional groups of the molecule with the Si(100)2×1 surface. The remaining unreacted functional group can undergo further reactions to construct more complex molecular structure on the surface.

The reactivity of the alkyl, alkenyl, carboxyl, hydroxyl, and carbonyl of the five molecules, including acetic acid, propanoic acid, acrylic acid, allyl alcohol, and allyl aldehyde, was investigated in the present work. Acetic acid, the second smallest carboxylic acids, was used as the reference molecule in the present research. Our XPS results showed that acetic acid adsorbs on the surface through O−H dissociation, forming bidentate and unidentate acetates at low and high exposures, respectively. The XPS results were supported by our DFT calculation, which showed that O−H dissociation products were more stable than the other thermodynamically plausible products. We have presented a model based on the electron delocalization to explain the observed C 1s chemical shifts of unidentate and bidentate carboxyl carbons based on the difference in the partial charge. Furthermore, TPD results showed that acetaldehyde, ketene, and CO are the main desorption products from the surface.

The study was followed by investigating the surface chemistry of acrylic acid, containing an ethenyl (CH_2=CH) group in addition to the carboxyl group, on the Si(100)2×1. It was observed that acrylic acid, as a conjugated molecule, attaches to the surface through Si−O bond after the O−H dissociation. Similar to acetic acid, the formation of bidentate and unidentate acrylates at low and high exposures, respectively, was revealed by our XPS results. Electron delocalization of acrylate can also be used to provide insights into the chemical shifts in the C 1s BEs of the both bidentate and unidentate adstructures. It is of

interest to note that C=C is known to form the [2+2] C=C cycloaddition product with the Si(100)2×1 surface. However, the present study demonstrates that acrylic acid prefers to attach to the surface through O−H dissociation rather than [2+2] C=C cycloaddition. Furthermore, propanoic acid, as the saturated form of acrylic acid, was studied in order to compare the effect of the presence of C−C *vs* C=C on the reactivity of carboxyl group with the surface. Formation of ethylene, acetylene, propene, and CO from acrylic acid, and of ethylene and CO from propanoic acid was observed in our TPD experiments.

In order to compare the reactivity of each of the two components of the carboxyl group: the hydroxyl and carbonyl groups, the reactions of allyl alcohol and allyl aldehyde (both with an ethenyl group) were investigated. The experimental results showed that O−H dissociation product for allyl alcohol and [2+2] C=O cycloaddition product for allyl aldehyde are favoured over the other possibilities, including [2+2] C=C cylcoaddition and the reactions through both functional groups with the surface. Our XPS results were used to further deduce the structures of the reaction products according to the observed C 1s BE shifts. Thermal evolution profiles also revealed the formation of ethylene, acetylene, propene for both allyl alcohol and allyl aldehyde.

For the five organic molecules studied in the present work, it was observed that the O-containing functional groups including carboxyl, hydroxyl, and carbonyl are favoured to react with the Si(100)2×1 surface. The presence of alkenyl (i.e. ethenyl in the present work) does not interfere with the reaction of these functional groups with the 2×1 surface. However, it is known that molecules containing only the alkenyl group readily form cycloaddition products with Si(100)2×1. It is concluded that the asymmetric buckled Si dimer atoms play the key role in reactions with the functional groups (that could get close to the surface) through electrophilic-nucleophilic interaction.

The present research provides the trend for the stronger relative reactivity of carboxyl, hydroxyl, and carbonyl functional groups over the ethenyl and methyl groups in reactions with the Si(100)2×1 surface. As a follow up of the present work, we propose to study the reactivity of more complex multifunctional molecules on Si(100)2×1 to provide the fundamental knowledge for using more complicated molecules (including three or more

functional groups) to imprint functionalization on the Si(100)2×1 surface. In particular, it would be of interest to study the reactions of the remaining C=C in the alkene-related reactions, including addition reactions with hydrogen halides such as HCl and HBr, in the halogen addition reactions with Cl_2 or Br_2, and in the [4+2] cycloaddition reactions with other alkene molecules (such as butadiene) or with the molecules containing C=C and C=O such as allyl aldehyde. The goal is to build an extended multifunctional molecular structure attached to the surface in a controlled way. If the reactions of C=C with hydrogen halide or halogen proceed as expected, the resulting carbon attached to the halogen atom will be a highly reactive site for further nucleophilic substitution reactions. The reaction of a halocarboxylic acid (such as chloroacrylic acid) with Si(100)2×1 can therefore be used instead of the multi-step functionalization reactions. However, it is expected that the high reactivity of the more complicated molecules will present more experimental challenges, in addition to producing undesirable reaction products with multiple attachments to the surface. As a second future project, the surface chemistry of 2-butenedioic (HOOC−CH=CH−COOH) on Si(100)2×1 should be investigated with the objective to determine whether one or both carboxyl groups will react with a surface. If only one of them attach to the surface through O−H dissociation, the other one can be used to attach to a second surface. In this case, the conjugated system in the whole molecule can be used for conducting the electron between two surfaces. However, if both of the carboxyl groups react with the surface, the current will go through one attached site and return to the surface through the other site. This molecular structure could provide a novel form of molecular electromagnet. By using state-of-the-art vacuum techniques, the functionalization of the surface can be achieved in a site-selective way to equip the surface with appropriate functional groups capable of interacting efficiently either with more complicated molecules including proteins, DNA, and living cells or indeed with a second surface.